NUCLEAR QUADRUPOLE RESONANCE STUDIES

OF MOLECULAR STRUCTURE.

by

RODERICK JOHN LYNCH

A thesis submitted in partial fulfilment of the requirements for the award of the degree of Doctor of Philosophy in the University of Warwick.

School of Molecular Sciences

July 1972

ACKNOWLEDGEMENTS

I wish to express my gratitude to my supervisor, Professor J.A.S. Smith, for his constant encouragement and helpful discussion throughout this work. Thanks are due also to Professor T.C. Waddington, while at Warwick for provision of research facilities, and with Dr C.J. Ludman, Dr K.B. Dillon, Dr T.A. O'Shea and Dr B. Bell for the loan of many compounds. I am indebted also to my colleagues within the n.q.r. group for their assistance on many occasions and to my wife for her patience and encouragement during the latter stages of this work.

SUMMARY

The theory of nuclear quadrupole resonance and quadrupolar relaxation is reviewed, and the chemical interpretation of n.q.r. data is discussed.

The super-regenerative oscillator system as employed in the Decca spectrometer for the detection of n.q.r. is described. Details of the measurement of relaxation times using a pulsed r.f. spectrometer are also given.

In a study of hydrogen-bonded anions containing conveniently situated chlorine atoms a combination of the relative value of the ^{35}Cl n.q.r. frequency and the magnitude of its shift on deuterium substitution is used to distinguish between centrosymmetric and asymmetric hydrogen bonds. The effect is clearly observed in the n.q.r. spectra of eight salts of the hydrogen or deuterium dichloride ion, and in four series of hydrogen di-chlorocarboxylate anions. For caesium and tetramethylammonium hydrogen dichlorides the direction of the n.q.r. frequency shift suggests that the asymmetry of the bond in the anion is increased on deuteriation. The very small deuteriation shift observed for the symmetrically hydrogen-bonded anion in tetraethylammonium hydrogen dichloride and caesium chloride, $^{1}/3$ hydronium hydrogen dichloride, is consistent with a single broad minimum potential function. The assignment to a torsional mode of a line at 85 cm^{-1} in the neutron inelastic scattering spectrum of the latter salt is consistent with the observed temperature dependence of the ^{35}Cl n.q.r. frequency.

The temperature dependences of the ^{35}Cl spin-lattice relaxation time in caesium and tetramethylammonium hydrogen dichlorides are not sensitive to deuteriation. It is proposed that below 250 K in the former salt and 300 K in the latter, relaxation occurs by field gradient fluctuations due to lattice vibrations, and that above these temperatures the severe decrease in T_1 with temperature may be explained by diffusion of hydrogen chloride molecules throughout the lattice.

The ^{35}Cl T_1 temperature dependence of the symmetrically bonded hydrogen dichloride ion in the hydronium dichloride salt is however sensitive to deuteriation, and this is consistent with a relaxation mechanism arising from field gradient fluctuations due to reorientation of the hydronium ions. Activation energies for this motion are estimated to be 8.1 k cals/mole for H_3O^+ and 10.5 k cals/mole for D_3O^+.

The n.q.r. spectra of acid salts of mono, di, and trichloroacetic acids and ortho-, meta- and para-chlorobenzoic acids are discussed with relevance to the particular hydrogen bond structure of the anion.

In a series of complexes of general formula trans-L_2OsCl_4, the measurement of the ^{35}Cl n.q.r. frequency provides the following order of cis-influence of ligands:

$$Cl < AsEt_3 < PEt_2Ph < PEt_3$$

A phase transition in trans-$(PEt_3)_2OsCl_4$ is indicated near 100 K. It is suggested that intramolecular non-bonding interactions for the earlier members of the series of complexes trans-L_2MCl_4 and K_2MCl_6 may have a significant effect on the magnitude of the chlorine n.q.r. frequency and its temperature coefficient.

The chlorine n.q.r. frequencies of some 3-chloroacetylacetonato-complexes are shown to vary considerably with the polarity or charge of the complex, and to depend very little on the central element. The differences can be explained in terms of linear intramolecular electric field shifts, the signs and magnitudes of which correlate with experimental values of the Stark coefficient.

The n.q.r. spectra of a series of six addition compounds of phosphorus pentachloride favour the ionic structure containing the tetrachloro-phosphonium ion in each case. Values for the libration frequency of the PCl_4^+ ion are predicted.

CONTENTS

FIGURES

CHAPTER 1

THEORY OF THE NUCLEAR QUADRUPOLE INTERACTION

1.1 Introduction

Nuclear quadrupole resonance (n.q.r.) is a branch of radio frequency spectroscopy, and is closely related to the more familiar nuclear magnetic resonance (n.m.r.). Both techniques involve the coupling of radio frequency radiation with a nuclear magnetic moment to bring about transitions between nuclear orientations of different energies. The difference between the two lies in the origin of the nuclear energy levels. In the case of nuclear magnetic resonance, the energy levels are governed by the interaction of the nuclear dipole moment with an externally applied magnetic field, whereas in nuclear quadrupole resonance, the levels result from an interaction of the nuclear electric quadrupole moment with the electric field gradient produced at the nucleus by the charge distribution of its environment. The way in which the quadrupole interaction is observed depends upon the relative magnitudes of the nuclear magnetic and nuclear quadrupole interactions. When the magnetic interaction is large in comparison with the quadrupole, the latter causes a splitting or broadening of the n.m.r. lines. When the quadrupole interaction is dominant, then the transition frequencies are largely determined by the electric field gradients at the nucleus and the magnetic interaction is seen as a splitting or broadening of the n.q.r. lines. In the absence of a magnetic field, there is no magnetic interaction and the unperturbed quadrupole resonance lines are observed. In this thesis we shall be dealing exclusively with the latter case, which is alternatively known as "zero field" or "pure" quadrupole resonance, and will from now on be referred to as n.q.r. With magnetic resonance, the transition frequencies

are proportional to the applied magnetic field, so that excitation is possible with a fixed frequency oscillator by sweeping the magnetic field. With n.q.r., the electric field gradient is a fixed property of the molecule or the crystal and is considerably larger than any practical externally-applied field gradient. This means that a variable frequency detection system must be used. The range of nuclear quadrupole interactions is such that transition frequencies can occur anywhere in the range between 100 kHz and 1 GHz making detection by a single spectrometer very difficult. An individual quadrupolar nucleus will have most frequencies within a more workable range, e.g. 5-60 MHz for ^{35}Cl so that spectrometers are usually designed with specific nuclei in mind.

Since the n.q.r. frequencies are specifically governed by the electron distribution in the neighbourhood of the nucleus, they are very sensitive to the type of bonding in which the quadrupolar nucleus is involved. Two extreme cases illustrate the point. If a halogen nucleus, for example, is involved in a purely ionic bond then the charge distribution around the nucleus is spherical so that the transition frequency is zero. If the halogen is involved in a purely covalent bond then the charge distribution is largely anisotropic because of differences in the valence shell p orbital populations, and the resonance frequency is considerable. Thus information about the chemical bond can be obtained directly from n.q.r. frequencies. Measurement of the rates of nuclear relaxation can also provide information about the types of molecular motion in the solid state. N.q.r. is essentially a kind of solid state spectroscopy because the very fast molecular motion in liquids and most gases averages to zero the effective electric field gradient experienced by the nucleus. This thesis is therefore concerned with the presentation and chemical interpretation of n.q.r. data obtained from solids where structure and molecular motion

are of considerable interest. Hydrogen bonded molecules form a fair proportion of the compounds studied, and the dichloride ion was also selected for further investigation by pulsed n.q.r., in order to measure relaxation times. The rest of this chapter deals with the theory of the quadrupole interaction, the effect of temperature on the transition frequencies, and the theoretical origin of quadrupole relaxation. Chapter 2 discusses some chemical applications of the technique, Chapter 3 deals with the experimental detection of n.q.r., and the remaining five chapters are each concerned with the presentation of results and discussion of the ^{35}Cl n.q.r. investigation on the following series of molecules: dichloride anions (Chapter 4), hydrogen bonded acid salts (Chapter 5), transition metal complexes of the type L_2MCl_4 and L_3MCl_3 (Chapter 6), 3-chloro-acetonylacetonate complexes (Chapter 7), and tetrachloro-phosphonium cations (Chapter 8).

1.2 The Resonance Frequencies of Pure Quadrupole Spectra

This section gives outlines of the relationship of the resonance frequencies to the electric field gradient and the nuclear electric quadrupole moment. Full derivations of the quadrupole Hamiltonian are given in refs. [1.1 and 1.2] and are therefore not discussed in any detail here.

A nucleus can have an electric quadrupole moment only if its spin quantum number, $I > \frac{1}{2}$. Such a nucleus does not have spherical symmetry, but is distorted along the axis of spin. The nuclear charge distribution is compressed or extended along this axis according to the sign of its quadrupole moment. A positive moment has a prolate spheroidal shape (extension along the spin axis), and a negative moment is an oblate

spheroid (contraction along the spin axis). Let us consider a volume element of positive charge within such a nucleus, $d\tau_n = dx\,dy\,dz$, of charge density ρ_n, distant r_n from the nuclear centre. If this charge element is under the influence of a potential, V, from the electronic charge distribution in the molecule, then the potential energy of the charge element in its environment is $-\rho_n d\tau_n V$. If we integrate over the complete nucleus

$$\text{energy of interaction, } E = -\int \rho_n V d\tau_n \tag{1}$$

V varies over the nuclear volume, and this variation can be expressed in a Taylor expansion

$$V = V_o + \left[x_n\left(\frac{\partial V}{\partial x_n}\right)_o + y_n\left(\frac{\partial V}{\partial y_n}\right)_o + z_n\left(\frac{\partial V}{\partial z_n}\right)_o\right]$$

$$+ \tfrac{1}{2}\left[x_n^2\left(\frac{\partial^2 V}{\partial x_n^2}\right)_o + x_n y_n\left(\frac{\partial^2 V}{\partial x_n \partial y_n}\right)_o + \ldots\ldots\right] \tag{2}$$

where the subscript o indicates the terms are to be evaluated at the origin and x_n, y_n, z_n are co-ordinates in the nuclear frame of reference. Substitution of (2) into (1) gives

$$\text{Interaction Energy, } E = -\int \rho_n d\tau_n \left[V_o + \sum_{\alpha = x_n, y_n, z_n} \alpha\left(\frac{\partial V}{\partial \alpha}\right)_o\right.$$

$$\left. + \tfrac{1}{2} \sum_{\alpha = x_n, y_n, z_n} \sum_{\beta = x_n, y_n, z_n} \alpha\beta\left(\frac{\partial^2 V}{\partial \alpha \partial \beta}\right)_o\right] \tag{3}$$

If we define

$$\int \alpha \rho_n d\tau_n = P_\alpha, \text{ the electric dipole moment} \tag{4}$$

$$\int \alpha\beta \rho_n d\tau_n = eQ'_{\alpha\beta}, \text{ the electric quadrupole moment tensor} \quad (5)$$

$$\left(\frac{\partial^2 V}{\partial\alpha\partial\beta}\right)_o = q_{\alpha\beta}, \text{ the electric field gradient tensor} \quad (6)$$

$$\text{then } E = ZeV_o + \sum_{\alpha} P_\alpha \left(\frac{\partial V}{\partial \alpha}\right)_o + \tfrac{1}{2} \sum_{\alpha\beta} e\, q_{\alpha\beta}\, Q'_{\alpha\beta} + \ldots\ldots \quad (7)$$

ZeV_o is the interaction energy of a point charge; it is orientation independent and therefore irrelevant. The second term, containing the electric dipole moment, is thought to be zero because of symmetry and also from experimental evidence. This leaves the quadrupolar and higher terms. The even polar terms are zero because of symmetry and the fifth term, the hexadecapole is negligible (zero if $I < 2$). Therefore it is fair to assume that the main orientation dependent term is the quadrupolar term.

The electric field gradient tensor can be redefined under a new co-ordinate system (x,y,z), in such a way that only the principal components of the field gradient are non-zero. Thus the potential energy for the quadrupole interaction, using the new co-ordinates, would be

$$E = -\int \tfrac{1}{2} \left[\rho_n x_n^2 \left(\frac{\partial^2 V}{\partial x^2}\right)_o + \rho_n y_n^2 \left(\frac{\partial^2 V}{\partial y^2}\right)_o + \rho_n z_n^2 \left(\frac{\partial^2 V}{\partial z^2}\right)_o\right] d\tau_n \quad (8)$$

Similarly the nuclear quadrupole moment tensor $Q'_{\alpha\beta}$ can be redefined such that the maximum component of the nuclear magnetic moment lies along the z axis ($I_z = I$) and the new tensor, $Q_{\alpha\beta}$ has zero trace (i.e. the sum of the diagonal elements is zero). This is done by defining [1.1].

$$Q_{\alpha\beta} = 3Q'_{\alpha\beta} - \delta_{\alpha\beta} \sum_{\alpha\alpha} Q'_{\alpha\alpha} \quad (9)$$

where $\delta_{\alpha\beta} = 1$ for $\alpha = \beta$ and 0 for $\alpha \neq \beta$.

$Q_{\alpha\beta}$ has only five independent components and the only part which is orientation-dependent gives the interaction energy

$$E = \frac{1}{6} \sum_{\alpha\beta} Q_{\alpha\beta} V_{\alpha\beta} \tag{10}$$

In quantum mechanical terms, the operator $\hat{Q}_{\alpha\beta}$ replaces $Q_{\alpha\beta}$ in (10) and the quadrupole Hamiltonian is given by

$$\hat{\mathcal{H}}_Q = \frac{1}{6} \sum_{\alpha\beta} \hat{Q}_{\alpha\beta} V_{\alpha\beta} \tag{11}$$

The Wigner-Eckart theorem [1.2] is now used to relate all nine terms in $\hat{Q}_{\alpha\beta}$ to a single nuclear constant, eQ. The Hamiltonian then becomes

$$\hat{\mathcal{H}}_Q = \frac{eQ}{6I(2I-1)} \sum_{\alpha\beta} V_{\alpha\beta} \left[\frac{3}{2} (I_\alpha I_\beta + I_\beta I_\alpha) - \delta_{\alpha\beta} I^2 \right] \tag{12}$$

eQ is a scalar quantity, the quadrupole moment of the nucleus and is defined as

$$eQ = \int \rho(3z^2 - r^2) d_\tau \qquad (I=I_z) \tag{13}$$

This is zero for a spherical charge distribution, positive if the spin axis is the major axis of the spheroidal nucleus, and negative if the spin axis (z axis) is a minor axis.

Typical quadrupole moments are given in the table below [1.3].

Nucleus	Spin I	Quadrupole moment Q, ($\times 10^{24}$ cm^2)
^{2}H	1	+0.0027965
^{14}N	1	+0.0166
^{35}Cl	3/2	-0.0802
^{37}Cl	3/2	-0.0632
^{79}Br	3/2	+0.332
^{81}Br	3/2	+0.282
^{127}I	5/2	-0.785

The electric field gradient tensor has already been redefined in a diagonal form so that all non-diagonal terms are zero, and the three azes x, y and z are called the principal axes of the tensor. Since Laplace's equation applies, i.e.

$$V_{xx} + V_{yy} + V_{zz} = 0 \tag{14}$$

only two parameters are required to define the field gradient. The convention is to to choose the principal axes in such a way that

$$|V_{zz}| \geq |V_{yy}| \geq |V_{xx}|$$

and to redefine $V_{zz} = eq$.

An asymmetry parameter, η , is also defined.

$$\eta = \frac{V_{xx} - V_{yy}}{V_{zz}} \tag{15}$$

η measures the departure of the field gradient from axial symmetry, and

can take values in the range $0 \leq \eta \leq 1$. When $V_{xx} = V_{yy}$, the field gradient is symmetric about the z axis and $\eta = 0$. Thus eq and η, together with the direction cosines of the principal axes relative to a crystal-based co-ordinate system fully define the electric field gradient. In terms of the principal axes of the EFG tensor the Hamiltonian is

$$\hat{\mathcal{H}}_Q = \frac{e^2Qq}{4I(2I-1)} [3I_z^2 - I^2 + \eta(I_x^2 - I_y^2)] \tag{16}$$

If the field gradient is described in terms of a non-principal set of axes, of which the components are

$$\begin{aligned} V_o &= V_{zz} \\ V_{\pm 1} &= V_{xz} \pm iV_{yz} \\ V_{\pm 2} &= \tfrac{1}{2}(V_{xx} - V_{yy}) \pm iV_{xy} \end{aligned} \tag{17}$$

$(I_+ = I_x + iI_y)$
$(I_- = I_x - iI_y)$

then the quadrupole Hamiltonian has the form [1.2]

$$\begin{aligned} \hat{\mathcal{H}}_Q = \frac{eQ}{4I(2I-1)} [&V_o(3I_z^2 - I^2) + V_{\pm 1}(I^-I_z + I_zI^-) \\ &+ V_{-1}(I^+I_z + I_zI^+) + V_{+2}(I^-)^2 + V_{-2}(I^+)^2] \end{aligned} \tag{18}$$

This form of the Hamiltonian is useful when considering relaxation for which the principal axes are not fixed in space, but are functions of time.

Returning to the form of equation (16), when axial symmetry prevails and η is zero, the expression for the energy levels of the quadrupolar interaction is

$$E = \frac{e^2Qq}{4I(2I-1)} [3m^2 - I(I+1)] \tag{19}$$

Because of the m^2 term, the energy levels for $\pm$ m are degenerate. For nuclei of spin 3/2, the possible energy levels are

$$m = \pm \tfrac{1}{2} \qquad E = \frac{-e^2Qq}{4}$$

$$m = \pm 3/2 \qquad E = \frac{e^2Qq}{4} \tag{20}$$

The selection rule for magnetic dipole transitions is

$$\Delta m = \pm 1$$

so for spin 3/2 just one transition is observed at a frequency

$$\nu = \frac{E_{\pm 3/2} - E_{\pm 1/2}}{h} = \frac{1}{2}\frac{e^2Qq}{h} \tag{21}$$

Measurement of the transition frequency therefore gives the value of $\frac{e^2Qq}{h}$, the quadrupole coupling constant, expressed in Hz.

When the field gradient is not axially symmetric, then η is non-zero and the transition frequency becomes

$$\nu = \frac{1}{2}\frac{e^2Qq}{h}\left(1 + \eta^2/3\right)^{\frac{1}{2}} \tag{22}$$

The degeneracy of $\pm$ m is not lifted for half-integral spins. For spin 3/2, the quadrupole coupling constant cannot be accurately derived from the transition frequency unless η is known. In practice, if $\eta < 0.1$ as is often the case for chlorine, then the error in neglecting the η^2 term in equation (22) is less than 0.15%, and the coupling constant can be taken as twice the resonance frequency.

For spins other than 3/2, more than one frequency transition occurs and both $\frac{e^2Qq}{h}$ and η can be obtained. The expressions for transition frequencies for various spins are given in the table below [1.3].

Spin	Transition Frequency ($\eta \neq 0$)
1	$\nu_1 = \frac{1}{2}\left(\frac{e^2Qq}{h}\right)\eta$
	$\nu_2 = \frac{3}{4}$ " $\left(1 - \frac{\eta}{3}\right)$
	$\nu_3 = \frac{3}{4}$ " $\left(1 + \frac{\eta}{3}\right)$
$\frac{3}{2}$	$\nu_1 = \frac{1}{2}$ " $\left(1 + \frac{\eta^2}{3}\right)^{\frac{1}{2}}$
$\frac{5}{2}$	$\nu_1 = \frac{3}{20}$ " $(1 + 0.09259\eta^2 - 0.63403\eta^4)$
	$\nu_2 = \frac{3}{10}$ " $(1 + 0.20370\eta^2 + 0.16215\eta^4)$
$\frac{7}{2}$	$\nu_1 = \frac{1}{14}$ " $(1 + 3.63333\eta^2 - 7.26070\eta^4)$
	$\nu_2 = \frac{2}{14}$ " $(1 - 0.56667\eta^2 + 1.85952\eta^4)$
	$\nu_3 = \frac{3}{14}$ " $(1 - 0.1001\eta^2 - 0.01804\eta^4)$

The expressions for spins $\frac{5}{2}$ and $\frac{7}{2}$ are sufficiently accurate for values of $\eta < 0.25$; more terms in the series expansion are necessary for greater η values [1.4] or a direct solution can be used for $\eta \sim 1$ [1.18]. In practice, for spins $\frac{5}{2}$, $\frac{7}{2}$ and $\frac{9}{2}$, η values are obtained from tabulated frequency ratios which have been calculated for various asymmetry parameters [1.5]. For unity spin e.g. ^{14}N, η is derived from the ratio of ν_2 to ν_3, since ν_1 is usually too low to be observed unless η is large. For spin $\frac{3}{2}$, the only way to determine η is by Zeeman studies, in which a small externally applied magnetic field splits the degeneracy of $\pm$ m. Usually it is required that the sample be a single crystal, so that the orientation of the crystal axes to the applied magnetic field direction is known. When η is fairly large (say, > 0.10) and signals are strong it is

sometimes possible to do Zeeman studies with a polycrystalline sample, and determine less accurate values of η from a dependence of the line splittings on the applied magnetic field [1.6].

The intensity of a pure quadrupole resonance line depends on the direction of the radio frequency field in relation to the symmetry axis of the electric field gradient. The line is of maximum intensity when the field is in a plane perpendicular to the symmetry axis and zero when it is parallel to the axis. Most n.q.r. experiments are carried out on polycrystalline samples and in these cases it is not possible to orient the crystal axes to best advantage, so an average intensity is obtained. Line intensity is also dependent upon a number of other factors: (1) the proportion of the necessary nuclei in the sample,(2) the volume or "filling factor" of the probe coil, (3) various forms of line broadening. There are at least three important sources of broadening; (1) static broadening, resulting from strains or dislocations in the crystal which can affect the electric field gradient at different crystal sites, (2) broadening due to magnetic dipole-dipole interactions, and (3) broadening from short state lifetimes caused by relaxation. The second effect arises from neighbouring nuclei with a magnetic moment which generate random Zeeman splittings, either directly through space or indirectly through the bonding electrons, where the effect is intra-molecular. In very narrow lines, a broadening effect due to Zeeman splittings from the earth's magnetic field may be observed. The broadening is expected to be of the order of 0.2 kHz for chlorine which is much less than usual linewidths [1.4]. The third source of broadening is that due to transitions induced by the molecular motion, and is called "lifetime broadening". The contribution to the line width will be inversely

proportional to the spin-lattice relaxation rate, so this form of broadening becomes important when T_1 becomes very short (< 100 μsec.). Relaxation effects will be discussed in section 1.4. Another interaction which can give rise to line-splitting or line-broadening is the isotope effect, e.g. in BCl_3 the ^{35}Cl resonance is a doublet because of the different averaging that occurs in isotopically-related species such as $B^{37}Cl^{35}Cl_2$ and $B^{35}Cl_3$ as a result of their differing amplitudes of thermal motion.

1.3 Temperature Effects

Measurement of n.q.r. frequencies at different temperatures usually reveals a negative temperature coefficient. This is normally explained in terms of increasing vibrational amplitudes, which cause an averaging of the electric field gradient. The effect has been investigated by Bayer [1.8] who assumes that it is the torsional component of the motion that causes the field gradient averaging process. If we take the simple case where only one torsional motion is important and consider a rotation of OZ, the symmetry axis, by a small angle θ around a position of stable equilibrium Oz, in a plane perpendicular to an axis Ox in the laboratory frame. The molecular frame electric field gradients are:

$$\begin{aligned} V_{ZZ} &= eq \\ V_{XX} &= V_{YY} = -\frac{1}{2} eq \end{aligned} \qquad (23)$$

In the laboratory frame:

$$
\begin{aligned}
V_{zz} &= eq\ (1 - \frac{3e\theta^2}{2}) \\
V_{xx} &= -\ \tfrac{1}{2}\, eq \\
V_{yy} &= -\ \tfrac{1}{2}\, eq\ (1 - 3\theta^2) \\
V_{yz} &= \frac{3eq\theta}{2} \\
V_{xz} &= V_{xy} = 0
\end{aligned}
\tag{24}
$$

In the laboratory frame, the quadrupole Hamiltonian becomes [1.14]

$$
\hat{\mathcal{H}}_Q = \frac{e^2Qq}{4I(2I-1)} \left[\left(1 - \frac{3\theta^2}{2}\right)\left(3I_z^{\,2} - I^2\right) - \frac{3}{4}\,\theta^2(I_+^{\,2} + I_-^{\,2}) + 3\theta(I_zI_y + I_yI_z)\right] \tag{25}
$$

Thermal motion causes θ to fluctuate, so this is now a time dependent Hamiltonian. When averaged over all values of θ, the last term in the square bracket disappears since $< \theta > = 0$. The second term, $-\frac{3}{4} < \theta^2 > (I_+^{\,2} + I_-^{\,2})$, represents a small departure from cylindrical symmetry and affects the energy levels only by a contribution proportional to $< \theta^2 >^2$; therefore for small θ this term can be neglected. The first term is therefore dominant and the resonance frequencies will be changed by factor of $(1 - \frac{3}{2} < \theta^2 >)$. $< \theta^2 >$ will increase with temperature for low enough torsional frequencies so n.q.r. frequencies are expected to decrease with temperature, as is normally observed.

The torsional motion can be described by a simple harmonic oscillator model,

$$
A_t\omega_t^{\,2} < \theta_t^2 > \;=\; \hbar\omega_t\left(\tfrac{1}{2} + \frac{1}{\exp(\hbar\omega/kT)-1}\right)
$$

where ω_t is the torsional frequency; if there are more than one torsional mode, then $\omega_t = \omega_x$, ω_y, ω_z, and A_t are the corresponding moments of

inertia. From this is derived the expression for the temperature dependent n.q.r. frequency [1.4]

$$\nu = \nu_o \left[1 - \frac{3}{2}\hbar \left(\frac{1 + \eta/3}{2A_x\omega_x} + \frac{1 - \eta/3}{2A_y\omega_y} \right) - \frac{3}{2}\hbar \left(\frac{1 + \eta/3}{A_x\omega_x(\exp(\hbar\omega_x/kT)-1)} \right.\right.$$

$$\left.\left. + \frac{1 - \eta/3}{A_y\omega_y(\exp(\hbar\omega_y/kT)-1)} \right) \right] \qquad (27)$$

where ν_o is the n.q.r. frequency for the stationary molecule. If the terms in η are neglected, then the temperature coefficient is given by:

$$\frac{1}{\nu_o}\frac{\partial\nu}{\partial T} = \frac{3\hbar^2}{2kT^2}\left[\frac{\exp(\hbar\omega_x/kT)}{A_x(\exp(\hbar\omega_x/kT)-1)^2} + \frac{\exp(\hbar\omega_y/kT)}{A_y(\exp(\hbar\omega_y/kT)-1)^2} \right] \qquad (28)$$

The Bayer theory has been extended [1.9] by taking into account the temperature dependences of the torsional frequencies and the corresponding moments of inertia, thus providing a better fit to experimental data. The Bayer theory is essentially a constant volume theory, whereas experimental measurements are usually made at constant pressure. The temperature dependence of the n.q.r. frequency ν, at constant pressure may be written

$$\left(\frac{\partial\nu}{\partial T}\right)_P = \left[\sum_i \frac{\partial\nu}{\partial\omega_i}\frac{\partial\omega_i}{\partial V} + \frac{\partial\nu}{\partial V} \right]\left(\frac{\partial V}{\partial T}\right)_P + \left(\frac{\partial\nu}{\partial T}\right)_V \qquad (29)$$

where ω_i are the lattice frequencies. The last term is the contribution already discussed - the Bayer term. The first two take into account the temperature dependence of the lattice frequencies and the change in volume. The pressure dependence may be similarly formulated

$$\left(\frac{\partial\nu}{\partial P}\right)_T = \left[\sum_i \frac{\partial\nu}{\partial\omega_i}\frac{\partial\omega_i}{\partial V} + \frac{\partial\nu}{\partial V} \right]\left(\frac{\partial V}{\partial P}\right)_T \qquad (30)$$

Elimination of the square-bracketed term gives

$$\left(\frac{\partial \nu}{\partial T}\right)_P = \left[\left(\frac{\partial V}{\partial T} \right)_P \Big/ \left(\frac{\partial V}{\partial P}\right)_T \right] \left(\frac{\partial \nu}{\partial P}\right)_T + \left(\frac{\partial \nu}{\partial T}\right)_V \qquad (31)$$

The term in the square brackets in equation (31) is the ratio of coefficient of thermal expansion to the compressibility, which normally is a negative quantity.

If the n.q.r. frequency pressure dependence is also negative then the overall temperature coefficient is the sum of two oppositely signed terms. In most cases the Bayer term predominates and a negative temperature dependence is observed. If however the pressure coefficient is large and negative, then the first term in equation (31) may predominate and a positive temperature dependence is observed.

An example of these effects has been seen in the temperature study of ^{81}Br resonance in $TiBr_4$[1.15]. At low temperatures, the volume dependent term is dominant and the observed temperature coefficient is positive. As the temperature increases, the Bayer term increases because of increased molecular oscillations and so overrides the first term giving an overall negative temperature coefficient.

The volume dependent term is often important in ionic lattices where the field gradient largely depends upon $1/R^3$, where R is the inter-ionic distance, and in this case the pressure dependent term is positive. ^{63}Cu resonance in cuprous oxide is such an example. [1.9]. Volume effects are less important in highly covalent structures since the intermolecular contribution to the field gradient is only a small fraction of the total contribution.

In some cases, discontinuities are observed in the temperature dependence of an n.q.r. frequency. These are usually due to phase transitions, or the onset of molecular motion (for example, hindered rotation). Phase transitions are usually accompanied by a sharp change in the resonance frequency whereas rotational effects cause a broadening and perhaps loss of the signal at temperatures where the rotational frequency is comparable with that of the frequency width of the line. This effect has been observed in 1,2 dichloroethane [1.16], in which rotation occurs about the Cl .... Cl axis. At higher temperatures when the rotation rate is in excess of the n.q.r. frequency, an average field gradient is experienced by the chlorine nuclei, which is less than the original field gradient by a factor of $\left(\frac{3\cos^2\theta-1}{2}\right)$, where θ is the angle between the Cl-C bond and the rotation axis. For this molecule, θ is 19^{o}, so that this factor predicts a reduction in frequency of $\sim 5{\cdot}5$ MHz. This compares reasonably well with the observed reduction of $\sim 4{\cdot}5$ MHz. The discrepancy has been attributed to the neglect of the asymmetry parameter and the non-rigorous nature of the calculation [1.4].

1.4 Quadrupolar Relaxation

As in nuclear magnetic resonance, the response of a system of quadrupolar nuclei to radiofrequency power is governed by the relaxation times of the spin system. In quadrupole relaxation the important ones are:

T_1, the spin-lattice relaxation time

T_2^*, the inverse line-width parameter

T_2, the spin-phase memory time.

T_1 governs the rate at which the energy acquired by the spin system from the radio-frequency field can be dissipated into thermal energy. It is analogous to the longitudinal relaxation time in n.m.r. i.e. the rate constant for the recovery of the nuclear magnetisation vector in the field direction. The parallel in n.q.r. for the case I = 3/2 would be the rate constant for the return of the nuclear quadrupole moment to its minimum energy position in relation to the electric field gradient.

Both T_2 and T_2^* are related to the relaxation of the spin components among themselves, and the difference between them lies in the way in which they are measured. T_2^* governs the overall rate of decay and includes a contribution from static broadening effects due to slight inequivalences in the individual electronic field gradients. Thus the rate of decay of magnetisation following a 90° radiofrequency pulse is governed by T_2^*. There should be an inverse relationship between T_2^* and line-width, $\Delta\nu$, as measured on a spectrometer giving true lineshapes. T_2 would be the inverse linewidth if all static broadening in the crystal could be removed; in fact this broadening is compensated for in the pulse combinations used to measure T_2. So that we now define T_2 as governing the rate of decay of the echo amplitude after a $90^\circ/180^\circ$ pulse sequence. Again this is analogous to the compensation for the loss of spin-phase memory time in n.m.r., due to inhomogeneity in the applied magnetic field. T_2^* is therefore often considerably shorter than T_2.

T_2^* values can be estimated from linewidth studies, but for T_1 measurement pulse methods are normally required. Since T_1 is more sensitive to the dynamic structure of a solid than are T_2 and T_2^*, it will receive more attention here and also in Chapter 4. It should be noted that whereas T_1 decays for I = 3/2 are exponential, T_2 and T_2^* decays are not necessarily so.

To a first approximation, the electrical and magnetic contributions to T_1, arising from a particular lattice motion, are proportional to the square of the respective interaction energies [1.4]. For ^{35}Cl, the electric quadrupole interaction (e^2Qq/h) is 10^4-10^5 times the magnetic dipole energy $\left(\frac{\mu_1\mu_2}{r_{12}^3}\right)$, so that the electrical contribution to T_1 is 10^8-10^{10} times more important than the magnetic contribution.

In the Bayer theory of quadrupolar relaxation [1.8], the torsional motions of the molecule in the crystal are continuously interrupted by other vibrational and torsional modes, leading to random changes in the electric field gradient at the quadrupolar nucleus. There will be a frequency distribution of these random fluctuations and if this distribution has components at frequencies corresponding to $\Delta m = \pm 1$ and $\Delta m = \pm 2$ transitions between quadrupolar energy levels, then these components, which are equivalent to oscillating electric field gradients, can bring about such transitions.

The effect of the transitions will be to restore the Boltzmann distribution to the spin states and so this constitutes a relaxation mechanism.

The frequency distribution of the random fluctuations can be expressed by spectral density functions, $J_1(\omega)$ and $J_2(\omega)$ at the two frequencies of interest, namely those corresponding to $\Delta m = \pm 1$ and ± 2 transitions respectively. Spectral density functions are defined in terms of a correlation function, $K(\tau)$ which is variable with time (τ). If the relaxation is brought about by a torsional component of the motion, then two correlation functions may be defined

$$K_1(\tau) = \langle \theta(t)\ \theta^*(t+\tau) \rangle$$
$$K_2(\tau) = \langle \theta^2(t)\ \theta^{2*}(t+\tau) \rangle \qquad (32)$$

where θ is again the angle of displacement from the mean positive of the symmetry axis of the field gradient. The corresponding spectral densities are

$$J_1(\omega) = \int_{-\infty}^{\infty} K_1(\tau) e^{-i\omega\tau} d\tau$$

and
$$J_2(\omega) = \int_{-\infty}^{\infty} K_2(\tau) e^{-i\omega\tau} d\tau \qquad (33)$$

where ω is the n.q.r. frequency (Hz) x 2π.

From the expression for the time dependent quadrupole Hamiltonian in equation (25), the random part of it will be

$$\hat{\mathcal{H}}_1 = \mathcal{H} - \bar{\mathcal{H}} = A[-\frac{3}{2}(\theta^2 - \overline{\theta^2})(3I_z - I(I+1)) - \frac{3}{4}(\theta^2 - \overline{\theta^2})$$
$$.(I_+^2 + I_-^2) + 3\theta(I_zI_y + I_yI_z)] \qquad (34)$$

where $A = \frac{e^2Qq}{4I(2I-1)}$

It follows from Bloembergen, Purcell and Pound theory [1.7] that

$$W_1 = |\langle m \pm 1 | \hat{\mathcal{H}}_1 | m \rangle|^2 J_1(\omega)$$
and
$$W_2 = |\langle m \pm 2 | \hat{\mathcal{H}}_1 | m \rangle|^2 J_2(\omega) \qquad (35)$$

Using equations (33), (34) and (35) the following transition probabilities are derived

$$W_1 = \frac{3}{4}\omega^2 \int_{-\infty}^{\infty} K_1(\tau) e^{-i\omega\tau} d\tau \qquad (36)$$

$$W_2 = \frac{3}{16}\omega^2 \int_{-\infty}^{\infty} K_2(\tau)e^{-i\omega\tau}d\tau \qquad (37)$$

From the rates of change of population densities it can be shown that [1.14]

$$\frac{1}{T_1} = 2(W_1 + W_2) \qquad (38)$$

Substitution of equation (36) and (37) into (38) gives

$$\frac{1}{T_1} = \frac{3}{8}\omega^2[4J_1(\omega) + J_2(\omega)] \qquad (39)$$

The form taken by $J(\omega)$ and $K(\tau)$ depends upon the type of motion producing the field gradient fluctuations. Expressions for $K(\tau)$ usually include the definition of a correlation time, τ_c. As an example, a purely exponential correlation function would be of the form

$$K_1(\tau) = < \theta(0)\theta^*(0) > \exp\left(\frac{-|\tau|}{\tau_c}\right) \qquad (40)$$

where $< \theta(0)\theta^*(0) >$ is the mean square average at $\tau = 0$.

τ_c is therefore calculable from the T_1 data and gives the time scale of the particular molecular motion responsible for the relaxation. For example, hindered rotations in intramolecular groups have been shown to be efficient at generating fluctuating field gradients of the correct order, and in this case τ_c describes the time between rotations. This mechanism has been proposed for the ^{35}Cl quadrupolar relaxation in 1,2 dichloroethane [1.10, 1.11] and in 2,2 dichloropropane [1.10]. In the latter case, rotating methyl groups cause the field gradient fluctuations. Spin-lattice relaxation data in p-dichlorobenzene have been explained in terms of a pure torsional oscillation about an axis perpendicular to the ring [1.8, 1.13].

For relaxation in ionic lattices, Van Kranendonk [1.12] has derived a theory due to lattice vibrations, in which a Raman type spin-phonon

coupling is the source of the time dependence of the field gradients. At temperatures above the Debye temperature of the lattice, the relaxation rate is proportional to the square of the temperature (^{o}K).

^{35}Cl relaxation in sodium chlorate has been accounted for by Chang [1.17] in terms of lattice vibrations using an essentially similar theory.

The theoretical interpretation of spin-lattice relaxation times is usually based upon individual calculations of transition probabilities for the particular molecule, and the results obtained in Chapter 4 on the dichloride ion will be treated in a similar manner.

CHAPTER 2

THE CHEMICAL INTERPRETATION OF NUCLEAR QUADRUPOLE RESONANCE

2.1 Introduction.

In Chapter 1 it has been shown that measurement of nuclear quadrupole resonance frequencies can yield a value for the quadrupole coupling constant, $\frac{e^2Qq}{h}$. This quantity may be used in two ways.

Firstly, an accurate calculation of the electric field gradient at the nucleus can be carried out, which will give a value for a theoretical coupling constant, provided that the nuclear quadrupole moment, eQ, is known. Comparison with the experimentally determined coupling constant then provides a test for the accuracy of the wave functions used. Field gradient calculations are a useful test for electronic behaviour near the nucleus, since the function has an inverse cubed dependence on the electron-nucleus distance.

Secondly, coupling constants can be experimentally determined for a series of related molecules, from which approximate electron distributions may be derived, and these correlated with other physical properties e.g. bond distance. It is this procedure which has been used exclusively in this thesis. The semi-empirical theory for the treatment of quadrupole coupling constants is due to Townes and Dailey [2.1]. This method has been used extensively to explain a large proportion of halogen n.q.r. data and has been found to give a reasonably consistent interpretation [2.2]. It will be fully described in the next section.

In addition to elucidating the nature of chemical bonds, n.q.r. can provide crystallographic information. This is apparent in n.q.r.

single crystal studies, in which the directions of the principle components of the electric field gradient tensor are obtained, and this has been used to provide an almost full structural determination [2.3]. On polycrystalline samples, the multiplicity of the resonance can help to differentiate between space groups provided that the number of molecules per unit cell is known. Even without this information it is possible in some cases to determine the symmetry of a molecule from the crystallographic equivalence of the quadrupolar nuclei. Examples of this type will be given in chapters 4 and 5.

2.2 The Townes and Dailey Theory.

This theory rests on the assumptions that the observed nuclear quadrupole coupling constant in a molecule can be expressed in terms of the coupling constant in the free atom, and that the field gradient is generated predominantly by the valence shell p-electrons. Using these assumptions, $e^2Qq_{mol.}$ can be related to e^2Qq_{atom} by a simple equation in which the bond hybridisation, the ionic character and double bond character all appear as variables. The derivation is as follows.

Consider an element of charge of dimensions $d\tau$ and charge density ρ distant r from a quadrupolar nucleus. Let the angle θ describe the angle between the axis of quantisation of the nucleus, the z axis, and the position of the charge element. The potential due to the charge element at the nucleus is

$$V = \frac{\rho d\tau}{r} \qquad (1)$$

Hence $\frac{dV}{dz} = -\frac{\rho d\tau}{r^2} \cos\theta$, since $\frac{dr}{dz} = \cos\theta$

and $\frac{d^2V}{dz^2} = \rho \left(\frac{3\cos^2\theta - 1}{r^3} \right) d\tau$. $\qquad (2)$

For the field gradient due to the total electron cloud around the nucleus, equation (2) must be integrated over all space

$$Vzz = \int \rho \left(\frac{3\cos^2\theta - 1}{r^3}\right) d\tau \qquad (3)$$

In quantum-mechanical terms, the charge density, ρ can be replaced by $-e\Psi^*\Psi$.

$$Vzz = -e\int \Psi^*\left(\frac{3\cos^2\theta - 1}{r^3}\right) \Psi d\tau \qquad (4)$$

This is the total field gradient generated by the electrons at the quadrupolar nucleus. There exists also a contribution from other nuclei in the molecule. Including this term, the expression for the field gradient becomes

$$eq = -e\int \Psi^*\left(\frac{3\cos^2\theta - 1}{r^3}\right) \Psi d\tau + \sum_i Z_i e\left(\frac{3\cos^2\theta - 1}{R_i^3}\right) \qquad (5)$$

where $Z_i e$ is the nuclear charge on atom i, distant R_i from our nucleus. Contributions to the electronic part of the field gradient will of course come from all electrons in the molecule. At this stage we shall consider the nucleus in question to be involved in a covalent bond with another atom in a diatomic molecule, A-B. The sigma bond is formed by the overlap of hybrid atomic orbitals on A and B, Ψ_A and Ψ_B. The distribution of the two electrons in the bond is described by a molecular orbital, Φ, which is a linear combination of the two atomic orbitals.

$$\Phi = a\Psi_A + b\Psi_B \qquad (6)$$

Ψ_A and Ψ_B are both normalised. If Φ is also normalised,

$$a^2 + b^2 + 2abS = 1 \tag{7}$$

where S is the overlap integral, $\int \Psi_A^* \Psi_B \, d\tau$. The ionic character of the bond is

$$i = a^2 - b^2 \tag{8}$$

Both Ψ_A and Ψ_B will be hybrid orbitals of the form

$$\Psi_A = s\varphi_A^s + p\varphi_A^p + d\varphi_A^d \tag{9}$$

$$\Psi_B = s'\varphi_B^s + p'\varphi_B^p + d\varphi_B^d \tag{10}$$

where φ^s, φ^p and φ^d are s, p_z and d_z^2 orbitals. Because of the normalisation conditions $s^2 + p^2 + d^2 = 1$ and $s'^2 + p'^2 + d'^2 = 1$. The relative importance of the various contributions to the field gradient given by equation (5) can now be assessed. Suppose that atom A is a chlorine atom. Contributions to eq will come from

1. The two electrons in the molecular orbital Φ.
2. The $3p_x$ and $3p_y$ electrons on atom A.
3. The electrons which occupy the 3s level in the free atom.
4. The inner shell electrons on atom A, $1s^2\ 2s^2\ 2p^6$.
5. The nucleus of atom B and all its electrons, with the exception of the one in Φ.

These will now be considered separately.

1. The electrons in the molecular orbital Φ, give rise to a field gradient eq_{MO}.

where $q_{MO} = 2\ (a^2 q_A + b^2 q_B + 2ab q_{AB})$ (11)

from equations (4) and (6).

$$q_A = \int \Psi_A^* \left(\frac{3\cos^2\theta - 1}{r^3}\right) \Psi_A \, d\tau \tag{12}$$

$$q_B = \int \Psi_B^* \left(\frac{3\cos^2\theta - 1}{r^3}\right) \Psi_B \, d\tau \tag{13}$$

$$q_{AB} = \int \Psi_A^* \left(\frac{3\cos^2\theta - 1}{r^3}\right) \Psi_B \, d\tau \tag{14}$$

Using equation (9)

$$q_A = s^2 q_s + p^2 q_p + d^2 q_d + 2sp\ q_{sp} + 2sd\ q_{sd} + 2pd\ q_{pd} \tag{15}$$

q_s is zero because of spherical symmetry of the s orbital. q_{sd} is the only non-zero crossterm because it is the product of two even functions. Since $p^2 = 1-s^2-d^2$,

$$q_A = (1-s^2-d^2)q_p + d^2 q_d + 2sd\ q_{sd} \tag{16}$$

where $q_{sd} = \int \varphi_A^{s*} \left(\frac{3\cos^2\theta - 1}{r^3}\right) \varphi_A^d \, d\tau$. and eq_p, eq_d are field gradients due to a single electron in p_z and d_{z2} orbitals respectively.

2. By substitution of the hydrogen-like wavefunction for a $3p_z$ orbital into equation (4) it may be shown [1.3] that

$$eq_p = \frac{-4e}{15}\left(\frac{Z}{3a_o}\right)^3 \tag{17}$$

Z is the atomic number, a_o is the Bohr radius. Similarly for p_x and p_y orbitals

$$eq_{xx} = eq_{yy} = \frac{2e}{15}\left(\frac{Z}{3a_o}\right)^3 \tag{18}$$

so that

$$eq_p = eq_{zz} = -2eq_{xx} = -2eq_{yy} \tag{19}$$

Each electron in a p_x or p_y orbital produces $-\frac{1}{2}eq_p$ of field gradient, so that the total π electron contribution is

$$eq_\pi = -2eq_p \tag{20}$$

3. In the free atom there is no contribution to the field gradient from the 3s orbital. Due to sp hybridisation, the s electrons now occupy the counter-hybridised orbital, $\Psi = s\varphi_p + p\varphi_s$ and contribute

$$eq_{A^+} = 2s^2eq_p \tag{21}$$

to the total field gradient.

4. We now come to the contribution from the inner shells of the chlorine atom. As has been pointed out by Sternheimer [2.4], the inner shells cannot be regarded as spherically symmetrical charge distributions because of two effects. 1. Polarisation of the inner shells by the charge distributions of the valence electrons and other charges external to the nucleus, which brings about a shielding effect. 2. In addition, the nucleus induces a quadrupole moment in the inner shells. This latter effect is brought about in two ways (a) by a radial distortion of the inner shell due to repulsion from the negative (or less positive) ends of the nuclear quadrupole and a similar attraction to the more positive ends of the nucleus; and (b) by an angular distortion, in which chage in the electron shell opposite the "negative" part of the nucleus would tend to migrate towards the preferred position opposite the more positive ends of the quadrupole. Sternheimer showed

that the two polarisation effects, 1. and 2. above, are of equal magnitude [2.4]. However, the net effect is not the sum of the two parts calculated separately because of the cancellation of half of each interaction [2.2]. The total polarisation effect would be to multiply all the components of the field gradient which appear in equations (11), (20) and (21) by a factor of $(1 - R_1)$, where R_1 is the Sternheimer polarisation factor. The field gradient at the chlorine nucleus in the molecule will be expressed later in terms of the field gradient in the free atom, and it is implicit in the Townes-Dailey theory that the polarisation term is common to both and therefore does not appear in the final expression.

5. The effective positive charge at nucleus B produces a field gradient at the chlorine nucleus of

$$eq_{B^+} = \frac{d^2(e/r)}{dz^2} = \frac{2e}{R^3} \qquad (22)$$

This must be multiplied by a polarisation factor to allow for shielding. The shielding factor will be different from R_1 because the chlorine valence shell will contribute some additional shielding. The factor γ is normally used for charges external to the atom concerned.

$$eq_{B^+} = \frac{2e}{R^3}(1 - \gamma) \qquad (23)$$

In a free chlorine atom, the field gradient at the nucleus is generated by the absence of one p electron from a complete valence shell. Therefore the term q_p can be set to equal $-q_{atom}$. Summing all the contributions in equations (11), (16), (20), (21) and (23), the

total field gradient is $eq_{mol.}$ where

$$q_{mol} = q_{MO} + q_{\pi} + q_{Cl+} + q_{B+}$$

$$q_{mol} = 2a^2[-(1-s^2-d^2)q_{atom} + d^2 q_d + 2sd\, q_{sd}]$$

$$+ 2b^2 q_B(1-R_1) + 4abq_{AB} + 2q_{atom} - 2s^2 q_{atom} + \frac{2}{R^3}(1-\gamma) \qquad (24)$$

Equation (24) is drastically simplified by Townes and Dailey. If the field gradient due to a d_{z^2} orbital is calculated in a manner similar to equation (17), then it is apparent that q_d is negligible in comparison with q_p for electrons with the same principal quantum number. Therefore the second term in the square brackets can be neglected. So, also, can the third term, because the amount of d character is always less than the s character for chlorine. The terms $2b^2 q_B(1-R_1)$ and $\frac{2}{R^3}(1-\gamma)$ are neglected because of their dependence on R^{-3}[2.1]. Das and Hahn further point out that R_1 and γ are of opposite sign and will cancel unless the bond is highly ionic. The overlap term, $4ab\, q_{AB}$ is also neglected, since Townes and Dailey showed it to be less than 5% in ICl; and for more ionic molecules its value would be expected to be even smaller.

These approximations reduce equation (24) to

$$q_{mol} = 2q_{atom}[(1-s^2) - a^2(1-s^2-d^2)] \qquad (25)$$

From equations (7) and (8), $2a^2 = i + 1 - 2abS$. Therefore

$$q_{mol} = q_{atom}[1-s^2+d^2-i(1-s^2-d^2)+2abS(1-s^2-d^2)] \qquad (26)$$

If, in the last term, S is calculated using Slater-type orbitals, then this leads to fairly high values of s character to explain experimentally determined coupling constants. Gordy has indicated that these wavefunctions are not always accurate for electronic properties near the nucleus [2.5]. and the overlap term has therefore been neglected in the Townes-Dailey theory. Equation (26) becomes

$$q_{mol} = q_{atom}[1-s^2+d^2-i(1-s^2-d^2)] \tag{27}$$

In cases where d hybridisation is improbable, e.g. chlorine, the Townes-Dailey expression reduces to its simplest form

$$\frac{e^2Qq_{mol}}{e^2Qq_{atom}} = (1-s^2)(1-i) \tag{28}$$

Where there exists the possibility of π bonding with the chlorine $3p_x$ and $3p_y$ orbitals, the contribution to eq_{mol} from equation (20) will be modified, since the number of π electrons on chlorine will be reduced from 4 to $2(2-\pi)$, where π is defined as the difference in electron density between a bound and free atom p_π orbital.

Therefore eq_π becomes $-(2-\pi)eq_p$. This changes equation (27) to

$$\frac{e^2Qq_{mol}}{e^2Qq_{atom}} = (1-i)(1-s^2+d^2)-\pi \tag{29}$$

If the chlorine atom is bonded to a more electronegative atom than itself, it will carry an effective positive charge. The interaction between a p electron and the nucleus is therefore increased [2.6]. The coupling constant is increased by a factor of $(1+\epsilon)^i \simeq (1+i\epsilon)$,

if ϵ is small, where ϵ is a constant determined from atomic spectroscopy and is due to the change in value of $\langle r^{-3} \rangle$ for the p-electron. Values of ϵ are given in refs [2.6] and [2.2] where the value of 0.14 is quoted for chlorine. For Cl^+, equation (29) therefore becomes,

$$\frac{e^2Qq_{mol}}{e^2Qq_{atom}} = \rho = [(1-i)(1-s^2+d^2)-\pi](1+i\epsilon). \qquad (30)$$

The symbol ρ is often used for the ratio of the coupling constant in the molecule to that in the free atom.

As an alternative to equation (28) the contributions to the field gradient may be expressed in terms of the populations of the chlorine 3p orbitals. The approximations involved are the same as before. The following table gives the contributions to the field gradient in the z direction. n_1 and n_2 are the populations of Ψ_A and Ψ_{A^+} (the counter-hybridised orbital) respectively.

Orbital	E.F.G along z.	Orbital population	Total contribution to E.F.G
Ψ_A	p^2q_p	n_1	$n_1p^2q_p$
Ψ_{A^+}	s^2q_p	n_2	$n_2s^2q_p$
$\Psi(3p_x)$	$-\frac{1}{2}q_p$	2	$-q_p$
$\Psi(3p_y)$	$-\frac{1}{2}q_p$	2	$-q_p$

$$q_{mol} = -q_{atom}\,[n_1p^2 + n_2s^2 - 2] \qquad (30)$$

Assuming that no d hybridisation is involved in Ψ_A $p^2 + s^2 = 1$ and

$$q_{mol} = -q_{atom}[n_1(1-s^2) + n_2s^2 - 2] \qquad (31)$$

if $n_2 = 2$, the electrons in the non-bonding orbital,

$$q_{mol} = -q_{atom}[n_1(1-s^2) + 2(s^2-1)]$$

and

$$\rho = [(1-s^2)(2-n_1)] \qquad (32)$$

Note the similarity to equation (28). Within the approximate nature of the analysis, equation (32) directly relates the ratio of the coupling constants to the population of the p_σ atomic orbital in a singly coordinated atom. When ρ is large, ~ 1, $n_1 \sim 1$, corresponding to delocalisation of charge in the covalently bonded structure. When ρ is small, n_1 approaches 2 which corresponds to localised charge on the atom, in which case an ionic structure predominates.

The value of ρ is calculated using the atomic coupling constant uncorrected for Sternheimer effects since the latter is assumed to cancel with a similar factor in e^2Qq_{mol}. This coupling constant for spin $^3/2$ is usually taken as twice the observed resonance frequency unless there is any reason to believe η to be large. (equation (22), chapter 1). This approximation can cause a maximum error of 15% (if $\eta = 1$), but typically the error is much less (-0.15% if $\eta = 0.1$).

Taking again the case of spin $^3/2$, if the n.q.r. spectrum shows more than one line, the multiplicity may be due to either chemical or physical differences in the field gradient. Splittings due to chemical differences in the interaction are usually significantly larger than those due to physical or solid state effects (apart from solid-state hydrogen bonding) and are treated separately by the Townes-Dailey equation. Solid state splittings may be due to differences in the E.F.G. tensor in magnitude and direction or in direction alone. It is not possible to separate the two, however, without single crystal Zeeman studies.

If coupling constants are to be analysed using equation (28) or (32), then some estimate for the amount of sp hybridisation is required. This will be discussed in Section 2.4.

2.3 The Cotton and Harris Equation.

Cotton and Harris [2.7] have more recently derived a general theory for relating nuclear quadrupole coupling constants to electronic structure by a molecular orbital method. Their approach has been to deal with the problem in the opposite manner, to calculate a quadrupole coupling constant from known molecular orbitals derived from a minimum energy criterion.

The theory starts from a set of N orthogonal molecular orbitals, Φ_p, each of which is formed from a linear combination of n orthogonal atomic orbitals, φ_i.

$$\Phi_p = c_{1p}\varphi_1 + c_{2p}\varphi_2 \ldots . c_{np}\varphi_n = \sum_i c_{ip}\varphi_i$$

If each molecular orbital contains N_p electrons the electronic contribution to the field gradient at the quadrupolar nucleus, α, is

$$q^{\alpha}_{z.electronic} = \sum_p \sum_i \sum_j N_p c_{ip} c_{jp} q^{\alpha}_{ij} \qquad (33)$$

where $q^{\alpha}_{ij} = e \int \varphi_i^* \left(\frac{3\cos^2\theta - 1}{r^3}\right) \varphi_j d\tau.$

The q_{ij} terms in equation (33) can be one, two, or three centre integrals.

$$q^{\alpha}_z = \sum_p N_p \Big[\sum_i (c_{ip})^2 q^{\alpha}_{ii} + \sum_j (c_{jp})^2 q^{\alpha}_{jj} + \sum_i \sum_j c_{ip} c_{jp} q^{\alpha}_{ij} + \sum_j \sum_k c_{jp} c_{kp} q^{\alpha}_{jk} \Big] \qquad (34)$$

i indicates an atomic orbital centred on nucleus α, while j and k are atomic orbitals on other nuclei. Equation (34) is simplified by the

following assumptions:

1. The field gradient contribution from the inner electrons on nucleus α is set equal to a constant, P.

2. The contributions from other nuclei and their inner electron shells are collectively termed q^{α}_{core}.

3. All non-core integrals, q_{jj}, plus half of the sum of the q_{ij} overlap terms are set to cancel with q^{α}_{core}. This is said to be justified on the basis of their numerical results [2.17,2.18]. A typical error in this approximation is claimed to be 2.5% of the total field gradient.

4. All three centre integrals are neglected.

Equation (34) then becomes

$$q^{\alpha}_{z} = \sum_{p} N_{p} \left[\sum_{i} c^{2}_{ip} \overline{q_{ii}{}^{\alpha}} + \sum_{i} \sum_{j>i} c_{ip} c_{jp} \overline{q^{\alpha}_{ij}} \right] + P \qquad (35)$$

The bar over the q^{α} terms indicates that the summation is restricted to non-core orbitals. If q^{α}_{ij} can be approximated by $S_{ij} q_{ii}$ where S_{ij} is the overlap integral

$$\int \varphi^{*}_{i} \varphi_{j} d\tau$$

q^{α}_{z} then becomes

$$q^{\alpha}_{z} = \sum_{i} f_{i} q^{\alpha}_{ii} + P \qquad (36)$$

where $f_{i} = \sum_{p} N_{p} \left[c^{2}_{ip} + c_{ip} \sum_{j>i} c_{jp} S_{ij} \right]$

The coupling constant in the molecule is

$$e^{2} Q^{\alpha} q^{\alpha} = \sum_{i} f_{i} \left[e^{2} Q^{\alpha} q^{\alpha}_{ii} + \frac{e^{2} Q^{\alpha} P}{\sum_{i} f_{i}} \right] \qquad (37)$$

The polarisation term, P, although large, is assumed to be similar in the atom and molecule. Therefore the term in square brackets in equation (37) may be replaced by the coupling constant in the free atom. For chlorine, the latter is equal to the negative of the field gradient from one p electron so that N_p is replaced by $2-N_p$ in equation (37). The final expression is

$$e^2Qq_{mol} = 109.7 \sum_p (2-N_p)\left[c_{ip}^2 + \sum_{j>i} c_{ip}c_{jp}S_{ij}\right] \qquad (38)$$

This equation reduces to that of Townes and Dailey, when overlap is neglected. Cotton and Harris have applied equation (38) to the results of their molecular orbital calculations on transition metal complexes of the type MCl_6^{2-} where M = Re, Os, Ir, and Pt. [2.18], and $PtCl_4^{2-}$ [2.17]. The calculated coupling constants agree with the measured values within an error of 10%.

2.4 Hybridisation.

In molecules containing multi-coordinated atoms the use of atomic orbitals for bond formation often fails to predict the correct molecular geometry. In many cases the use of hybridised atomic orbitals explains satisfactorily the observed molecular structure and leads to greater orbital overlap. In singly coordinated atoms however the effects of hybridisation are less apparent. When the Townes and Dailey theory was first presented considerable dispute arose over the question of hybridisation in singly coordinated halogen atoms. The authors of the theory derived an empirical rule which proposed that the sigma bonding orbital contains 15% s character when the halogen has an electronegativity of more than 0.25 units (Pauling scale) than the atom to which it is bonded. In all other cases, s is set to zero. In addition, the d hybridisation is always less than 5%.

Townes and Dailey based this rule on the following reasons:

1. s hybridisation involves promotion of electrons to a higher state, which should be easier for a negative halogen ion than for a neutral or positive atom.

2. In the Townes-Dailey expression, equation (29), the effects of s and d hybridisation oppose each other so that even a small amount of d character could lead to unreasonable values for the amount of s character.

The alternative ~~opinion~~ approach, due to Gordy [2.5] was to neglect s hybridisation altogether, and consider that bonds were constructed from pure p orbitals. This is supported by the experimental coupling constants in halogen molecules, in which the bonding is 100% covalent. The ratio of molecular to atomic coupling constants is unity so that use of the Townes-Dailey expression requires that the amounts of s and d characters are equal. For chlorine, d is known to be negligible. On this basis, Gordy proposed that s character could be neglected in all single bonds in which halogen was the most electronegative atom. Neither procedure is entirely satisfactory but at least Gordy's approximation does not have the sudden discontinuity of the Townes-Dailey rule.

The question of hybridisation has been reviewed by Lucken [2.2], who considers the factors which lead to a mixing of s and p orbitals in a diatomic molecule.

1. Electrostatic effects, which arise from a polarisation of pure s and p orbitals by an electrostatic field gradient. This can be responsible for up to 10% s character.

2. The overlap of an s-p hybrid σ-orbital with the orbital of the neighbouring atom is usually greater than that of either an s or p orbital alone. If the value of the Slater overlap integral is calculated for various proportions of s character, then it is apparent that a small

amount of s character considerably increases overlap. This is shown in ref. [2.2] for HCl and Cl_2. Also it is obvious that there is little increase in overlap above 20-25% s character.

3. Orbital energies must also be considered. Again taking the case of a halogen atom involved in a single bond in a diatomic molecule, if the other atom is more electronegative than the halogen then its atomic orbital with which it is to form a bond with the halogen will have a lower orbital energy than its partner. Since strongest bonds are formed by orbitals of most similar energies, some s character would be expected in the chlorine bonding orbital. Conversely, if the other atom is less electronegative than chlorine, then its bonding orbital would be of higher energy than the chlorine p orbitals, and considerably higher than the chlorine s orbitals, which in this case would not be expected to be involved in the bonding. This conclusion is opposite to the Townes and Dailey view, but agrees with that of Gordy.

Whitehead and Jaffé [2.8] have used the ionisation potential of an atomic orbital as a measure of its energy and have related this quantity to hybridisation. They later introduced the concept of orbital electronegativity and used this to treat the hybridisation problem [2.9]. The method is illustrated by application to HCl.

The Gordy definition of ionic character is used

$$i = \tfrac{1}{2}|X_{Cl} - X_H| \qquad (38)$$

where X_H, X_{Cl} are the corresponding orbital electronegativities. When an s-p hybrid orbital is used for bonding the hybrid orbital is given by

$$X_{hyb.} = sX_s + (1-s)X_p \qquad (39)$$

where s is the fractional s character of the hybrid orbital. For HCl,

$$i = \tfrac{1}{2}\left[s X_s^{Cl} + (1-s)\, X_p^{Cl} - X_H \right] \qquad (40)$$

The Townes-Dailey equation (28), can then be re-expressed as

$$\frac{e^2 Qq_{mol}}{e^2 Qq_{atom}} = \left(\frac{X_s^{Cl} - X_p^{Cl}}{2} \right) s^2 - \left(\frac{X_s^{Cl}}{2} - X_p^{Cl} + 1 + \frac{X^H}{2} \right) s + \left(1 + \frac{X^H}{2} - \frac{X_p^{Cl}}{2} \right) \qquad (41)$$

Values of the orbital electronegativities, X_H, X_s^{Cl}, X_p^{Cl}, have been calculated by Hinze and Jaffé from spectroscopic data and are listed in ref [2.10]. Using the ^{35}Cl coupling constant of 53MHz equation (41) may be solved to give a value of 6.9% s hybridisation in HCl.

This is, however, a considerably larger value than that apparent in an SCFMO calculation [2.11], in which the amount of s character in the bonding orbital is only 0.7%.

An independent estimate of hybridisation in a molecular orbital has been obtained from e.s.r studies [2.12]. The nuclear electron spin-spin hyperfine coupling tensor of a free radical consists of isotropic and anisotropic parts which can be related to the s and p contributions to the molecular orbital in which the unpaired electron is located. A series of interhalogen diatomic radical-anions, trapped in alkali halide matrices have been studied in this way [2.12]. In these radicals, the unpaired electron is moving in the antibonding sigma orbital but the proportion of s:p character in this orbital will be the same as in the bonding orbital. The results show that in ions of the type FCl^-, FBr^- and FI^- the amount of s character is small, less than 5% in all cases. Also the trend is that s character is greatest for the atom at the positive end of the dipole. This disagrees with the Townes-Dailey rule but of course agrees with the orbital energy hypothesis.

It appears therefore that the amount of hybridisation in the sigma bond of singly coordinated halogen nuclei is often small, and may be negligible in some cases. It is often more reasonable not to attempt to separate the effects of ionic character and hybridisation, but to interpret quadrupole coupling constants in terms of the electronic population in the p_σ orbital.

For other multi-coordinated nuclei, hybridisation information may be derived from bond angles, in cases where the structure has been fully ascertained. If a nucleus forms two ~~similar~~ equivalent s-p hybrid bonds, at an interbond angle of θ, then the expression for the s character in each bond is given by [1.4].

$$s = \frac{\cos\ \theta}{(\cos\ \theta - 1)} \qquad (42)$$

This simple expression neglects the effects of any d hybridisation and also any intramolecular repulsion effects. Equation (42) has been used to provide approximate s values for interpretation of ^{14}N and ^{33}S quadrupole coupling constants [2.13]. This approach is of course not possible in the vast majority of halogen compounds.

2.5 Double Bond Character.

It follows from the definition of the asymmetry parameter, η, given in chapter 1, that this quantity will be closely related with the amount of double bond character present in a bond. If we consider a molecule in which one of the p_π orbitals on a halogen atom is involved in a π bond, for example the p_y orbital, we can derive expression for the principal components of the field gradient tensor in the following way. If the bond order of the π bond is π, and the number of electrons in the p_x, p_y and p_z

orbitals are N_x, N_y and N_z respectively, we can use equation (19) and obtain:

$$q_{xx} = [N_x - \tfrac{1}{2}(N_y + N_z)]\, q_{at}$$

$$q_{yy} = [N_y - \tfrac{1}{2}(N_x + N_z)]\, q_{at}$$

$$q_{zz} = [N_z - \tfrac{1}{2}(N_x + N_y)]\, q_{at} \qquad (43)$$

As given in chapter 1, η is defined as

$$\eta = \frac{q_{xx} - q_{yy}}{q_{zz}} \qquad (44)$$

Substitution of equation (43) into (44) gives

$$\eta = \frac{\frac{3}{2}(N_x - N_y)q_{at}}{q_{zz}} = \frac{\frac{3}{2}(N_x - N_y)}{\rho} \qquad (45)$$

Since $N_y = 2-\pi$ and $N_x = 2$ in this case, the π character of the bond,

$$\pi = \frac{2}{3}\,\rho.\eta \qquad (46)$$

This equation, due to Bersohn [2.14] is very convenient in that π is immediately obtainable from experimental η and ρ values. Unfortunately η is not determined for nuclei of spin $\frac{3}{2}$ without resort to Zeeman studies, and further, η will be zero, regardless of π bonding if the bond axis should lie along a three or more-fold axis of symmetry [1.1]. In some molecules in solids, a contribution to asymmetry in the e.f.g. tensor may arise from intermolecular effects, in which case π will be overestimated.

Double bond character has been related to bond length data by a

semi-empirical rule proposed by Pauling [2.15]

$$\pi = \frac{R_1 - R}{R_1 + 2R - 3R_2} \tag{47}$$

where R is the length of the bond in question, and R_1, R_2 are the lengths of pure single and double bonds. In the absence of experimental data R_1 and R_2 are approximated by the Stevenson-Schomaker relationship *

$$R_1 = R_{1A} + R_{1B} - 0.09\,|X_A - X_B|$$

R_{1A}, R_{1B} are values for the singly bonded covalent radii of atoms A and B; X_A and X_B are electronegativities.

The accuracy of this expression has, however been questioned [2.16]. The agreement between the Pauling method and the Bersohn equation has not been outstanding, partly because of the very approximate nature of the former method. For example, in vinyl chloride, the η method gives π to be 5% but bond length data give 15% [2.14]. A large uncertainty in bond lengths together with extrapolation errors in R_1 and R_2 for atoms other than carbon may be responsible for the discrepancies.

π bonding in a number of chlorobenzenes has been investigated using Bersohn's equation [2.2]. In ortho- and meta-substituted molecules not all the assymetry in the field gradient will be due to π bonding so that Bersohn's equation leads to higher values than is expected. For para-substituted species, equation (46) gives more reliable π values. For example the π character of the C-Cl bond in p-chloroaniline is observed to be less than that in p-dichlorobenzene. This is expected owing to more favourable π bonding in the C-N bond [2.19]. In p-chlorophenol there are two distinct resonance frequencies, one of which has a very high asymmetry parameter. The crystal structure indicates that this could arise from hydrogen bonding to an hydroxyl group. The asymmetry of the other chlorine is low for a similar reason to p-chloroaniline [2.20].

* V. Schomaker and D. P. Stevenson, JACS, (1941), 63, 37.

CHAPTER 3

THE EXPERIMENTAL DETECTION OF NUCLEAR QUADRUPOLE RESONANCE.

3.1 Introduction.

The detection of n.q.r. signals is dependant upon the coupling of the nuclear magnetic moment with a suitably applied rotating magnetic field, H_1. In this respect it resembles detection in nuclear magnetic resonance but the following differences exist:-

1. As indicated in chapter 1, the n.q.r. frequency is determined by the electric field gradient within the crystal, so that a variable frequency detector is necessary. In the case of n.m.r. the oscillator frequency used is determined largely by the magnitude of the applied magnetic field.

2. Spin-lattice relaxation times (T_1) of quadrupolar nuclei tend to be shorter than those of nuclei which possess only a magnetic moment, because of the greater efficiency of quadrupole relaxation processes in comparison with dipolar processes. This means that a higher power is required in order to observe resonance.

3. The degeneracy of the quadrupole spin states causes a net cancellation of the nuclear induction in a direction perpendicular to the axis of the transmitting coil. Therefore crossed coil detection is not possible in zero magnetic field and single coil systems are used (although small magnetic fields remove this degeneracy and crossed coil systems can then be used).

The variable frequency requirement immediately rules out the bridge form of detection used in n.m.r [3.1] since this system is very frequency sensitive. The three usual methods for n.q.r. detection employ

(1) a marginal oscillator,

(2) a super-regenerative oscillator, or

(3) a pulsed r.f. or spin-echo spectrometer.

(The latter, however, is not well suited for frequency searching at the present time).

The marginal oscillator gives good lineshapes and operates over a wide frequency range. A typical detector of this type is described in [3.2]. Super-regenerative detection however tends to have a higher sensitivity and moreover operates well at higher r.f. levels. It also can be swept over a wide frequency range; on the other hand, it gives in general poor lineshapes, and each fundamental is accompanied by a host of sideband responses. This method however has been used most extensively and the majority of the results described in this thesis were obtained using this type of detector. Pulsed methods have also been used and these will be described in Section 3.3. Although sensitive, the frequency range that can be swept before retuning is required, is fairly limited.

In Section 3.2 the Decca N.Q.R. Spectrometer is described, the prototype version of which was used for detecting signals in all the compounds studied. The general principles of the super-regenerative detector are included in this section.

3.2 The Decca NQR Spectrometer.

The Decca spectrometer is based on a design by Smith and Tong [3.3]. It uses conventional super-regenerative detection, and has a number of

refinements:- automatic gain control, sideband elimination and automatic frequency measurement. A block diagram of the spectrometer is given in Figure 3-1. The essential elements will be discussed in order, beginning with the detection system.

(a) The Super-regenerative Detector.

The super-regenerative oscillator (s.r.o.) was the first circuit to be used in the detection of n.q.r. in solids, by Dehmelt and Krüger in 1950 [3.4]. Essentially, it consists of an r.f. oscillator which is periodically turned off at a far lower rate than the oscillator frequency. When turned on again, the oscillations build up either from noise (incoherent mode) or the tail of the preceeding pulse (coherent mode) until they reach their limiting value. The sample is situated in the inductance coil of the tank circuit, and the parameters are adjusted to give operations in the coherent mode. If an input signal due to the exchange of r.f. energy with the sample, appears in the tank circuit of the oscillator at the tuned circuit frequency, then the oscillations build up sooner and the overall area of the r.f. envelope is increased (see Figure 3-2). This increases the level of the oscillator valve anode current, which is then detected, either directly on an oscilloscope or by other means. The rate at which the oscillator is 'quenched' determines the phase relationship between bursts of r.f. and also, in the extreme cases determines whether the oscillator is operating in the linear or logarithmic mode. The former mode requires a rapid quench frequency so that the oscillations never reach their limiting value. In this (the linear) mode the output is a linear function of input. When the oscillations are allowed to limit, with a slower quench frequency, the relationship between input and output is logarithmic, and it is this mode of operation which is useful for n.q.r. detection. If the quench frequency is such that each burst of r.f. dies away completely before the next one starts up, we have

FIG. 3-1 DECCA N.Q.R. SPECTROMETER BLOCK DIAGRAM

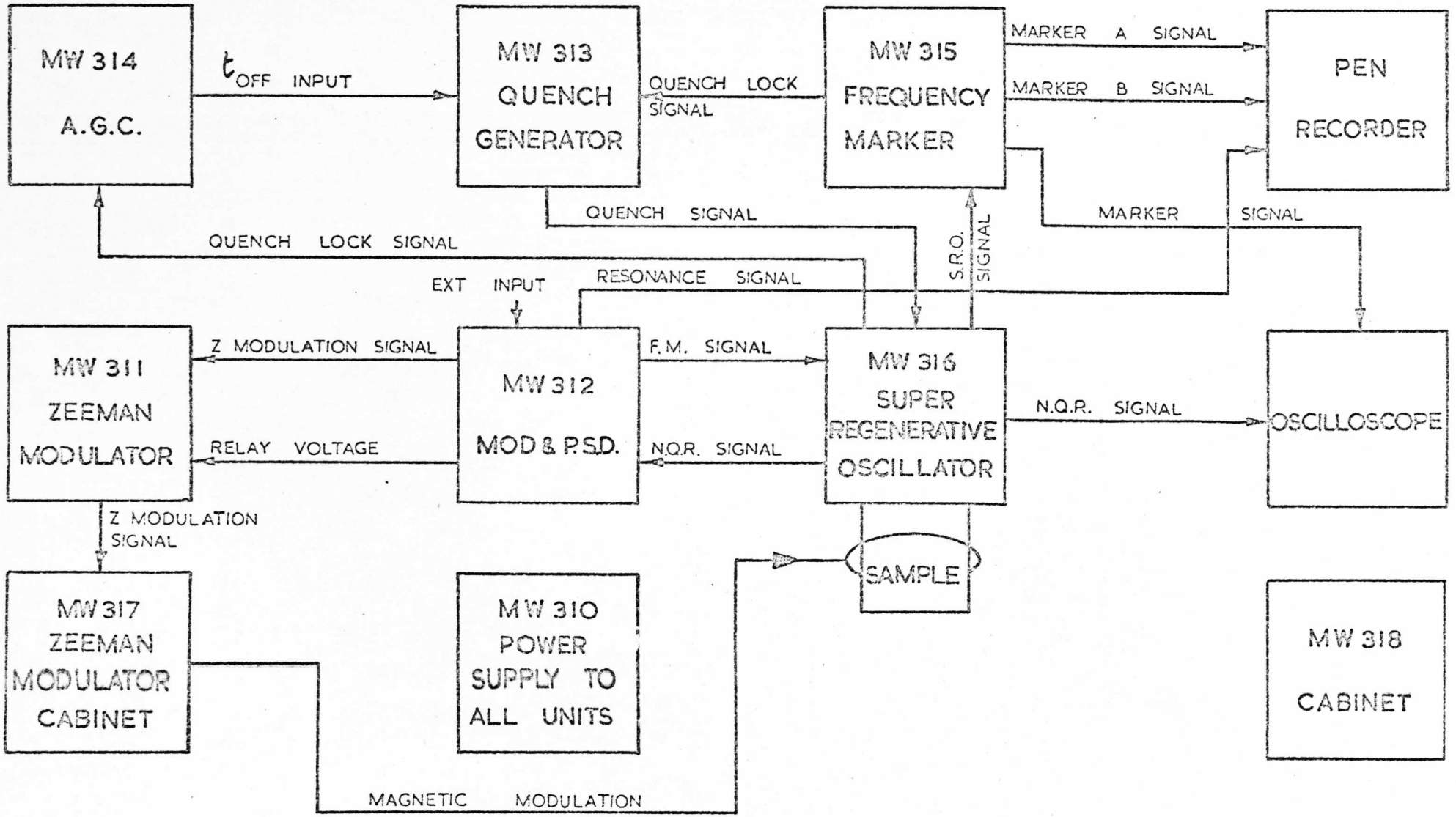

Fig. 3-2 R.F. Envelope of S.R.O.

(a) QUENCH WAVEFORM

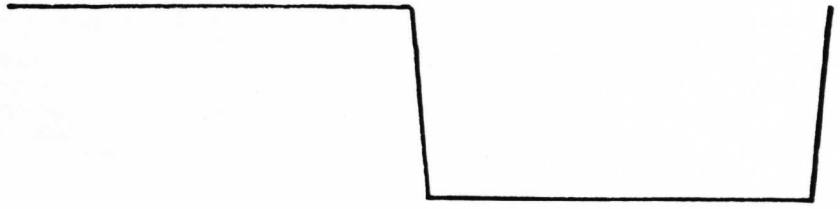

(b) INCOHERENT

Leading edge diffuse since oscillations build up from noise.

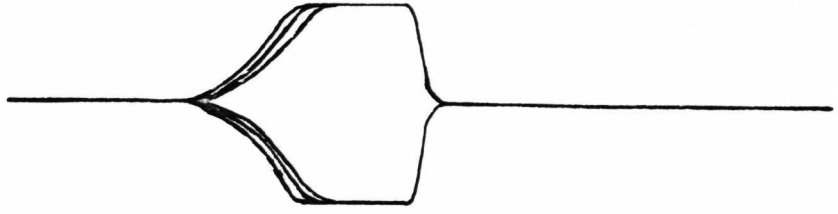

(c) COHERENT

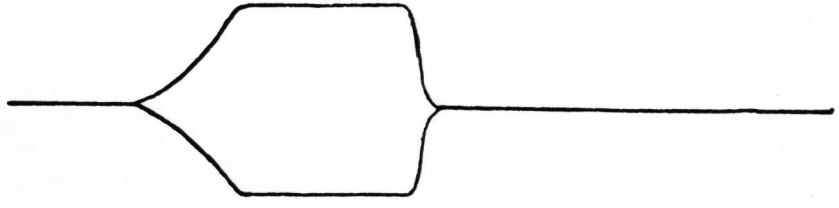

(d) COHERENT and with large input signal.

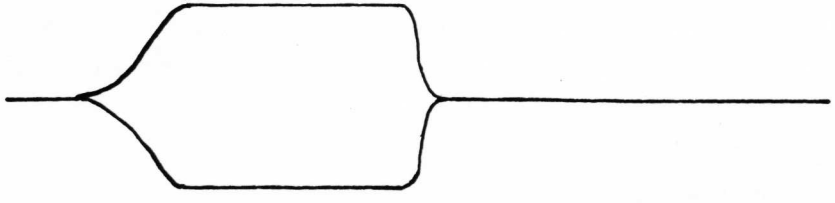

'incoherent' operation (see Figure 3-2b). When the r.f. bursts are allowed to come together, so that each pulse is initiated by the tail of the preceding one, we have 'coherent' operation (Figure 3-2c). Thus by varying the quench frequency, or else t_{OFF}, the time for which the quenching pulse is off, the s.r.o. can be made to have variable coherence. This has a drastic effect on the power spectrum of the oscillator. Since the quenching of the oscillator is an extreme form of amplitude modulation, the power spectrum will contain sidebands separated from the carrier frequency by integral multiples of the quench frequency. Figures 3-3(a),(b)(c) and (d) show the change in power spectrum with varying coherence as t_{OFF} is increased, from the totally coherent condition (Fig. 3-3(a)) to the totally incoherent (Fig. 3-3(d)). The amplitude of the sidebands is obtained by a Fourier analysis of the r.f. envelope shape. Since the rise and fall times of the oscillations are short, the Fourier analysis of the square envelope shape contains mostly odd harmonics, and this results in the odd numbered sidebands being stronger than the even ones. The coherence is important: firstly by decreasing it, the gain of the detector is increased, and secondly, it also changes the line width in the power spectrum. Sensitivity as an n.q.r. detector is increased by decreasing the coherence until the power spectrum line width is comparable with that of the natural line width of the nuclear resonance. Under optimum conditions, even in lines as broad as 5-10 KHz, all the nuclei can be simultaneously excited by an s.r.o. system. The s.r.o. in this respect is superior to the marginal oscillator, where the oscillator line width is less than the width of the resonance line, so that only a proportion of the nuclei are excited. Since the power spectrum of a suitably adjusted s.r.o. will always contain sidebands which are also capable of exciting resonances, a frequency swept spectrum will contain multiple lines for a single n.q.r. signal. However, these sideband responses may be suppressed in the Decca spectrometer (see Section (c)).

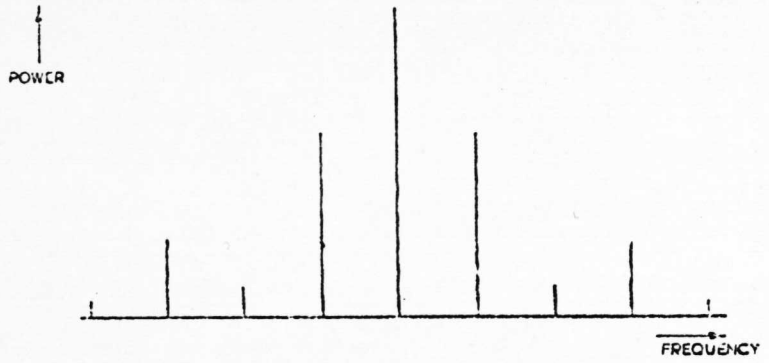

(a)

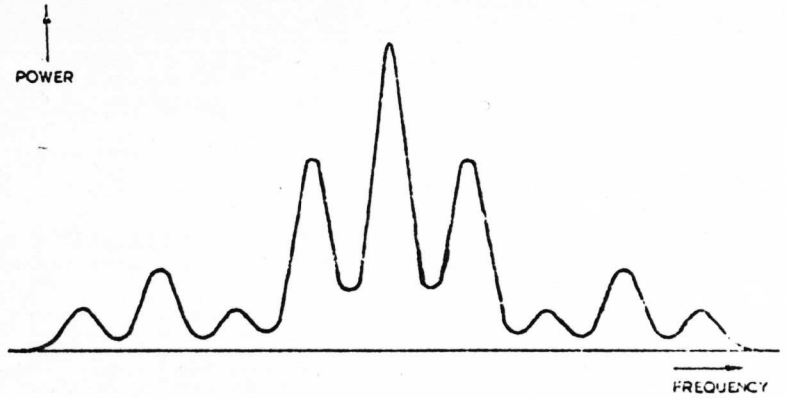

(c)

Fig. 3-3 Changes in Power Spectrum as t_{OFF} is increased.

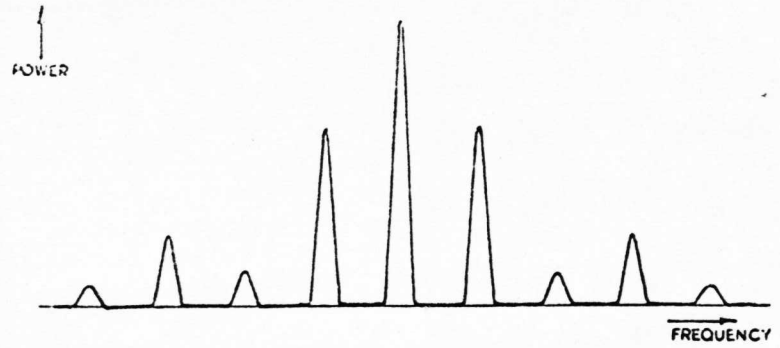

(b)

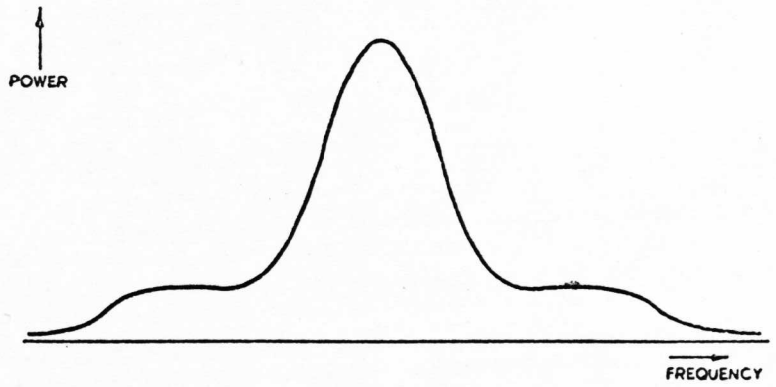

(d)

If the s.r.o. is in the partially coherent mode, suitable for n.q.r. detection, there will be three contributions to the signal immediately following a pulse. These are the residual noise, the tail of the preceeding pulse and the n.q.r. signal. An r.f. pulse will have the phase corresponding to the vector sum of all three, and since this includes a noise term, of random phase, there will be a random change of phase between successive pulses. However, if the magnitude of the noise contribution is small then the phase change will also be small, and will average almost to zero within the overall spin-phase relaxation time, T_2^*, of the nucleus, so that the system will be sufficiently coherent for good sensitivity. In practice the switching of the quench alters slightly the overall capacitance of the tank circuit, which results in a frequency shift, or phase change, as the pulse decays. Since the phase of the tail controls the phase of the next pulse there will consequently be a large phase shift between pulses, which will cause the carrier frequency to vary.

In the Decca spectrometer the effect is compensated for by switching an additional capacitance into the tank circuit when the quench is applied. The capacitance varies according to the phase difference, and takes the form of the centre shift compensation control on the s.r.o. unit. It is adjusted manually for minimum movement of the nearest fundamental frequency marker when viewed on an oscilloscope.

The quality of the n.q.r. signal will depend, apart from molecular parameters, on the filling factor and 'Q' factor of the tank circuit induction coil. These are optimised by using a thin-walled sample tube which is tightly packed with the polycrystalline sample, and also by using an inductance coil which closely fits the sample tube. In fact when signals are weak, a sample of larger than average size is sometimes used, together with a custom-built coil of as high a Q factor as possible.

(b) Automatic Gain Control.

The gain of the super-regenerative detector depends exponentially on the quench frequency and the total capacitance of the oscillator tank circuit. The carrier frequency of the oscillator is determined by

$$f_o = \frac{1}{2\pi\sqrt{LC}}$$

where L and C are the inductance (in Henries) and capacitance (in Farads) of the tank circuit respectively, so that for a frequency swept oscillator C will change, drastically affecting the gain. In the Decca spectrometer, a system for controlling the gain is incorporated, which keeps the noise output at a constant level. After detection, noise from the output is filtered using suitable time constants to eliminate any components of modulation, < 2 KHz, and quench frequency, > 7 KHz, and the resulting narrow band is amplified and rectified to provide a d.c. level. This is compared with a reference level in a differential amplifier, and the result is fed back to the quench pulse generator to control t_{OFF}. The gain may also be changed by alteration of the effective damping of the oscillator which is a function of G_o, the effective conductance in parallel with the tank circuit during the off-period. A similar feedback loop is used to control G_o, should insufficient gain control result from controlling t_{OFF}. If the noise output is too low, then the feedback loop will increase t_{OFF} until the noise level rises. If for some reason this does not happen, eg. the probe coil is not connected or the manual coherence control is incorrectly set, then t_{OFF} rises until the oscillator is stopped and a warning lamp indicates this. The a.g.c. system is able to control the gain for most of the range of any particular probe coil, i.e. in a frequency range of 2:1.

(c) Sideband Suppression.

The quenching system for the s.r.o. is derived from a pulse generator which can provide quench pulses, of variable duration, t_{OFF} at a repetition rate in the range 7 to 40 kHz. In addition the quench frequency may be stabilised by locking to a suitable crystal in the marker unit, providing locked quench frequencies of 10, 25 and 50 kHz. The final spectrum would then be expected to contain sidebands produced at multiples of 10, 25 and 50 kHz. These sidebands can be removed by the method suggested by Dean and Pollack [3.5], in which the quench frequency is modulated at a rate which is fast in comparison with the time constant of the detector, but slow compared with the modulation frequency. In this way sidebands become smeared out and disappear into the noise. The Decca spectrometer uses a modulation frequency of 50 Hz, and an overall recording time constant of up to 10 sec, so that a convenient quench modulation frequency is 1 Hz. Since the coherence is affected by changes in t_{OFF}, the latter must be kept constant (within 2%) when sideband suppression is used, so that only t_{ON} varies at the 1 Hz rate. The quench frequency is set to vary steadily from 10 kHz to $\sim$ 25 kHz. for most frequency ranges. For lower frequency searches, the upper limit may need to be reduced, to comply with the approximate rule that t_{ON} should equal t_{OFF} for good sensitivity.

(d) Frequency Sweep and Modulation.

In order to record a signal on the chart recorder the carrier frequency is slowly swept through the resonance. This is done using a variable capacitor, C in the oscillator tank circuit which has a linear change of capacitance with $\frac{1}{\theta^2}$. In this way an approximately linear frequency sweep is obtained. The drive is provided by a variable geared synchronous motor, via magnetic clutch which allows for manual setting of the capacitor before commencing the slow sweep. In the prototype version of the instrument

used in this laboratory, considerable backlash is present between motor and capacitor, which is taken up using the fastest motor sweep before starting the run on the selected sweep range. The motor is reversible so that the resonance may be swept through in either direction.

As an alternative, strong resonances may be displayed on an oscilloscope, in which case the capacitor sweep is provided by a ramp voltage taken from an external time base on the oscilloscope to a varactor diode in the oscillator. This diode acts as a voltage-dependent capacitor and provides sufficient change in capacitance for a sweep of approximately 50 kHz of the oscillator frequency.

In Section (b) it was indicated that the width of the quench pulse, t_{OFF} will change as the oscillator frequency is swept. Therefore the voltage output will be changing which will result in a slow drift in the output as the frequency is changed. The n.q.r. signal is comparatively weak and is extracted from this drift, and from the noise, by the use of modulation and phase sensitive detection. The modulation has the effect of introducing an amplitude-modulated component into the s.r.o. output when the frequency is close to that of the line. The phase-sensitive detector is then used to extract the a.m. part of the signal, by comparison with the reference modulation. Basically the p.s.d. consists of two bridges each of which is switched in and out of circuit by positive and negative going pulses from the square-wave referance modulation. When the a.m.-modulated signal is in phase with the reference, the positive part of the a.c. component will be allowed through one bridge and the negative part through the other. Any discrepancy in phase between the signal and references causes a net cancellation and a reduced signal appears at the output of the p.s.d.

The overall band width of the detector is controlled by the value of capacitance placed across the output (between the positive terminal and earth, and the negative terminal and earth). Time constants of 0.1, 0.3,

1,3, and 10 seconds are included in the p.s.d. unit, but it was found beneficial when searching for very weak signals to use an additional time constant unit with a unity gain amplifier which provided double section filtering and time constants up to 30 seconds, giving a significant signal to noise improvement on overnight runs. Dr A. Royston provided the circuit for this unit.

The three types of modulation used are frequency modulation, of both symmetric (F.M.1) and bisymmetric (F.M.2) square waveform, and Zeeman modulation. In the first of these, the fundamental oscillator frequency is made to vary by a small amount at a rate equal to the modulation frequency. As the oscillator frequency approaches that of an n.q.r. absorption line, then the modulation will create an a.m. component in the s.r.o. output, the amplitude of which will be proportional to the gradient of that part of the line swept by the modulation (see Figure 3-4). The lineshape recorded from this square-wave modulation is therefore a first derivative. In a similar way, bisymmetric square wave frequency modulation produces an output proportional to differences of gradient so that a second derivative lineshape is recorded (Figure 3-5). In both cases, the lineshape will however broaden with the depth of modulation (the extent of the change in frequency).

With Zeeman modulation a fixed magnetic field of up to 200 gauss is periodically applied to the sample at a modulation frequency of 50 Hz., during which the signal is erased by the broadening of the many Zeeman splittings caused by the magnetic field. A large coil surrounding the sample is supplied with a bisymmetric waveform to provide the modulating field. In this case the amplitude of the a.m. component is proportional only to the height of the absorption so as the line is swept, the absorption curve should be reproduced (see Figure 3-6). However the response of the oscillator rarely gives a pure absorption curve, which may be a mixture of first and second derivatives, so the lineshape as normally detected has no

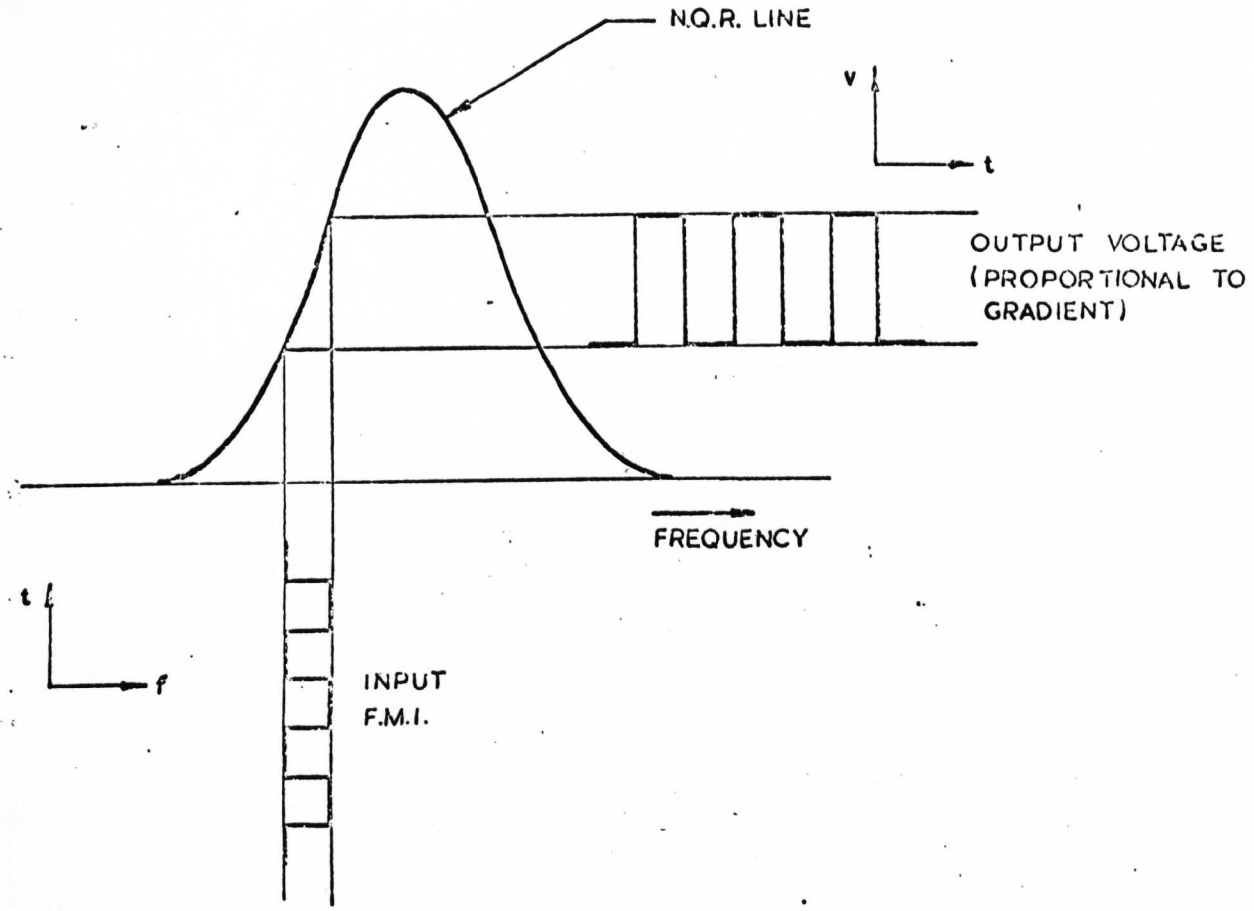

FIG . 3-4a. RESPONSE TO F.M.I.

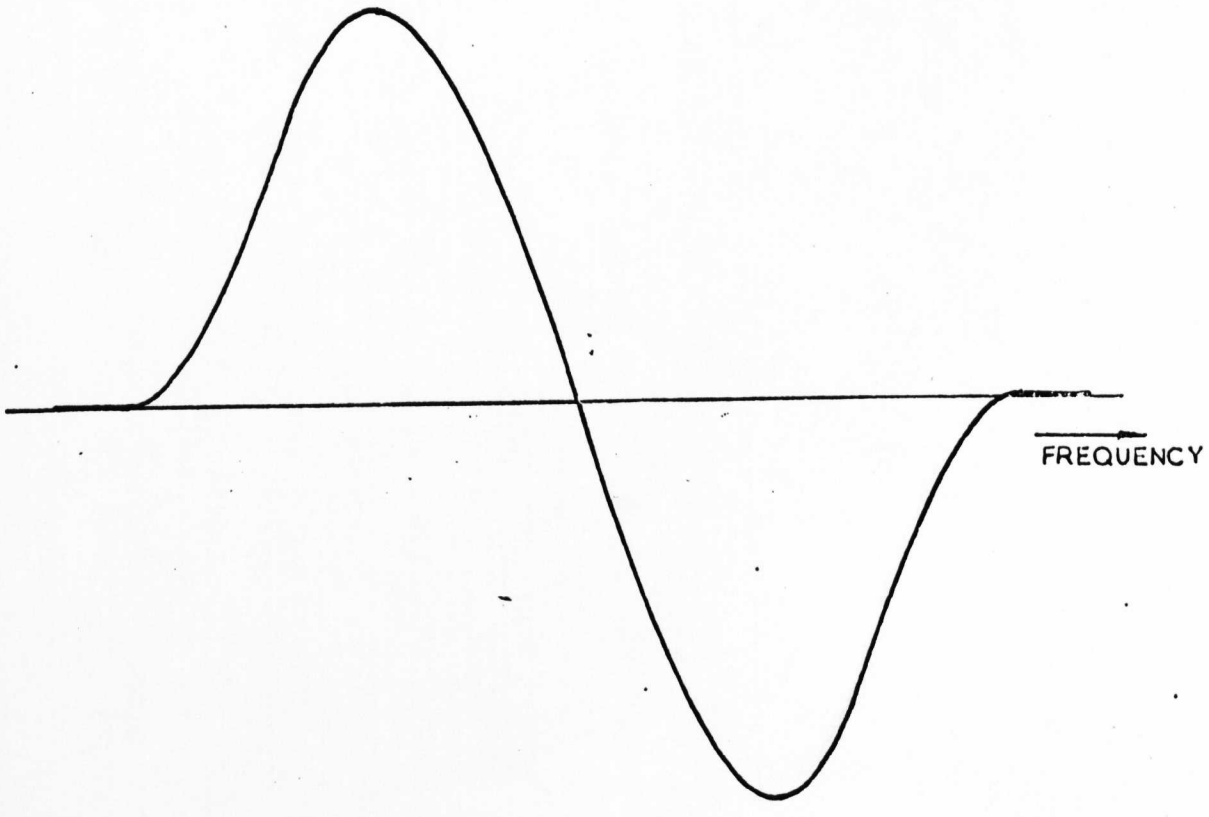

FIG. 3-4b. LINE SHAPE WITH NARROW F.M.I.

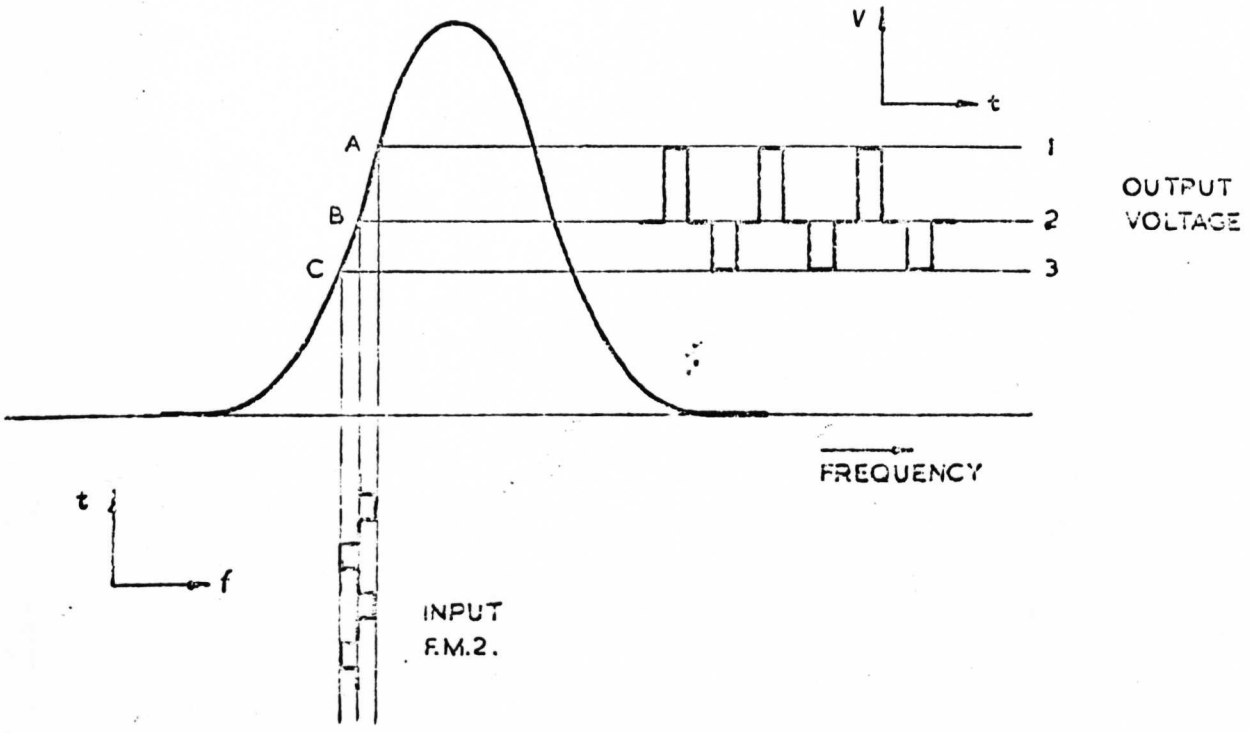

FIG. 3-5a. RESPONSE TO F.M.2.

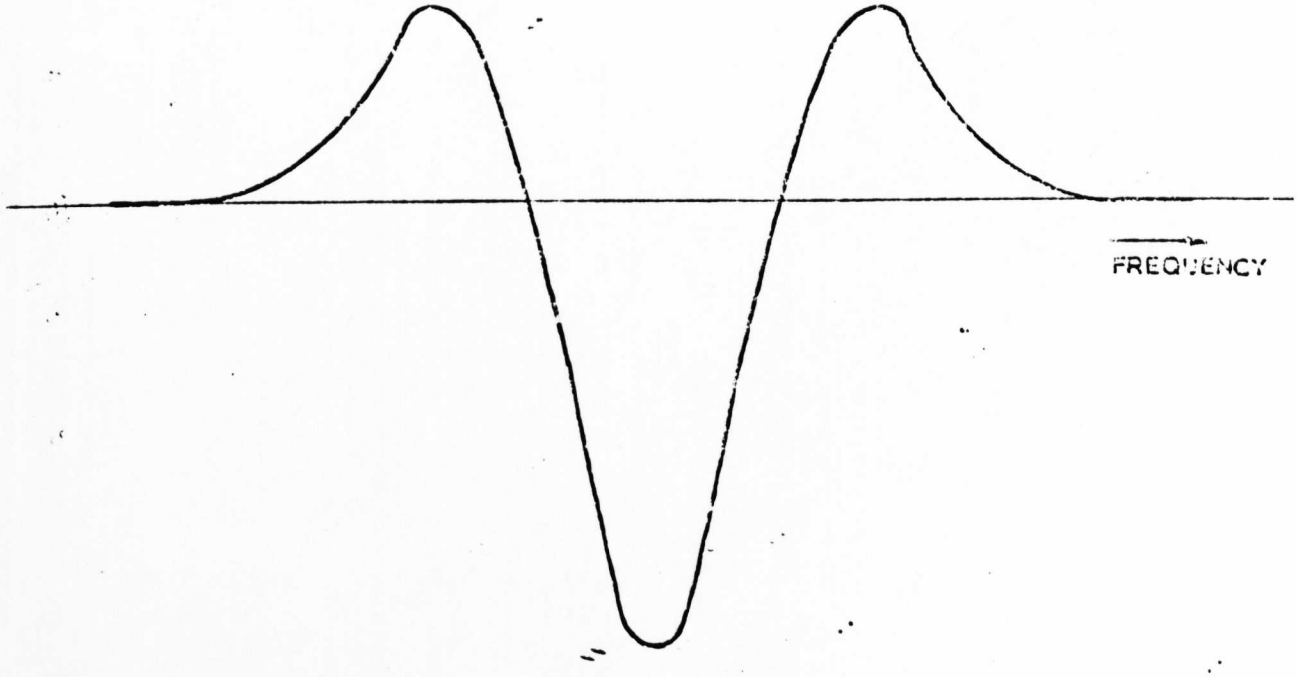

FIG. 3-5b. LINE SHAPE DIFFERENTIATED TWICE

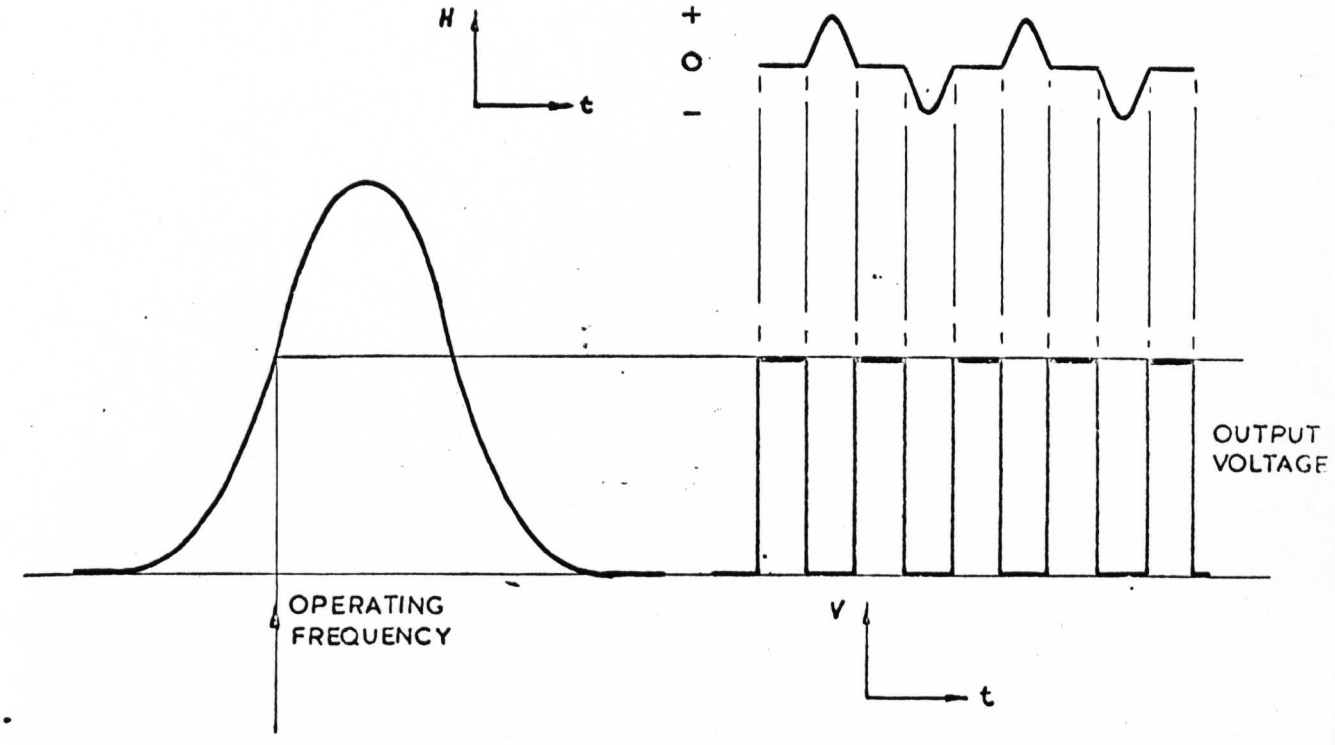

FIG. 3-6a. RESPONSE TO ZEEMAN MODULATION

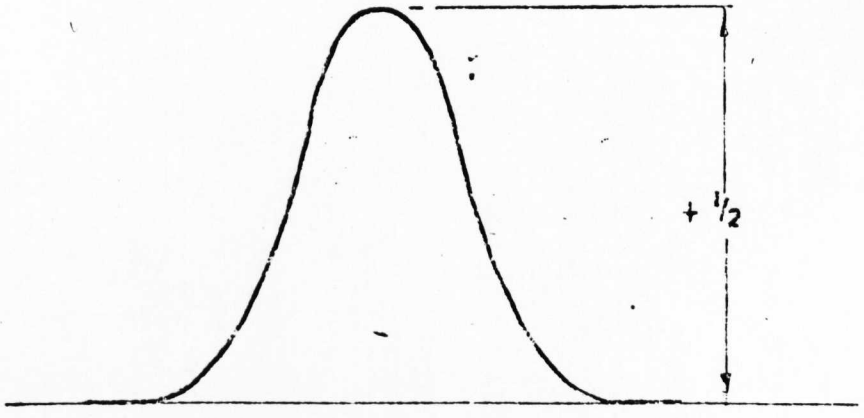

FIG. 3-6b. RECORDED LINE WITH ZEEMAN MODULATION

simple structure. Practically all of the spectra discussed in the following Chapters were recorded using Zeeman modulation, mainly for the reason that the use of frequency modulation gives rise to many spurious responses from sources such as strong radio stations, instrumental resonances e.g. from the oscillator valve itself, and also piezoelectric responses which may occur with non-centrosymmetric crystals. For best use of f.m. the modulation depth should be comparable with the line width, but this is usually unknown for initial searches.

Because of the complex lineshapes, it is sometimes difficult to assign the number of lines and the line centres to a spectrum where splittings are very small and lines overlap. To assist in assignment a computer program (from Dr J. Royston) has been used in which singlet lineshapes are simulated using different combinations of first and second derivatives of a pure Gaussian lineshape. The best combination for a singlet, chosen by comparison with experimental lineshapes is then used for more than one line at various line centres. The resulting graphical output is compared with the experimental lineshape and in favourable cases the number of lines and their line centres may be determined in this way. A comparison of a simulated spectrum with the corresponding experimentally determined one is shown in Figure 3-7.

(e) Frequency Measurement.

The measurement of frequency of a super-regenerative oscillator detecting system is not as straight forward as with the marginal oscillator, in which a sample of the output may be monitored by a digital frequency meter. Such a method cannot be used for a s.r.o. because of direct interference from the quench frequency. A possible method is to introduce a known frequency at a low level, from a frequency generator, into the oscillator tank circuit. This causes a spike to appear on the recorded output at

TEXT BOUND INTO

THE SPINE

Fig. 3-7 Lineshape Comparison of an observed Doublet from $(CCl_3COO)_2HK$ with a Computer Simulation.

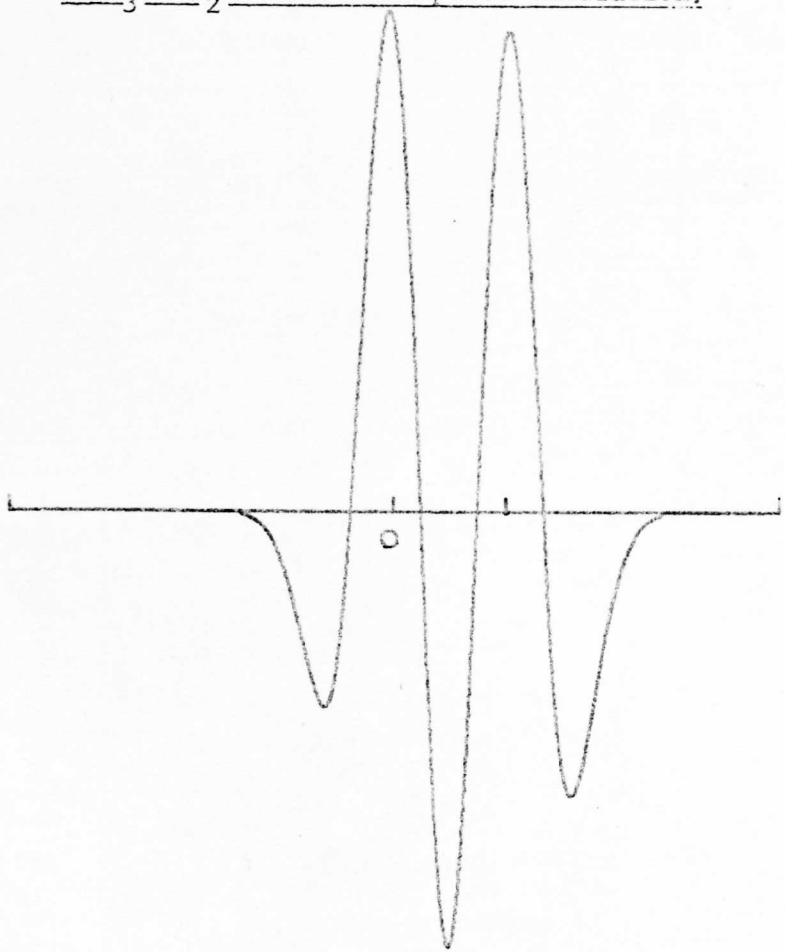

Obtained from the combination of two singlet lines each synthesised from 30% Gaussian 1st derivative and 70% 2nd derivative.

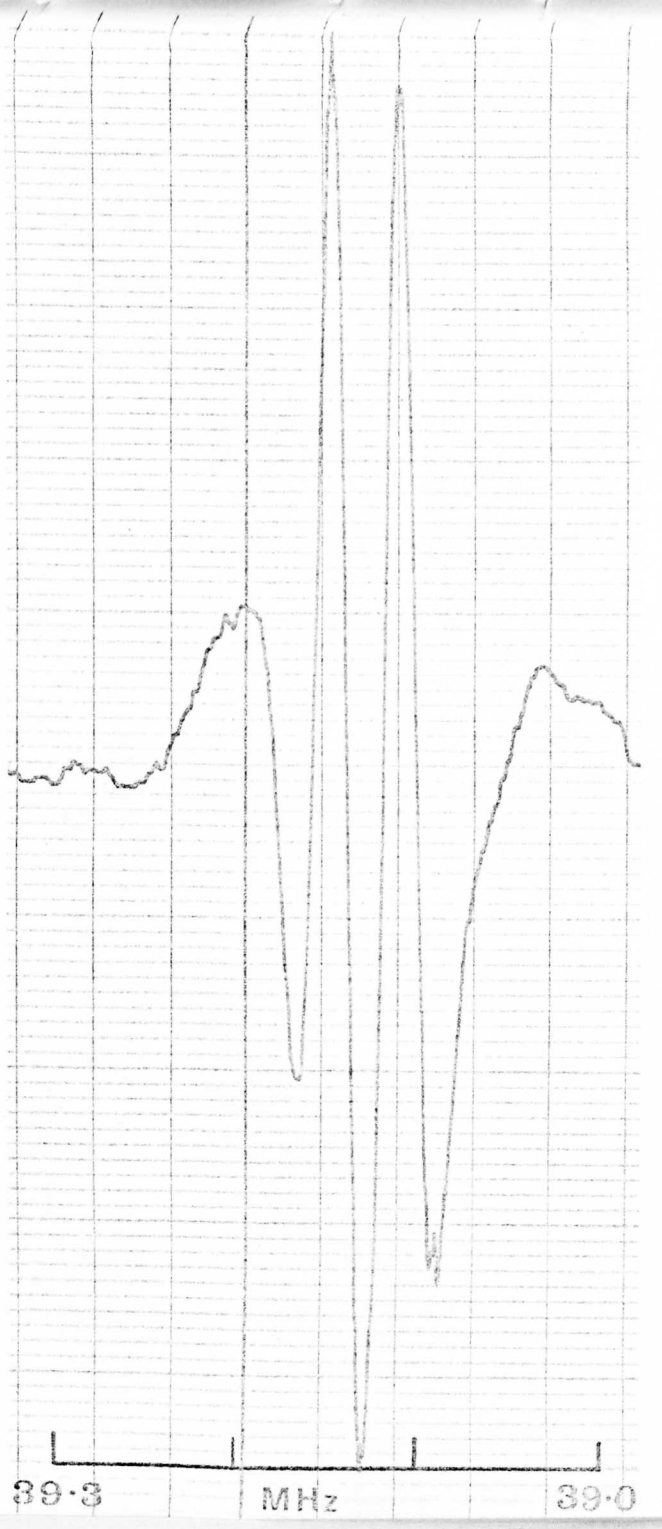

the appropriate frequency. However, since the added signal will be detected in precisely the same way as a true n.q.r. signal, sidebands of the marker frequency will also be recorded, and may lead to confusion of the true marker position.

Sideband suppression does overcome this, but this method does have the disadvantage that the signal itself may be distorted by the extra peak, which may not be recorded as a sharp spike because of broadening by the long time constants used for the detection. In addition the method is time-consuming and tedious.

The Decca spectrometer is equipped with an automatic marking system which does not disturb the n.q.r. spectra in any way. Calibration marks are made along the edge of the chart so that frequencies of the line centres may be read directly from the chart. The method used is to feed a sample of the r.f. voltage from the s.r.o. tank circuit into a diode mixer which is also fed with a set of harmonics of a standard frequency. When the spectrometer frequency sweeps through that of one of the harmonics, an audio beat frequency is fed out of the mixer. This is filtered and amplified and used to operate an event marker recording on the edge of the chart. During the sweep, approaching harmonics may be heard on a loudspeaker which monitors the audio output. When sideband suppression is not in use, sidebands will also cause markers to appear. The system is simplified by using the same standard frequencies to drive the quench generator as well as the marker unit. Then the sidebands of one harmonic will coincide with other sidebands of the next harmonic. The marker unit in the prototype instrument used here was capable of providing calibration marks at intervals of 10, 25, 50 and 100 kHz. An additional marker unit has since been added; similar to that in the normal production version of the instrument, which produces markers at larger intervals of 100, 250, 500kHz

and 1 MHz. When two marker channels are used the spectrometer frequency need only be known to the nearest MHz. for full calibration of the spectrum. This is easily done using a radio receiver which need not be accurately calibrated. For most of the spectra recorded on the prototype instrument only one marker channel was available so that each run was calibrated at its beginning (after the backlash in the drive linkage was taken up) and its end. This was carried out using an Eddystone radio receiver, which contained built-in crystal calibration. The radio was easily able to pick up the characteristic audio signal of the marker beat notes and could be tuned to the fundamental by ear, listening for an unmodulated component, as the sideband suppression caused the audio signal of the marker sidebands to fluctuate.

Frequencies were checked using a frequency meter (J.A.C. Electronics Ltd model 331) to generate the same frequency which was detected on the radio. All the frequency markers in the spectrum were then calibrated by interpolation. For long searches, 100 kHz is a convenient range to use for markers, in which case the frequency may be read easily within 10 kHz. Using markers at smaller intervals on slower scans gives an accuracy in favourable cases of 1 kHz. An example of a calibrated spectrum is shown in Figure 3-8.

(f) Variable Temperature Operation.

The probe unit for variable temperature operation is provided with low thermal conductivity but high electric conductivity connections (German silver) to the rest of the spectrometer, and consists of a copper screw-topped can which acts as an r.f. screen for the tank circuit inductance containing the sample. For operation at liquid nitrogen temperature, the probe unit is immersed in the coolant contained in a Dewar vessel which fits inside the Zeeman modulation coils of the instrument. For safety

FIG. 3-8 CALIBRATED ^{35}Cl N.Q.R. SPECTRUM OF $trans\text{-}(PEt_3)_2ReCl_4$ AT 293 K.

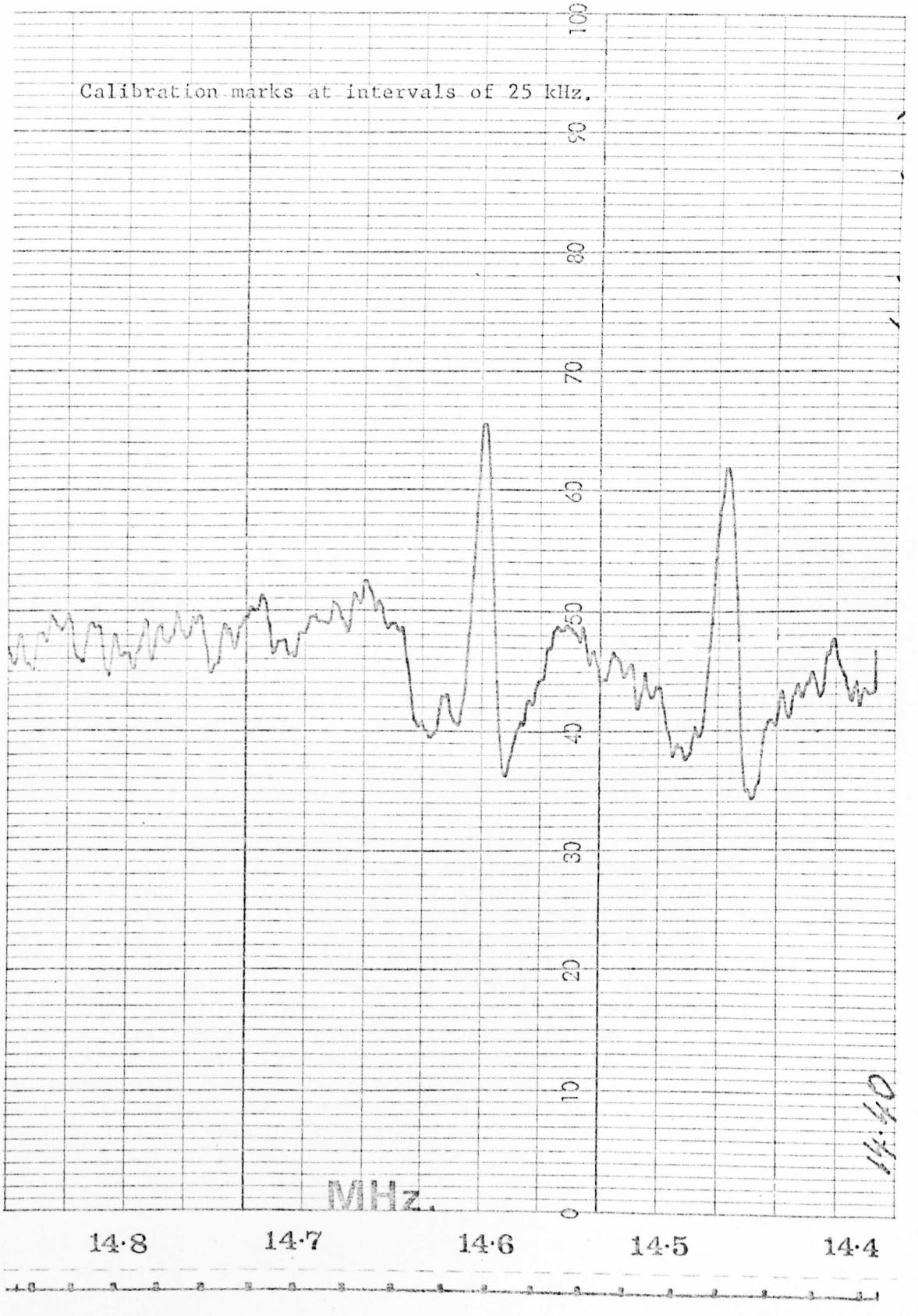

reasons it is important that liquid oxygen is prevented from condensing inside the probe can, so liquid nitrogen is allowed to enter through an aperture in the top of the probe. Alternatively the probe may be sealed, including any opening inside the coaxial German silver connections. Provided that the coil is firmly mounted the presence of nitrogen in the probe appears to have no adverse effect. A badly mounted coil may vibrate in the boiling refrigerant and introduce additional noise through microphonics. The probe is of course sealed when used with other coolants.

Approximate temperature coefficients are derived from the change in frequency from liquid nitrogen to room or ice temperature. For a more exact study of the temperature dependence of the n.q.r. frequency, it is necessary to record spectra at a range of temperatures, especially in cases where lines are not detectable continuously from 77 K to room temperature. This is done either by using slush baths at a variety of temperatures, or more expediently, by allowing the probe assembly to warm up slowly to 77 K while the resonance is repeatedly scanned. In the latter dynamic method, there will be a slight discrepancy in temperature between that recorded by a thermocouple attached to the probe assembly and the actual sample temperature. The temperature lag has been determined by performing this experiment on the ^{35}Cl resonance in potassium chlorate, for which the temperature dependence is known, [3.6]. For a warm-up rate of 0.5 K per minute, the average difference between the sample temperature and that of the probe can was only 1 K. If the frequency is to be measured to an accuracy of 5kHz then this degree of error in temperature is acceptable, since an average value for a temperature coefficient is 5 kHz/K. It was found that the warm-up rate could be varied by adjustment of the amount of liquid nitrogen remaining in the base of the Dewar vessel.

The temperature is monitored using a copper/constantan thermocouple placed as close to the sample as possible, i.e. attached to part of the

sample tube protruding from the r.f. coil. Even in this position the thermocouple voltage was considerably modulated by the quench modulation, until copper braid screening was used for the thermocouple. In this arrangement the point of temperature measurement is quite close to the sample so the temperature lag should be less than 1 K which was measured from a thermocouple attached to the can.

The thermocouple is used in conjunction with a Comark 165 CL electronic thermometer. This device uses a reference junction at ambient temperature and changes in this are compensated for by a manual adjustment. The instrument gives a direct reading of temperature for the range -200°C to + 30°C, at an accuracy of $\pm$ 0.5°C, which is within that required.

Spectra were also recorded at one or two fixed temperatures, such as solid carbon dioxide/isopropanol (195 K), liquid nitrogen/isopentane (112.7 K), or liquid nitrogen/isoamyl/alcohol (156.0 K) slush baths. The results showed that any temperature lag was small and that line widths did not appear to be increased by the warm-up method, as might be expected from the existence of a temperature gradient across the sample.

In some samples, spectra were recorded at temperatures higher than ambient. In these cases a similar technique was employed, using hot oil in the Dewar vessel. Frequencies were measured as the probe cooled from $\sim$ 60°C to ambient temperature.

3.3 Detection by R.F. Pulse Methods and Measurement of Relaxation Times.

The use of pulsed methods for the detection of n.q.r. is not a new technique; in fact the first experiments were carried out in 1954 [3.7]. It has not been as widely adopted as the super-regenerative detection system, due largely to the more complex circuitry, high r.f. powers and short recovery times required. However, the amount of information obtainable is greater; for example nuclear relaxation times can be studied by this method.

The resonance principle is analogous to that of n.m.r., except that instead of the nuclear magnetic moments changing their orientation in an external magnetic field, the nuclei now change their orientation with respect to the direction of the principal component of the electric field gradient in the crystal, defined in chapter 1 as the z axis. In a polycrystalline sample the z axes of the e.f.g. tensor will lie in all possible directions with respect to the coil so that there will always be a proportion of crystallites so arranged in the sample that their z axes coincide with a particular direction in the laboratory frame of reference. This direction we shall call the 'z direction'and it may be compared to the direction of H_o, the applied magnetic field in the n.m.r. experiment. In the latter, the nuclei will precess about the H_o direction at a rate of γH_o, where γ is the gyromagnetic ratio of nucleus; in quadrupole resonance, we may assume that nuclear precession occurs at the n.q.r. frequency specified in chapter 1 (e.g. $\nu_Q = \frac{e^2Qq}{2h}$ for nuclei of spin $^3/2$). If an intense radiofrequency field H_1 is switched on, the nuclei (in both cases) will also precess about the H_1 direction at a rate of γH_1. If this field is applied at right angles to H_o, say along the x axis in a rectangular coordinate system, xyz, then the new rotation will be in the yz plane. For n.q.r. of polycrystalline samples, there is no directional requirement of the r.f. field since the choice of a laboratory frame 'z direction' is arbitrary. The length of time for which H_1 is switched on controls the amount of rotation of the macroscopic nuclear moment, M. Two periods are commonly used:

(1) The length of time in which M travels through 90^o, at right angles to H_o, or the z direction, and (2) the length of time in which M travels through 180^o, to a position antiparallel with H_o, or the -z direction. R.f. pulses corresponding to (1) and (2) are normally referred to as 90^o and 180^o pulses. When the r.f. pulse is switched off, M continues its precession about z (or H_o) but then a number of relaxation effects become

apparent. Suppose that M has been turned into the y direction by a 90^{o} pulse (applied along the x direction) then the magnitude of M will be diminished by two separate effects:

(1) The return of M to the z direction, in the yz plane and

(2) The dispersal of components of M in the xy plane, ie. the plane perpendicular to H_o or the z axis.

The process described in (1) is found to be governed by a single rate constant when only two nuclear energy levels exist, as in the case of spin $^{3}/2$. The rate of return to equilibrium is given by the Bloch equation [3.8].

$$\frac{dM_z}{dt} = -\frac{(M_z - M_o)}{T_1}$$

The rate constant, T_1 is described as the spin-lattice relaxation time, since the return of M to the z direction is dependant upon energy exchanges between the nuclear spin system and the thermal energy bath of the lattice. M_o is the original magnitude of M and M_z is the component in the z direction.

Two different relaxation effects contribute to the process described in (2) above:

(a) A macroscopic sample will have nuclei in a distribution of electric field gradients, so that their precession rates about z will not be identical. In our frame of reference, xyz, which can be considered to be rotating at the average n.q.r. frequency, the non-equivalence of nuclear sites will cause a fanning out of the contributions to M in the xy plane.

(b) Internuclear interactions also occur in which the magnetic moments of neighbouring nuclei cause fluctuations in the precessional frequencies and so a similar fanning-out process occurs. In liquid-state

n.m.r. the rate equations for this process are simply [3.8].

$$\frac{dM_x}{dt} = \frac{-M_x}{T_2} \qquad \frac{dM_y}{dt} = \frac{-M_y}{T_2}$$

The rate constant, T_2 is called the spin-spin or transverse relaxation time, or alternatively the spin-phase memory time, since a frequency fluctuation is equivalent to a fluctuation in phase. Unfortunately, in solids, transverse decays are rarely if ever truly exponential.

The difference between the two effects in (a) and (b) is that the process described in (a) takes place at a fixed function of time, ie. it is reversible, whereas in (b) the spin-spin interactions are random in nature and are therefore irreversible. This difference is demonstrated by a particular pulsed r.f. experiment. If a 90^o pulse is followed after an interval τ by a 180^o pulse, then the magnetisation vector M is first turned through 90^o into (say) the y direction (Figure 3-9(b)). The transverse components of M immediately begin to fan out (Figure 3-9(d)) during time τ. The 180^o pulse then causes a complete reversal of the spin system and after a further time τ the components of M coalesce to give again a magnetisation in the y direction (Figure 3-9(f)). The magnetisation in this direction induces a current in the receiver coil, and this 'spin-echo' is detected by the spectrometer. Of course only the reversible part of the relaxation process, 2(a) above, is detected in the spin echo, so that if further 180^o echo producing pulses are applied, the spin echo amplitude gradually decreases, at a rate governed by T_2. This procedure forms the basis of the Carr-Purcell pulse sequence for T_2 measurement [3.9]. The reversible processes are usually dominant in determining the transverse relaxation of M, and the decay of signal following a 90^o pulse is often quite rapid in n.q.r., as it is in broad-line n.m.r. in solids. The rate constant for this (the 2(a)) process is

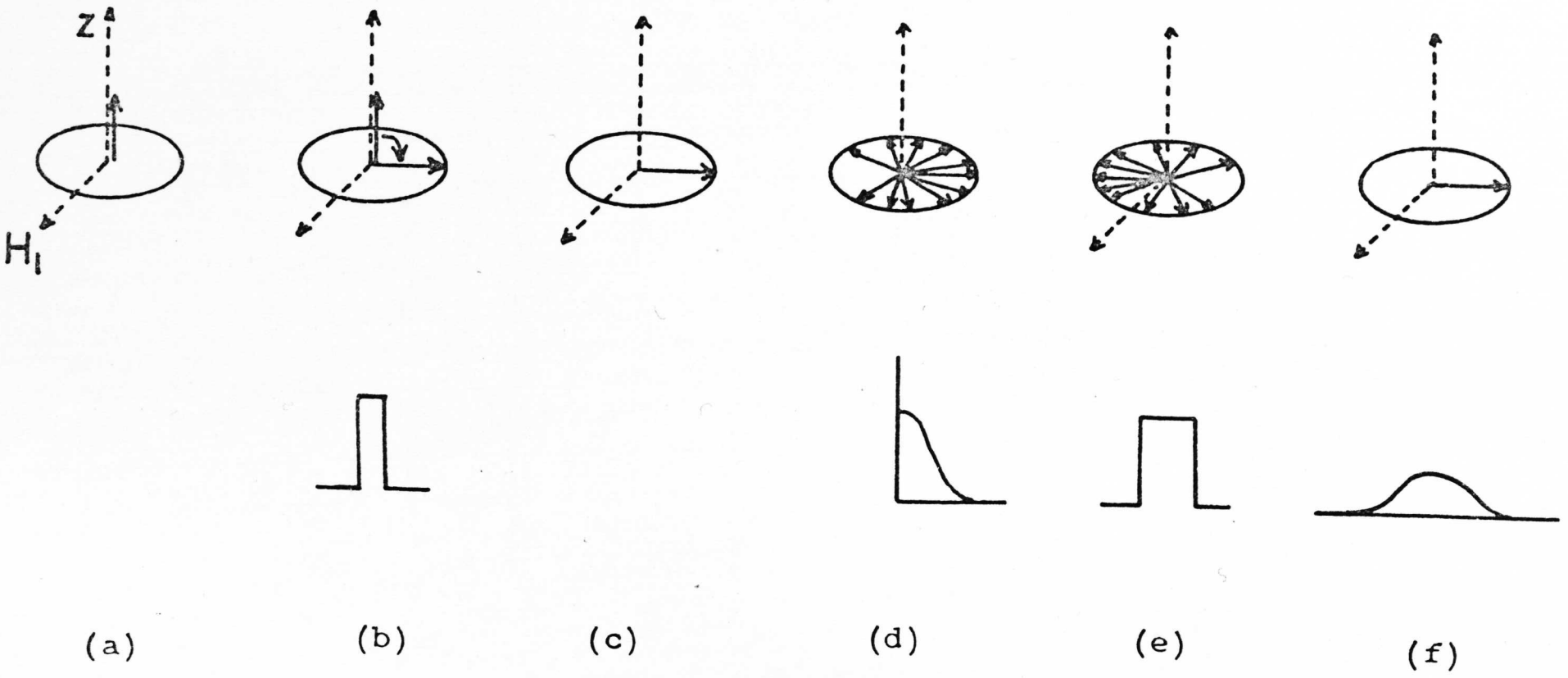

Fig.3-9 Magnetization vectors (upper line) and pulse responses (lower line) in pulsed experiments.

called T_2^*, the inverse line-width parameter. The short T_2^* values are therefore a reflection of the broad lines that are characteristic of n.q.r.

The spin-lattice relaxation time, T_1, is determined by a pulse sequence such as 180-τ-90 or 90-τ-90. The initial pulse turns M into the -z direction, (or if the second pulse sequence is used, into the y direction). The purpose of this pulse is to remove the magnetisation from the z direction.

After an interval, τ, an 'inspection' 90^o pulse is applied and the free induction decay signal which immediately follows it will be a measure of the magnetisation that has returned to the z direction. As τ is increased the free induction decay following the second pulse will follow the value of M_z. For the 180-τ-90 sequence the signal will initially decrease as M_z decays from a negative value to zero, and then it will build up as M_z returns to its initial positive value. The 90-τ-90 sequence excludes the decreasing signal part of the experiment. A further refinement is to follow the second pulse by a 180^o pulse to produce an echo, the amplitude of which is taken as the measure of M_z. These pulse sequences form the basis of spin-lattice relaxation time measurements. T_1 is obtained directly from the expression for M(t), the height of the free induction decay signal or echo

$$M(t) = M(o)\ [1-2\ \exp(-\tau/T_1)]$$

where M(o) is the height of the signal produced with a single 90^o pulse.

Signal detection in a new sample is usually carried out using a single pulse of length approximately 90^o. An exact 90^o pulse is set up by observing the f.i.d. on the oscilloscope adjusting the pulse width for maximum amplitude following the pulse. However an approximate setting is usually sufficient for initial signal detection. After instrumental tuning, the frequency is slowly adjusted until a signal appears on the

oscilloscope. Searching for a signal is more difficult than for magnetic resonance where the frequency range of any particular nucleus is relatively narrow and can be predicted from the value of γH_o. In addition, searching over a wide range is tedious because constant retuning is necessary to maintain sensitivity as the frequency is swept.

Details of the spectrometer used in this laboratory for the detection of n.q.r. are given in the next section. The treatment of results is discussed in chapter 4.

3.4 The Bruker B-KR-322S Pulsed NMR Spectrometer.

The spectrometer is a variable frequency instrument of range 4-62 MHz. This partially covers the range for ^{14}N quadrupole resonance but is particularly suitable for ^{35}Cl and ^{37}Cl n.q.r. The spectrometer may be used for the detection of broad-line n.m.r. or n.q.r. and only differs from a standard n.m.r. spectrometer in the construction of the probe unit. The dimensions of the interchangeable transmitter/receiver coils have been made compatible with those of the Decca probe unit for ease of sample handling and to preserve a maximum filling factor. This compatibility is important when samples are required to be sealed in ampules. A block diagram of the instrument is given in Figure 3-10. An outline of the function of the important sections will be described in their natural sequence.

(a) The Frequency Synthesiser.

The operating frequency of the spectrometer is produced by the frequency synthesiser, in this case a Schlumberger FSX 3000 unit. The desired frequency is obtained from a combination of the frequency elements derived from multiplication and division of the basic 1MHz. frequency produced by a quartz oscillator. In this way frequencies of up to 100MHz may be generated, crystal locked at intervals of 1kHz. Using harmonics even higher frequencies are attainable but these are of no use

Text cut off in original

FIG. 3-10 BLOCK DIAGRAM PULSE SPECTROMETER

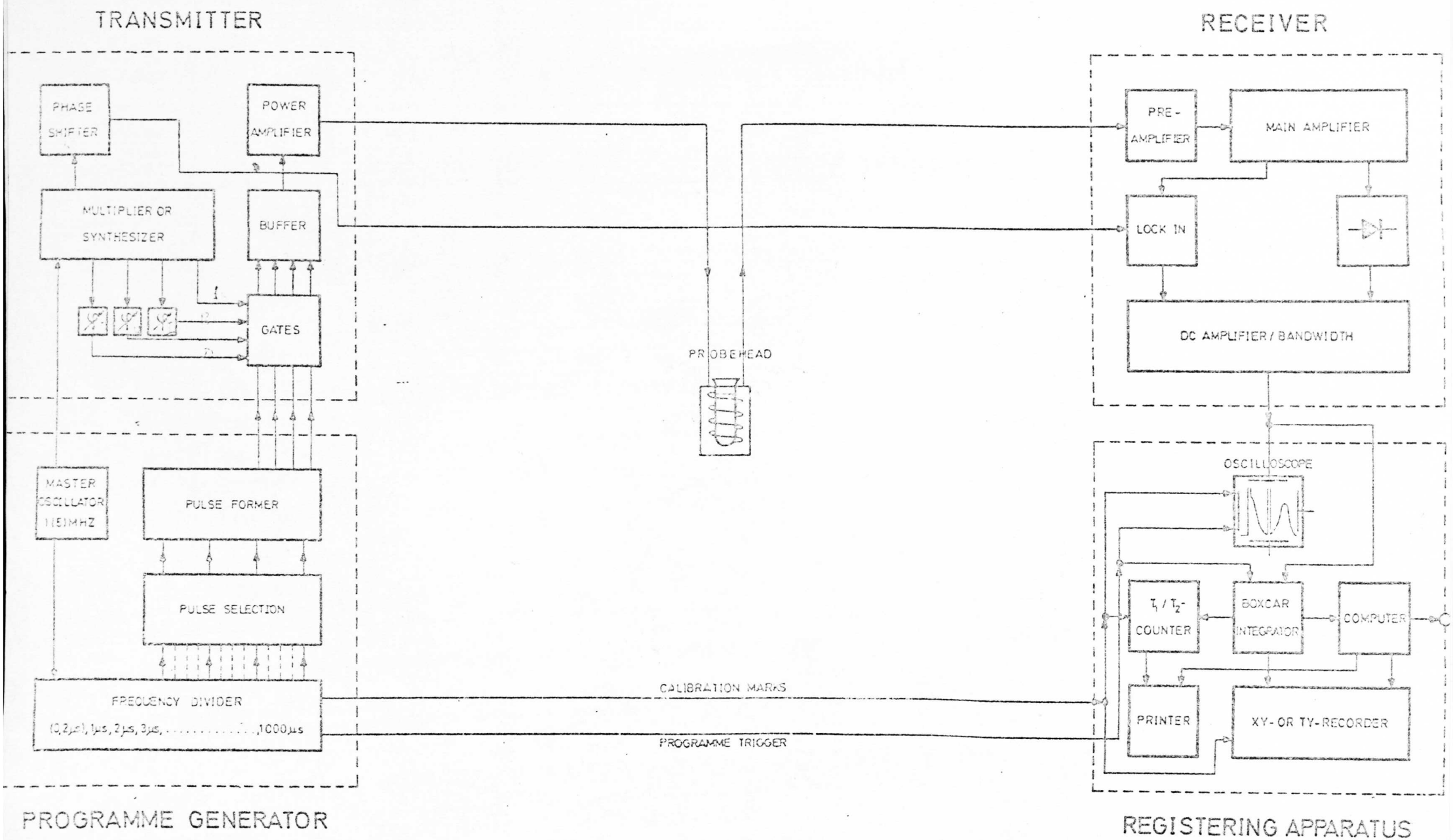

with the present spectrometer. Interpolation between the 1kHz frequencies to 10 Hz. is also possible but a frequency locked to the nearest kHz. was found to be satisfactory for most n.q.r. work. The 1MHz crystal frequency is also used as the basic 'clock' from which are derived all the digital timings in the pulse programme generator. In this way phase coherence between consecutive pulses is preserved.

(b) The Pulse Programme Generator.

This unit controls the spacings and duration of all pulses in a pulse sequence, and also the repetition rate of the complete pulse programme. All timings are derived digitally from the 1MHz. quartz oscillator in the frequency synthesiser. This eliminates any 'jitter' in pulse power due to phase incoherence between pulses. Four pulse former units use monostable 'flip-flop' circuits to each control a pulse width and its corresponding inter-pulse time. Pulse times are variable between 1μS. and 1mS. except in the case of the second pulse former which can provide pulses of up to 1 sec. which are useful for saturation sequences. Delays between pulses are adjustable (on pulse formers 1, 3 and 4) between 1μS and 10mS. They are digitally linked to the 1MHz 'clock' to preserve coherence. The second pulse unit has a wider selection of delays, from 1μS to 99 sec. in six overlapping ranges, each range having 99 different delay settings. Also this unit is provided with a device for automatically incrementing the inter-pulse delay by a fixed amount after a set number of pulse programmes have been carried out. This is a convenient feature for measurement of T_1 values, where the value of τ, in a 180-τ-90 pulse sequence, is successively increased.

In addition, three well-used pulse sequences are provided. These are the Carr-Purcell sequence (90-τ-n180) for T_2 measurement, the triplet sequence (180-τ-n(90-180-90)) for measurement of long values of T_1, and a saturation sequence (n90-τ-90), also useful when T_1 values are long.

The principle of the triplet sequence is as follows: The first pulse reverses the direction of the nuclear magnetisation and after a time, τ, a 90^{o} pulse turns it into the measuring (xy) plane, and produces a free induction decay signal; the 180^{o} pulse produces an echo, the height of which measures the magnitude of the magnetisation in the $z(H_o)$ direction and the final 90^{o} pulse in the triplet returns the magnetisation to its original position at time τ. Triplets occur at fixed intervals to obtain a series of echoes, the heights of which are a function of T_1.

$$M(t) = M(o)\ [1-2\ \exp(-\tau/T_1)]$$

This method gives a measure of T_1 in a single pulse sequence.

The saturation sequence is also useful for measurements of long T_1 values. A series of n-90^{o} pulses remove all magnetisation from the +z direction and after a time τ a 90^{o} pulse measures the amount that has returned to this direction. This method is most useful for the measurement of T_1 values in excess of 10 seconds.

The pulse programme unit also controls the rate of repetition of the pulse programmes (variables from 10 mS to 200S.) and provides calibration marks at any decade rate.

(c) Transmitting Section.

Each pulse formed by the pulse programme generator is set to control a gate through which passes the r.f. signal, after amplification and phase shifting according to requirements of the pulse programme.

The complete pulse sequence then passes to a high gain power amplifier. From a typical input of 0.1W this is amplified to 1-3kW depending on the frequency. Two different variable gain power amplifiers are used to cover the full range of the instrument, 4-16 MHz and 16-64 MHz, which are interchanged as required. Both input and output stages are of narrow bandwidth so that their tuning is frequency dependent. The output from

the power amplifier is applied directly to the transmitting coil in the probe unit. The single coil is wound in two sections, a doubly wound part which forms the transmitter coil, and a singly wound portion in which the signal is induced. The receiving part has approximately four times as many turns as the transmitting section, and eight interchangeable coils are used to cover the range from 4-62 MHz.

(d) The Receiver.

The preamplifier of the receiver is mounted closely to the probe unit in order to minimise pick up from external sources. Crossed diodes in the probe limit the input to the preamplifier and these protect the receiver from the transmitter pulses. In the preamplifier the complete frequency range is subdivided into smaller ranges each covering $1:\sqrt{2}$ of the lowest frequency in that range. The main amplifier is of wide band-width so that no tuning is necessary. The band-width is further limited after the main amplifier by selection of a time constant suitable for the signal. The signal is retrieved by either diode or phase sensitive detection, the latter using the carrier frequency from the frequency synthesiser as its reference (See Section 3.4(a)). Phase sensitive detection is to be preferred for weak signals because of a slight false baseline effect with diode detection. This arises because only noise that is positive relative to the true baseline is passed by the diode, and may lead to a false measurement of M(o) in the determination of T_1 values. Strong signals are observed directly on an oscilloscope which is triggered from the start of the pulse sequence, or alternatively from any of the pulses (often more convenient). Weak signals are enhanced using either a Boxcar Integrator or a Signal Averager (C.A.T.).

(e) The Boxcar Integrator.

This is an analogue device for improving the signal to noise ratio of a periodically repeated signal. The total signal is divided into very

small segments each of which is in turn progressively smoothed using a narrow band-width technique. The signal to noise of the whole signal can be improved in this way, by an amount depending on the segment sweep rate and repetition of the signal.

The Boxcar contains no store and its output is fed directly to the chart recorder. When measuring T_1 values using the 180-τ-90 method, the measuring position is not swept but is adjusted to measure a point on the free induction decay following the 90^{o} pulse. Automatic increment of τ then gives a curve, the rate constant of which is T_1.

(f) Signal Averager (Computer Averager of Transients).

In this instrument the input signal is systematically segmented and digitised for storing in the memory unit. Repetition of the signal causes the addition of corresponding segments in the store. The baseline random noise is thus reduced by the averaging process while the signal continues to increase in strength as the repeated sweeps are stored. The signal to noise improvement is equal to the square root of the number of scans, and for pulse programmes which on average are of mS. duration, this is a convenient and rapid method of signal enhancement. It is usually most convenient to trigger the C.A.T. sweep from the pulse immediately preceding the signal, which eliminates the recording of the unrequired part of the pulse programme.

When T_1 measurements are to be made, it is possible to use the trigger from the start of a pulse sequence to automatically advance the store index by one, so that when the τ value is incremented automatically at the end of each pulse sequence, a T_1 curve builds up in the memory of the signal averager. This is transferred to the chart recorder for analysis in the conventional manner. For the results described in chapter 4 signals were detected by both the Boxcar method and also using a Biomac 1000 signal averager. The fastest sweep on this instrument is 5mS., and since some

of the free induction decay signals to be recorded were only of 20μS duration, a sweep expander accessory was required which provided up to a 16 fold increase in sweep speed. This is achieved again by binary division: the signal level in the first segment is fed into channel 1 as before; the level in the second segment is fed not into channel 2 but into channel 17; the next into channel 33 and so on. After 16 sweeps the complete signal, of length 5mS/16 = 312μS, is recorded in the memory. This is sufficiently fast to record the very fast free induction decays from n.q.r. signals. Alternatively a transient recorder could be used, in conjunction with the signal averager.

(g) Variable Temperature Operation.

At temperatures other than ambient, a longer extension between coil and the base of the probe unit is required so that the coil and its screening can be enclosed in a Dewar vessel. For operation at liquid nitrogen temperature a stainless steel screening can was needed because of its low thermal conductivity. The conventional brass can caused frost build-up on the probe assembly, with an excessive nitrogen evaporation rate. A similar procedure to that used with the Decca spectrometer was used for obtaining results at intermediate temperatures; the probe in the partially emptied Dewar was allowed to warm up slowly as measurements were taken. The warm-up rate was more difficult to control than with the Decca spectrometer, due to a lower thermal capacity of the coil screening can. Progressive raising of the Dewar relative to the probe helped to decrease the warm-up rate, and it was found that in favourable cases measurements could be taken without the temperature varying by more than $2^{o}c$.

It proved to be difficult to locate the thermocouple inside the probe screening can near the coil because of increased noise in the preamplifier from pick-up in the thermocouple leads. Therefore the

thermocouple was attached to the outside of the screening can at the closest possible position to the coil. The same Comark electronic thermometer as used previously with the Decca spectrometer was used with the thermocouple for temperature measurement. This arrangement was only partially satisfactory because it gave only the temperature of the coil screen not of the sample itself. However, all the samples that were chosen for relaxation rate studies had previously been studied using the Decca spectrometer so that the temperature dependence of the frequencies were known. Since the n.q.r. frequency was measured to 1 kHz by adjusting the operating frequency of the spectrometer to produce a maximum free induction decay following a 90^{o} pulse, the sample temperature could be interpolated to within 1 K. Measurements were also carried out at fixed temperatures for checking purposes; ice (273 K), solid carbon dioxide and isopropanol mixture (195 K), and isoamyl alcohol slush bath (156 K) were normally used, as well as liquid nitrogen and room temperature. The warm-up method was an expedient technique that was used in the absence of any automatic temperature-controlling unit. The latter is now under construction.

CHAPTER 4

NUCLEAR QUADRUPOLE SPECTRA AND STRUCTURE OF THE HYDROGEN DICHLORIDE ANION.

4.1 Introduction.

The hydrogen dihalide ion $(X\text{-}H\text{-}X)^-$ is the simplest hydrogen-bonded structure, and for an n.q.r. investigation of hydrogen-bonded systems, the hydrogen dichloride ion is an obvious choice. In comparison with the hydrogen difluoride ion, which has been extensively studied by many techniques, other dihalide ions have received less attention. Compounds containing the hydrogen dichloride ion have been known for some years, in fact as early as 1903, Dilthey reported such a product which was formulated $[Si(acac)_3]Cl.HCl$. [4.1]. In 1906 he reported $[Si(dibenz)_3]Cl.HCl$ [4.2]. Similar compounds with tetra alkylammonium, pyridinium and quinolium cations were reported shortly afterwards by Kaufler and Kunz [4.3]. The reversible nature of the formation and dissociation of these compounds was established by Ephraim [4.4]. Not until 1954 were the alkylammonium complexes suggested to have a structure of the type $R_4N^+HCl_2^-$, postulating the existence of the hydrogen dichloride ion [4.5]. The early salts were prepared by the action of dry gaseous acid on amines or the substituted ammonium chloride. An alternative technique is to dissolve the tetraalkylammonium chloride in liquid HCl and remove the excess solvent, leaving the crystalline hydrogen dichloride [4.6]. West produced an interesting crystalline product from a concentrated aqueous solution of caesium chloride into which hydrogen chloride had been passed [4.8]. The ratio of Cs:H:Cl was found to be 1:1:2, but after much argument, an X-ray investigation by Schroeder and Ibers proved its structure to be, not

$Cs^+HCl_2^-$, but $CsCl^1/3[H_3O^+HCl_2^-]$ [4.9]. $CsHCl_2$ and $RbHCl_2$ have since been prepared, although they are stable only above the vapour pressure of liquid HCl. [4.7,4.10].

The samples used in the present n.q.r. study were kindly provided by Professor T.C. Waddington, Dr C.J. Ludman and Dr J.A. Salthouse. The samples were prepared using liquid HCl techniques, and sealed in glass ampules of 13 mm. diameter and ~20 mm. in length, giving maximum filling factor in the spectrometer probe coil.

4.2 ^{35}Cl NQR Frequencies.

(a) General Information.

In Table 4.1 the experimentally determined ^{35}Cl n.q.r. frequencies are given for the whole series of hydrogen dichlorides studied. Where resonances were not detected at liquid nitrogen temperature, the frequency at the lowest temperature at which the line was observed is given in column 3. The frequencies were measured using the prototype version of the Decca n.q.r. spectrometer described in Chapter 3. Line centres could be measured to $\pm$ 0.005 MHz with interpolation from the 100 kHz calibration marks. Greater accuracy in interpolation was possible with 10 kHz markers but owing to the lack of a second marker channel on this spectrometer the more widely-spaced markers were used to reduce the ambiguity in calibration.

The marker frequencies were checked before and after each run using a radio receiver and a frequency meter. Any non-linearity in the scale was only apparent on a wide frequency sweep. Sideband suppression was used so that the fundamental frequency alone was observed.

All the salts were studied over the temperature range from liquid nitrogen up to room temperature, and intermediate temperatures were obtained using either constant temperature slush baths or by the warm-up method

TABLE 4.1

^{35}Cl N.Q.R. FREQUENCIES IN THE HYDROGEN DICHLORIDE ANION, MHz.

	at 77K.	at intermediate temperature (K)	at 294 K.
Me_4NHCl_2	20.26	19.92_5(195)	19.51
	(20.22 a.)		(19.49 a.)
	(20.21 b.)		
Me_4NDCl_2	21.04	20.75 (195)	20.23_5
	(21.12 b.)		
$CsHCl_2$	-	21.17 (166)	20.47
$CsDCl_2$	-	22.18 (111)	21.28
$CsCl, {}^1/3[H_3O^+HCl_2^-]$	-	11.94 (203)	11.89_5
$CsCl, {}^1/3[D_3O^+DCl_2^-]$	-	12.07 (237)	12.05
Et_4NHCl_2	-	-	11.89
			(11.89 a.)
Et_4NDCl_2	-	-	12.01

a. J.C. Evans and G.Y-S.Lo, J. Phys. Chem, 70, 2702(1966); 71, 3697 (1967).

b. T.E. Haas and S.M. Welsh, J. Phys. Chem. 71, 3363 (1967).

described in Chapter 3. A graph showing the temperature dependences of the tetramethylammonium and caesium hydrogen dichloride frequencies for both the deuterated and undeuterated anions, is given in Figure 4-1. The temperature dependences of the hydronium dichloride frequencies are shown in Table 4.2.

In addition to the hydrogen dichlorides listed in Table 4.1, n.q.r. searches over the frequency range 9-35 MHz were also carried out on those with tetrapropylammonium, tetrabutylammonium, trimethyl ethylammonium and rubidium cations and also the mixed dihalides, RbHClBr, CsHClBr, CsIHCl and Bu_4NIDCl but in none of these could a resonance be positively identified. This is perhaps not surprising in the case of the larger alkyl ammonium salts where the number of observable nuclei is less than that in the tetraethyl-ammonium salt in which the signal was extremely weak. For the smaller cations however, other effects must be responsible for the lack of a response; for example, line broadening due to disorder in the crystal may be a contributory factor.

It is apparent from Table 4.1 that the n.q.r. frequencies for the hydrogen dichlorides fall into two groups at frequencies near 12 or 20-21 MHz. These may be compared with the chlorine frequency in solid HCl at 77 K which is 26.47 MHz. [4.11,4.12]

The bonding may be described in terms of two resonance hybrid structures, I and II, which contain an HCl molecule and a chlorine ion.

$$Cl \text{---} H \quad Cl^- \qquad\qquad Cl^- \quad H \text{---} Cl$$

I II

Fig. 4-1. Temperature Dependence of ^{35}Cl NQR Frequency, ν_Q, in the Dichloride Ion.

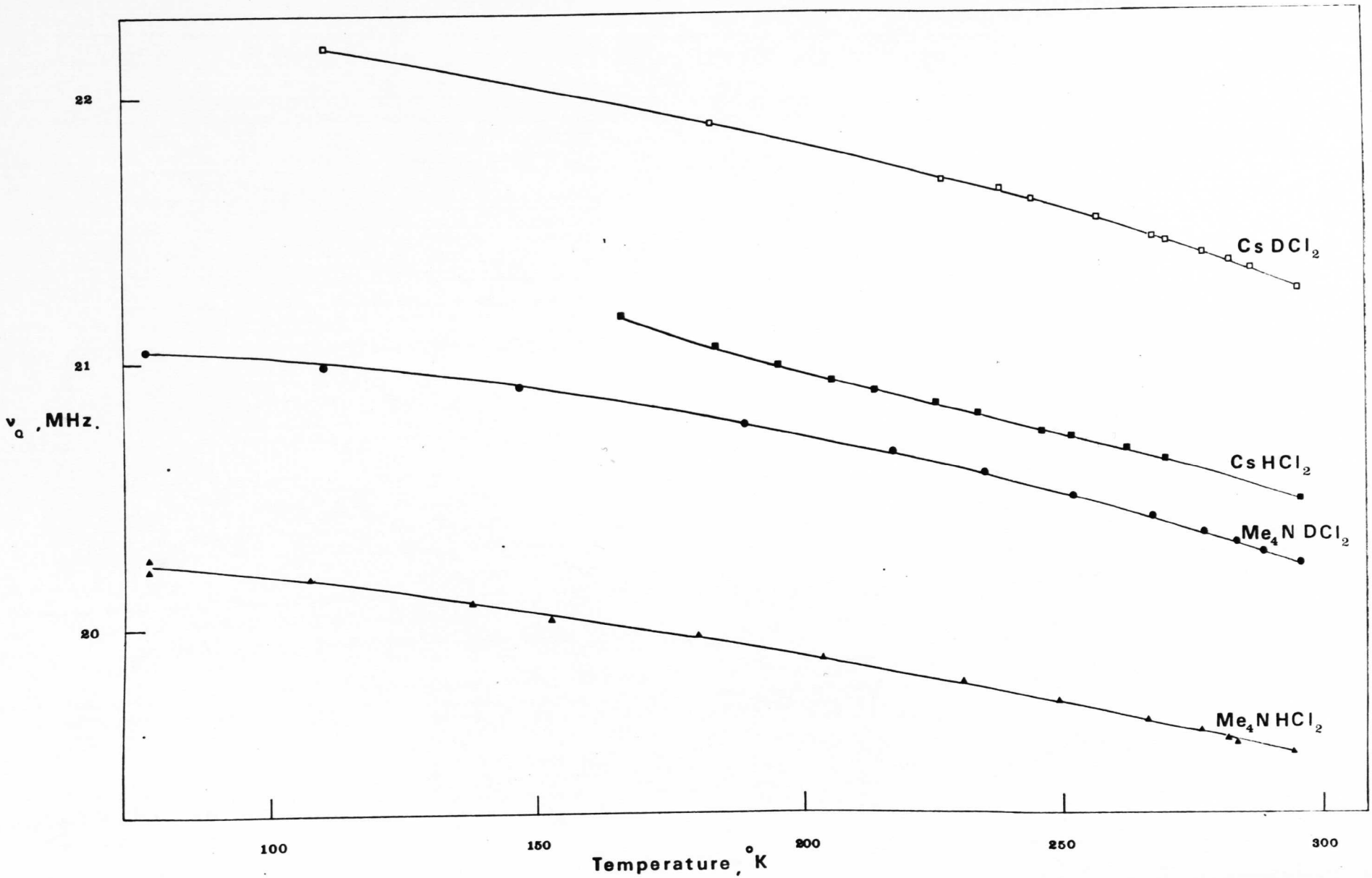

TABLE 4.2

TEMPERATURE DEPENDENCE OF ν_Q IN $CsCl^1/3(H_3O^+ HCl_2^-)$.

T(K)	ν_Q(MHz)
203	11.940
218	11.940
226	11.935
233	11.932
239	11.930
243	11.930
264	11.920
268	11.915
298	11.895

$CsCl^1/3 (D_3O^+DCl_2^-)$

237	12.070
245	12.065
252	12.065
266	12.060
278	12.055
298	12.050

If the contributions from I and II are equal, that is if the ion contains a symmetrically bound hydrogen atom, then the chlorine n.q.r. frequency would be expected to be the average of that of H-Cl and the chlorine ion ie. ~ 13 MHz [4.13].

This value is in near agreement with the group of frequencies near 12 MHz and so it is expected that this group of hydrogen dichloride anions contains a symmetrical hydrogen bond. This group includes both deuteriated and undeuteriated forms of tetraethylammonium hydrogen-dichloride and caesium chloride-$^1/3$ hydronium dichloride. The symmetrical nature of the bond is consistent with X-ray, I.R and neutron inelastic scattering spectra which will be discussed below.

The X-ray investigation of the caesium hydronium dichloride by Schroeder and Ibers [4.9] predicts a symmetrical structure from the presence of a mirror plane perpendicular to the Cl....Cl axis. Since this makes the chlorines crystallographically equivalent, only one line would be expected in the n.q.r. spectrum, which is as observed. The Cl....Cl distance reported is 3.14 ± 0.02 Å, which is somewhat shorter than the inter-chlorine distance of 3.22 ± 0.02 Å reported in tetramethylammonium hydrogen dichloride, the only other X-ray structure determination that has been carried out [4.14]. The unit cell structure in this compound is shown in Figure 4-2. In this case there is no mirror plane perpendicular to the inter-chlorine axis. The chlorine n.q.r. frequencies in the tetramethylammonium and caesium hydrogen dichlorides indicate a marked departure from symmetry in the bonding of the anion, and in terms of the resonance forms I and II a signal near 20 MHz. corresponds to approximately 75%: 25% contributions respectively. In these forms the bond between H and Cl is similar to that in the hydrogen chloride molecule, and not a fully covalent bond. With unequal contributions from the resonance forms, two lines are expected in the n.q.r. spectrum,

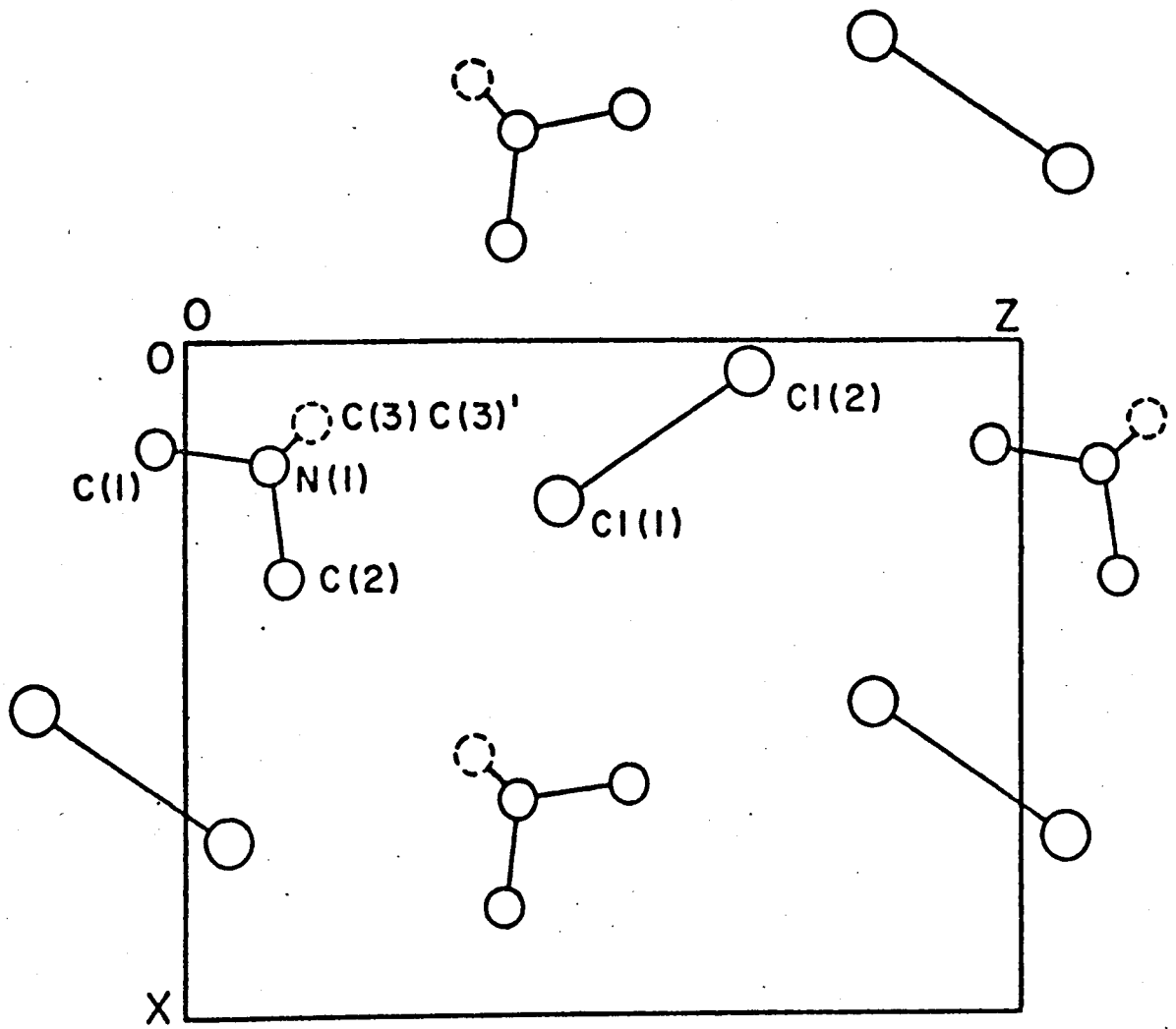

FIG. 4-2

View of the $(CH_3)_4N^+(Cl\text{-}H\text{-}Cl)^-$ structure perpendicular to the ac plane at y = 1/4. C(3) and C(3)' (dashed circles) lie outside of, but are projected on to the molecular plane. Primary bonding interactions are designated with solid lines.

one of which is observed near 20 MHz. and the other would be expected to be near 25% of 26.5 or 6.6 MHz. Since the frequency for the symmetrical hydrogen dichloride is nearer 12 than 13.25 MHz, the amount of asymmetry is equal to 20-12 = 8MHz, so that a signal near 4 MHz. is to be expected. This region is unfortunately out of the range of the Decca spectrometer in its present form, and on the lower limit of the pulsed spectrometer. No signal has yet been detected despite several searches at room and low temperatures.

The shorter bond length in the symmetrical hydrogen dichloride compared with the asymmetrical hydrogen dichloride reflects a stronger hydrogen bond in this type of anion. Further evidence of bond strength is provided by studies of the infra-red, Raman, and inelastic neutron scattering spectra. [4.15-4.20] As with the n.q.r. frequencies, the vibration spectra also divide the hydrogen dichlorides into two groups. Members of the group that are thought to have the unsymmetrical structure have been characterised by bands at 1520-1670 (ν_3), 1200 ($2\nu_2$) and 220 cm^{-1}. (ν_1) at room temperature, and include caesium, tetramethylammonium, tertiary butylammonium, and hexadecyltrimethylammonium hydrogen dichlorides [4.15]. In hydrogen bond formation, ν_3, the asymmetric stretch, is expected to shift to lower frequency as the A-H bond length increases in a hypothetical A-H ... B species; ν_2, the bending mode, is expected to increase in frequency; the value of ν_1, the symmetric stretch, is also expected to increase with bond strength. The general bands that characterise the second group, which are thought to be symmetrically hydrogen bonded, comply with these expectations for the formation of a stronger hydrogen bond: 700-800 (ν_3), 1000-1050(ν_2) and 260 cm^{-1}(ν_1). The salts in this group include tetraethylammonium, tetrapropylammonium, and tetrapentylammonium hydrogen dichlorides. Evans and Lo conclude that the vibration data for the first group could be explained by two inequivalent chlorine atoms with the proton

situated in an anharmonic potential well with a single minimum. The n.q.r. evidence verifies the inequivalence of the chlorine atoms but is unable to distinguish between single and double potential minima (see section (c)). Members of the second group are thought to have a symmetrical single minimum potential well, analogous to the difluoride ion, which has been shown to have a symmetrical structure by neutron diffraction in all salts so far examined [4.21].

Chang and Westrum [4.22] conducted heat capacity measurements on tetramethylammonium hydrogen dichloride and concluded that the compound had virtually zero residual entropy and therefore favoured a symmetrical structure with a single minimum potential function for the hydrogen dichloride ion. The point has been made, however [4.14] that zero residual entropy is not inconsistent with the unsymmetrical model if all the dipoles are oriented in an ordered fashion.

(b) Application of the Townes-Dailey Theory.

We assume in this section that the hydrogen dichloride ion is approximately linear, so that the field gradient at the chlorine nucleus is assumed to be axially symmetrical about the hydrogen bond, and the asymmetry parameter is therefore zero. The quadrupole coupling constant is therefore assumed to be equal to twice the resonance frequency. In the i.r. spectrum of caesium hydrogen dichloride a splitting of ν_2 has been observed which together with Raman evidence suggests that the ion may be bent [4.18]. However the error in neglecting a small η will be well within the approximate nature of the Townes-Dailey analysis (see Chapter 1). Measurement of ^{127}I resonance in HI_2^- would provide a check on the linearity. We shall use the Townes-Dailey procedure outlined in Chapter 2 for interpreting the coupling constants.

Text cut off in original

The Tomasi and Scrocco SCFMO calculation on the HCl molecule indicates that very little s hybridisation is present in the bonding molecular orbital, [2.11]. We shall therefore follow Gordy's approximation when applying the Townes-Dailey theory for calculating electronic charge densities. In Table 4.3 are given the expected populations of the p_σ atomic orbital on the n.q.r. monitored chlorine atom. If the bonding in the hydrogen dichloride is considered to be a four electron, three centre-bond as in ICl_2^- [4.23] then the total electron population must of course equal 4. For the symmetrical hydrogen dichloride ion, a σ electron density of 1.78 on each chlorine will mean an electron density on the proton of 0.44e so that the net atomic charge is +0.56e. We can compare the electroni charge densities with those of the dichloroiodide ion which is also symmetrical.

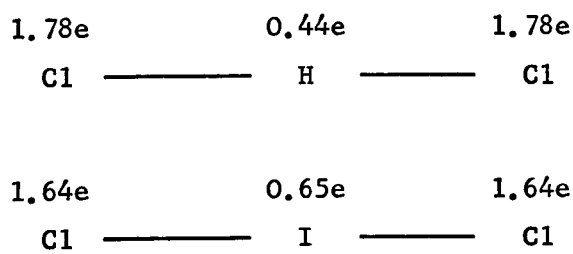

Since all the nuclei in the dichloroiodide ion have quadrupole moments it is possible to calculate each charge distribution independently. The fact that the electronic charges total approximately 4 lends weight to the theory that d hybridisation is negligible and only the three p_σ orbitals form the bonding molecular orbital. In comparison with the hydrogen dichloride ion, the charge distributions are compatible with the additional polar nature of the bond in the latter.

In the unsymmetrically-bonded hydrogen dichloride ion the quadrupole resonance of only one chlorine has been observed, so that only one p_σ population in the molecule may be calculated. However it has been pointed

TABLE 4.3

POPULATIONS OF CHLORINE $3p_\sigma$ ATOMIC ORBITAL

CALCULATED USING TOWNES-DAILEY THEORY

	$\frac{e^2Qq}{h}$ MHz.	$\frac{e^2Qq}{e^2Qq_{atom}}$	$3p_\sigma$ population
$Me_4N\ HCl_2$	40.52	0.370	1.63
$Me_4N\ DCl_2$	42.08	0.384	1.62
$Cs\ H\ Cl_2$	42.32	0.396	1.60
$Cs\ D\ Cl_2$	44.70	0.407	1.59
$CsCl^1/3[H_3O^+HCl_2^-]$	24.00	0.219	1.78
$CsCl^1/3[D_3O^+DCl_2^-]$	24.25	0.221	1.78
$Et_4N\ HCl_2$	24.01	0.218	1.78
$Et_4N\ DCl_2$	24.32	0.222	1.78
HCl	52.94	0.482	1.52
DCl	54.62	0.498	1.50

out that the difference between the coupling constant of the more ionic chlorine and that of the symmetrically bonded chlorine should correspond to the difference between the latter and the more covalently-bonded chlorine, [4.13].

This leads to an estimated coupling constant of 8 MHz. for the ionic chlorine which corresponds to a p_σ population of 1.93e on this atom. The electronic populations in the unsymmetrical hydrogen dichloride would then be

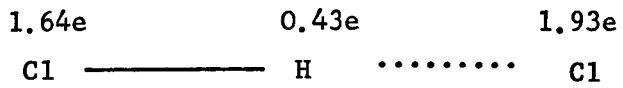

From this it appears that the protonic charge distribution is little affected by the symmetry of the anion. In comparison with the hydrogen chloride molecule,

there appears to be comparatively little change of electron population on the hydrogen atom. During hydrogen bond formation, in which a chlorine ion approaches the HCl molecule, the main transfer of charge is from one chlorine to the other, leaving the charge on the hydrogen atom comparatively unchanged.

On the basis of simple Huckel LCAO-MO theory a linear homonuclear triatomic molecule would be expected to have a p-electron population of 1.5 on the terminal atoms and 1 on the central atom (this neglects electron correlation effects). If the two terminal atoms are more electronegative than the central one then it is expected that the population

on the outer atoms will be greater than 1.5 and less than 1 on the central atom. If the bonding is not symmetrical in a homonuclear molecule, then the longer bonded atom will have a p population greater than 1.5 and the shorter bonded one, less than 1.5. The charge on the central atom should not be affected much by the asymmetry. These general conclusions agree with the approximate charge distributions calculated from the n.q.r. data.

(c) Deuteriation Shifts.

A further feature apparent in Table 4.1 is the change in the chlorine n.q.r. frequency produced by deuteriation. This deuteriation shift is not very temperature dependent (see Figure 4-1) but appears to be much greater in the asymmetrically bonded hydrogen dichlorides. Values of the deuteration shifts are given in Table 4.4, together with that of HCl for comparison. A change in the measured n.q.r. frequency on deuteriation will be due to the combined effect of two separate mechanisms:

(1) A change in the thermal vibrations which reduce ν_Q by motional averaging. (The temperature-independent part with which we are concerned here will be the change in the zero point energies of vibration, on deuteration);

(2) A shift in ν_o, the n.q.r. frequency of the static molecule, which results from changes in the bonding on deuteriation.

Before we can assess the changes in bonding on deuteriation, we must therefore estimate the change in ν_Q due to the zero point energy terms. The averaging effect of solid state motions can be predicted by the Bayer theory of n.q.r. frequency temperature dependence, which was discussed in Chapter 1. The expression which corresponds to equation (27) in Chapter 1, where no field gradient asymmetry is predicted, is

$$\nu_Q = \nu_o\left[1 - \frac{3}{2}\sum_i \frac{\hbar}{A_i\omega_i}\left(\tfrac{1}{2} + \frac{1}{e^x - 1}\right)\right] \qquad (1)$$

TABLE 4.4

DEUTERIATION SHIFTS in ν_Q, MHz.

	77K	294K
Me_4NHCl_2	+ 0.78	+ 0.725
$CsHCl_2$	-	+ 0.81
Et_4NHCl_2	-	+ 0.12
$CsCl^1/3[H_3O^+HCl_2^-]$	-	+ 0.155
HCl	+ 0.84	

+ indicates a higher frequency in the deuteriated ion.

Where ν_o is the n.q.r. frequency of the stationary molecule A_i, ω_i are the moment of inertia and torsional frequency of the ith mode of vibration, and $x = h\omega_i/kT$. The measured value of ν_Q is therefore reduced from the value of ν_o by a temperature dependent term and by a zero point energy contribution. In the Bayer theory the motions which most affect ν_Q are those which change the orientation of the electric field gradient with respect to the spin axis of the nucleus. In this case, there are at least two angular motions which will be responsible for this effect, namely the molecular bending mode ν_2, and any torsional lattice modes of the crystal. From equation (1), the reduction in ν_Q due to the zero point contribution of each angular motion, is

$$\frac{3}{4} \frac{\hbar}{A_i \omega_i} \nu_o \text{ Hz.} \qquad (2)$$

In order to apply this expression, it is necessary to estimate a value for the moment of inertia for each angular motion, in both types of dichloride ion. For a torsional lattice mode, the ion is treated as a linear triatomic molecule of the appropriate dimensions taken from the X-ray data. For the bending mode the moment of inertia term is probably nearer that of an HCl molecule calculated with the appropriate interatomic distance. In the symmetric ion this distance is half of the interchlorine distance ie 1.57Å, but in the asymmetric ion the proton position is not defined. A very approximate H-Cl distance can be estimated from the degree of covalency of the bond. In HCl the bond of length 1.28Å is 48% covalent (from n.q.r. data); the H-Cl distance in the symmetric ion is 1.57Å and the bond 28% covalent, so that for a 37% covalent bond (corresponding to $\nu_Q \sim 20$MHz.) linear interpolation gives a bond length of 1.44Å. Although this calculation is very approximate there is evidence [4.24] from a study of the ^{35}Cl n.q.r. frequency in

series of transition metal complexes, of a linear dependence of coupling constant upon the length of M-Cl bond. The moments of inertia of the various dichlorides for the two angular motions are then calculated.

TABLE 4.5

HYDROGEN DICHLORIDE ANION - MOMENTS OF INERTIA

Ion Type	Motion	M.ofI.(HCl_2^-) 10^{-40}g.cm^2	M.of I(DCl_2^-) 10^{-40}g.cm^2
Symmetric	torsional lattice mode	284	283
"	bending mode	4.00	7.78
Asymmetric	torsional lattice mode	306	308
"	bending mode	3.34	6.52

As may be expected, only the bending mode moment of inertia changes markedly on deuteriation . It has been observed in the neutron inelastic scattering spectra of caesium hydrogen dichloride that a large change in the bending mode frequency occurs on deuteriation (from 657cm^{-1} to 480 cm^{-1}) but change in the lattice frequencies is negligible [4.18]. For this asymmetric ion we can calculate the contribution to the deuteriation shift in ν_Q due to the zero point energy terms (equation (2)). Since the lattice mode frequencies are not affected by deuteriation and the corresponding moment of inertia terms are very similar, the contribution from the torsional lattice mode is very small and may be neglected. For the bending mode, which is assumed doubly degenerate, the difference in zero point energy terms causes a contribution to the deuteriation shift of ν_Q of 0.242MHz.

The measured deuteriation shift in caesium hydrogen dichloride is 0.81 MHz at room temperature, and from Figure 4-1 this appears to be virtually temperature independent. Therefore a shift in ν_o, the frequency in the static ion of 0.57 MHz. is to be expected due to changes in the bonding on deuteriation.

In terms of the simple bond length correlation, used earlier, this shift would correspond to a displacement of the deuterium of ~ 0.01Å nearer the more covalent chlorine atom. The direction of the shift is consistent with an anharmonic potential function with a single minimum, since the general lowering of vibrational levels on deuteriation will cause a shift in the position of maximum electron density in the well, nearer to the more covalently-bonded chlorine, and a corresponding rise in its n.q.r. frequency.

For the other group of hydrogen dichlorides, (those in which the ion is thought to be symmetrical), the observed deuteriation shift in ν_Q is much smaller than (but in the same direction as) the deuteriation shift in the asymmetric ion. One reason for this is that the contribution from the zero point energy term is reduced owing to the greater frequency of the bending mode in the symmetric ion. This contribution can be assessed as in the other case using the calculated moments of inertia (Table 4.5) and experimentally determined bending frequencies. Bond length data are provided by the Schroeder and Ibers X-ray structure analysis of the hydronium dichloride salt [4.9]. The bending mode is not observed in the i.r. spectrum because it falls under the broad band due to ν_2 of the hydronium ion [4.19]. However, it has been observed in the neutron inelastic scattering spectrum [4.20] at 795 cm^{-1}. The corresponding frequency in $CsCl^1/3[D_3O^+DCl_2^-]$ has not been determined, but a value can be estimated from the ν_2 values in tetraethylammonium hydrogen and deuterium dichlorides of 1050 and 750 cm^{-1} respectively [4.15]. This gives an

expected ν_2 value in symmetric DCl_2^- of 567 cm^{-1}. Estimation by comparison with HF_2^- and DF_2^- gives very nearly the same frequency (572cm^{-1}). The shift in ν_2 on deuteriation from 795 to 567 cm^{-1} is equivalent to a shift in ν_Q of 64 kHz, which compares with the observed value of 155 kHz in the hydronium salt. Within the very approximate nature of the analysis it appears that the electric field gradient at the chlorine nucleus is hardly affected by deuteriation of the hydrogen bond. This is to be expected if the potential function for the bond has a single broad minimum symmetrical well. The alternative is for the potential function to have a double minimum of the type proposed by Rundle [4.25, 4.26] to explain the observed increase in the overall bond length on deuteriation of O-H-O hydrogen bonds. His model is based upon the superposition of two potential functions for the O-H bond to give the double minimum. As the O-O distance decreases, the height of the barrier is expected to decrease and also the number of energy levels below the barrier will decrease. When the O-O distance has contracted sufficiently for the most occupied proton level to be comparable with the height of the barrier, then the lower-lying deuterium level will still be below the height of the barrier, and there will be consequently more electron density at the centre of the well (at the position of the barrier) for the O-H-O bond than for the corresponding O-D-O bond. Rundle's wavefunctions showed this effect, and it was maintained that the greater presence of the proton in the centre of the well, where it could attract both oxygen atoms simultaneously, led to the shortening of the bond. If the same situation occurred for the Cl-H-Cl bond, the greater electron density nearer the chlorine atoms in the deuteriated bond (compared with the undeuteriated bond) would give rise to a positive deuteriation shift in ν_Q. In view of the very small deuteriation shift observed for the tetraethylammonium hydrogen dichloride and the caesium chloride $^1/_3$ hydronium dichloride, it seems more

likely that the potential function has only a single broad minimum, or such a low central barrier that it is below the lowest H and D levels.

A deuteriation shift has also been observed in the ^{35}Cl NQR of $Na\ AuCl_4 2H_2O$ [4.24], but in this case ν_Q decreases on deuteriation (a negative shift), in contrast with hydrogen dichloride results. This can be rationalised as follows:- The O-H...Cl bond is certainly asymmetric and will have an anharmonic potential function. In contrast with the asymmetric dichloride, the n.q.r.-monitored nucleus is in the atom more weakly bound to hydrogen. With the lowering of vibrational levels on deuteriation the anharmonic nature of the well will cause the position of maximum charge density associated with the hydrogen (or deuterium) atom to move away from the chlorine atom so that its coupling constant is reduced.

In the ammonia molecule, the ^{14}N coupling constant decreases by 12% in the gas - solid transition, due to hydrogen bond formation. For ND_3, the decrease is 21.6%, which has been taken as evidence that deuterium bonds are stronger than hydrogen bonds [4.27]. An X-ray study showed that there is indeed a contraction of the N....N distance on deuteriation [4.28]. This would suggest that for a hydrogen bond between two similar atoms the total deuteriation shift in the ν_Q values for each atom would be an indication of the bond length isotope shift. Both positive and negative bond length shifts have been observed on deuteriation [4.25]. Only one frequency has been observed for the asymmetric hydrogen dichloride ion, but for the symmetric ion the value of the deuteriation shift, after allowance for the zero point energy contribution, is positive though small. This would suggest only a very small expansion of the Cl...Cl distance on deuteriation. However, in the hydrogen difluoride ion an apparent decrease in the F...F distance has been noted [4.25]. The measurement

of a bond length isotope shift by a structural investigation of the deuteriated hydronium dichloride salt would confirm this point.

(d) Temperature dependence of ν_Q.

A graph of the temperature dependence of ν_Q, the ^{35}Cl n.q.r. frequency, in the four unsymmetrical hydrogen dichlorides is given in Figure 4-1. In none of the four cases do the temperature dependences depart markedly from linearity. They are 'normal' - that is, the frequency decreases with temperature as predicted by the Bayer theory (Chapter 1). As with the deuteriation shifts, the temperature coefficients for the asymmetrically-bonded hydrogen dichlorides are considerably larger than those for the symmetric ions, in this case approximately an order of magnitude separates the two. This results from the difference in vibrational frequencies in the two types of hydrogen dichloride anion and their different averaging effects upon the n.q.r. frequency. The Bayer expression for the effect of these vibrational motions on ν_Q contains both temperature dependent and independent terms, of which the latter, the zero point energy terms, were discussed in section (c). The temperature dependent term for the reduction in ν_Q is

$$-\frac{3}{2}\nu_o \sum_i \frac{\hbar}{A_i\omega_i}\frac{1}{(e^x-1)} \qquad (3)$$

where $x = \hbar\omega_i/kT$. and ω_i is the ith angular frequency, which in this case represents ν_2, the molecular bending mode, and also a torsional lattice mode. Since the frequency of ν_2 is higher in the symmetrical dichloride ion, x will also be larger and therefore the temperature coefficient should be smaller for this ion. In the hydronium dichloride salt a lattice mode of frequency 85 cm^{-1} has been observed in the neutron scattering spectrum but it is not known whether this corresponds to a torsional mode [4.20]. If

this is the case then the increase in the torsional frequency from 35 to 85 cm^{-1} would also tend to reduce the temperature coefficient in the symmetrical ion. In Table 4.6 the experimentally observed values of the temperature coefficient, $\partial \nu_Q / \partial T$, are compared with the calculated values due to the bending mode, ν_2, and the torsional lattice mode. Both motions are assumed to be doubly degenerate which is to be expected if the ion is approximately linear. There is some evidence of non-linearity from a small splitting in ν_2 which has been observed in caesium hydrogen dichloride [4.18] and is interpreted as an indication of a slightly bent ion. The Bayer expression used for the calculation of the temperature coefficients is

$$\frac{1}{\nu_o} \frac{\nu_Q}{\partial T} = -\frac{3}{2} \frac{\hbar^2}{kT^2} \sum_i \left[\frac{e^x}{A_i (e^x - 1)^2} \right] \qquad (4)$$

From the results that are available the calculated temperature coefficients show reasonable agreement with the experimentally observed values, but there is a tendency for the Bayer theory to overestimate. This discrepancy could arise in the following way:

(1) It was indicated in Chapter 1 that the Bayer theory is essentially a constant volume theory and neglects changes in ν_Q due to pressure effects. If the pressure coefficient, $(\partial \nu_Q / \partial P)_T$ should be negative then this would have the effect of producing an extra term in the temperature dependence expression of opposite sign to the Bayer term, reducing the net temperature coefficient. Since this pressure coefficient has not yet been determined, the magnitude of this effect cannot be estimated.

TABLE 4.6

CONTRIBUTIONS FROM VIBRATIONAL MODES TO THE TEMPERATURE COEFFICIENT, $\partial\nu/\partial T$ at 300K AND COMPARISON WITH EXPERIMENTAL VALUES.

	ν_2, cm^{-1}	Contribution to $\partial\nu/\partial T$ (kHz/K)	$\nu_{torsion}$, cm^{-1}	Contribution to $\partial\nu/\partial T$ (kHz/K)	Total calculated $\partial\nu/\partial T$(kHz/K)	Observed $\partial\nu/\partial T$(kHz/K) (a)
$CsHCl_2$	657	-0.80	35	-6.5	-7.3	-5.8
$CsDCl_2$	480	-1.1	35	-6.5	-7.6	-6.5
Me_4NHCl_2	592	-0.78	-	-	-	-4.3
Me_4NDCl_2	440	-1.34	-	-	-	-6.4
$CsCl^1/3(H_3O^+HCl_2^-)$	795	-0.18	85	-0.67	-0.85	-0.46
$CsCl^1/3(D_3O^+DCl_2^-)$	(567)	-0.31	(85)	-0.67	-0.98	-0.53

Figures in brackets are estimated values.

(a) Taken from Figure 4-1, $\pm$ 0.1 kHz/K.

(2) The Bayer theory assumes that the angular vibration frequencies are temperature independent, which is not always true. In the study of chlorine resonance in potassium chlorate, for example, it was found that agreement between theory and experiment was increased by taking into account the effect of temperature on the frequency of the hindered rotation about axes parallel to the plane of the three oxygenatoms. In fact a squared dependence on temperature was found for these modes of vibration. In the present study, without any data of the temperature dependence of the torsional frequencies we must neglect this correction.

It appears therefore that the assignment of the 85 cm^{-1} line in the n.i.s. spectra of the hydronium dichloride salt, to a torsional mode, is consistent with the experimental data. In the asymmetrically bonded hydrogen dichlorides the situation arises that whereas the torsional lattice mode produces the greatest contribution to the temperature coefficient, it is the bending mode which dominates the zero point energy term and hence also its contribution to the deuteriation shift.

4.3 A Study of ^{35}Cl Quadrupole Relaxation and its Temperature Dependence.

(a) Measurement of relaxation times

In the study of the chlorine quadrupole frequencies of this series of hydrogen dichloride salts it was observed that line intensities increased markedly with temperature, up to 300 K.. Fig. 4-3 shows the large increase in signal intensity in the spectra of caesium hydrogen dichloride, recorded on the Decca spectrometer. This effect is the converse of that expected from a Boltzmann distribution of energy level populations and it was suspected that relaxation effects were responsible for this behaviour. If the spin-lattice relaxation time T_1 falls rapidly with temperature, and finally approaches the value of t_{OFF}, then the

Fig. 4-3 Change of Signal Intensity with Temperature.

Text cut off in original

induced voltage in the oscillator tank circuit increases with the more efficient relaxation.

Series of experiments using pulsed r.f. methods were carried out to measure spin-lattice relaxation times which would verify whether the foregoing condition applies, and also it was hoped, provide an indication of the time-scales and energies associated with the motional processes involved in the relaxation.

The relaxation times were measured using a Bruker KR-322S pulsed n.m.r. spectrometer, details of which are given in Chapter 3. The inverse linewidth parameter, T_2^*, was determined from the free-induction decay signal following a single 90^o pulse. This decay did not differ significantly from an exponential curve, and T_2^* was taken as the exponential constant of the curve.

Spin-lattice relaxation times, T_1, were measured by two methods. In the first, a two pulse sequence $180^o - \tau - 90^o$ is used in which the inter-pulse separation, τ, is incremented automatically and the amplitude of the signal at a fixed short time after the second pulse is monitored by a boxcar integrator. The rate of return of the free induction decay signal to its full amplitude is T_1 governed

$$M(t) = M(o)\,(1 - 2e^{-\tau/T_1}) \qquad (5)$$

Using the automatic incrementation of τ an exponential curve is recorded from the boxcar integrator, enabling T_1 to be calculated. It was not possibl as in some n.m.r. experiments, to follow the 90^o pulse with a 180^o pulse to produce an echo, the amplitude of which could be monitored by the boxcar. The signals obtained from these compounds were weak by conventional n.m.r. standards and the very short T_2^* values made it difficult to detect echoes, since the "fanning out" rate controlled by T_2^* was comparable with the width of the pulses. The curve taken from the output of the boxcar integrator, of M(t) against τ gives T_1 from a logarithm plot and a least squares fit to

a straight line of slope $\frac{1}{T_1}$. Fig. 4-4 shows a typical T_1 exponential curve obtained using the $180^o - \tau - 90^o$ automatic increment method for $CsDCl_2$ at 294K. Two pulses of 35 and 14 μS. duration were used and the inter-pulse spacing was increased by 10μS. every 6.4 secs. The pulse sequence was repeated every 100 mS. and the total recording time was 10 minutes.

The second method used for T_1 determination was that due to Alexander and Tzalmona [4.29] in which a continuous train of 90^o pulses are used, and the inter-pulse separation is varied. The amplitude of the free induction decay signal immediately following a pulse is monitored as before by the boxcar integrator or C.A.T. In the previous method, the overall pulse programme repetition time was kept constant, but in this method it becomes the time variable, t. In this case it is not necessary to wait for equilibrium between pulse sequences (normally $5 \times T_1$) as in the first method. However, it is only applicable when T_1 is larger than T_2.

It is shown in [4.29] that for intermediate pulse repetition rates T_1 is given by

$$\frac{M_o - M(t)}{M_o} = \exp(-t/T_1) \qquad (6)$$

where M_o is the signal amplitude for zero pulse repetition rate and M(t) is the signal amplitude at an inter-pulse spacing t. T_1 is then obtained from a logarithm plot and least squares analysis in the usual way or alternatively the time $t_{1/3}$ is measured where $t_{1/3}$ is defined by

$$\frac{M_o - M_{t_{1/3}}}{M_o} = 1/3 \qquad (7)$$

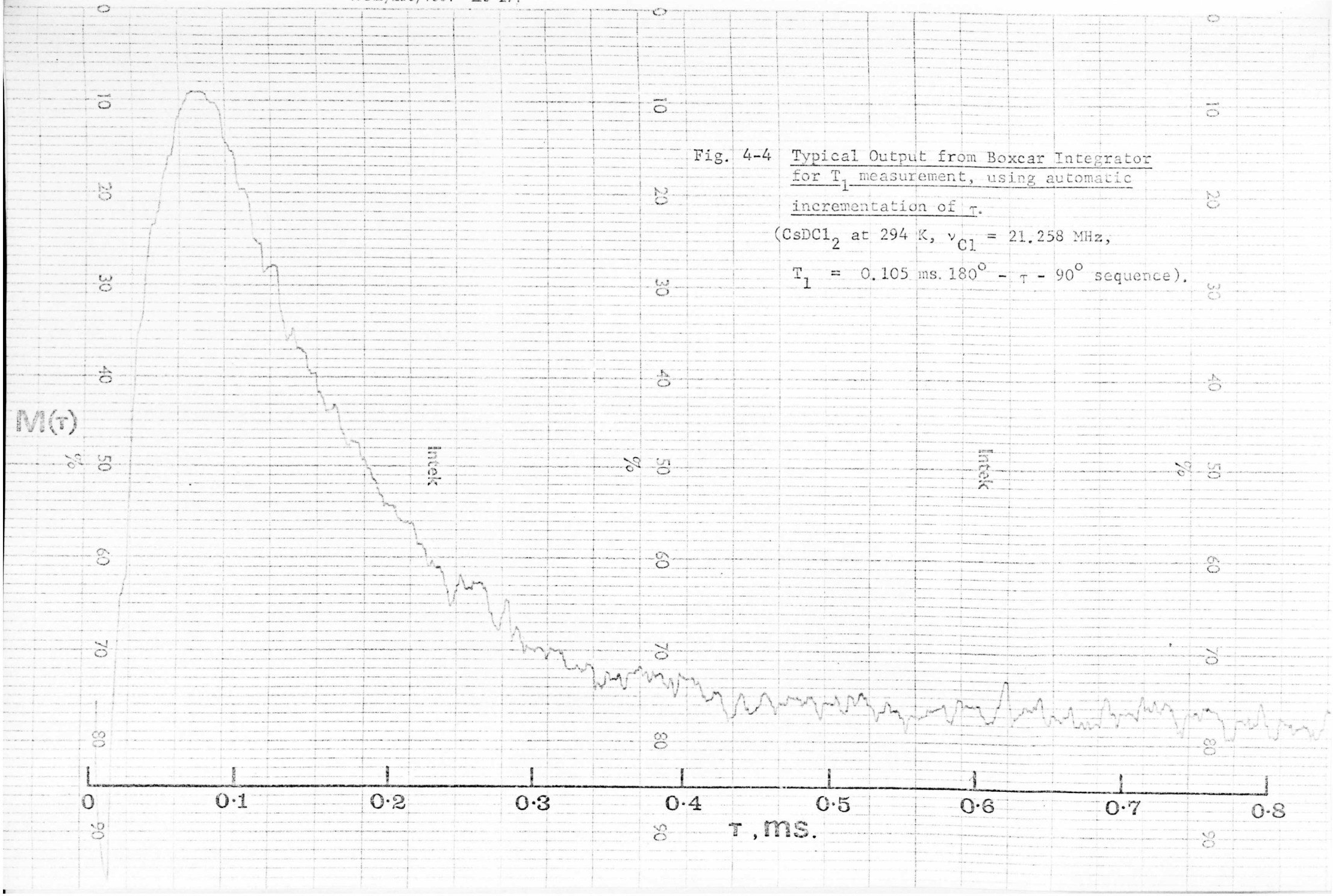

Fig. 4-4 Typical Output from Boxcar Integrator for T_1 measurement, using automatic incrementation of τ.

($CsDCl_2$ at 294 K, ν_{Cl} = 21.258 MHz, T_1 = 0.105 ms. 180° - τ - 90° sequence).

T_1 is simply calculated from the relation

$$1.1\ T_1 = t_{1/3} \qquad (8)$$

Both of these methods were used to evaluate T_1 from the data and showed agreement to within 15%.

Because of the difficulty in obtaining spin echoes it was not possible to measure T_2, since this requires the use of a Carr-Purcell type of sequence (see Chapter 3) in which the amplitude of a series of echoes provides the measure of T_2. In this relaxation study the values of T_1 and T_2^* were measured for the series of hydrogen dichlorides discussed in section 4.2, over as wide a range as the signals were visible, which in most cases were from 100-200 K up to 330 K.

Temperatures below ambient were obtained using constant temperature slush baths or the warm-up method detailed in Chapter 3.

Above ambient temperature, an oil bath was used to heat the probe unit.

(b) Spin-lattice Relaxation

The values obtained for the measured spin-lattice relaxation times over the temperature ranges studied are given in Table 4.7 for six of the dichlorides in the series. The very weak signal in the tetraethylammonium salt proved to be insufficient for T_1 or T_2^* measurements.

In all cases the T_1 values proved to very temperature dependent, and for hydrogen dichlorides for which the asymmetric structure is predicted T_1 decreased markedly with increase in temperature. For caesium hydrogen dichloride the range of spin-lattice relaxation times spanned five orders of magnitude. This salt showed the greatest changes in intensity with temperature when s.r.o. detection was used.

TABLE 4.7

MEASUREMENTS OF THE SPIN-LATTICE RELAXATION TIME IN THE HYDROGEN DICHLORIDE ION

(a) $CsHCl_2$

T(K)	T_1(mS)	T(K)	T_1(mS)
133.0	430	199.5	32.5
134.0	490	209.0	23.0
145.0	272	209.5	27.8
145.0	278	221.0	22.5
150.0	485	227.0	17.1
153.0	472	227.0	15.5
153.0	270	243.5	12.1
154.5	236	277.0	1.62
161.0	206	277.0	1.62
166.5	186	283.0	1.040
166.5	172	297.0	0.115
171.0	180	297.0	0.096
172.0	182	297.0	0.082
173.0	184	297.0	0.0645
176.0	157	297.0	0.0694
186.0	85	297.0	0.0878
199.5	42.5	297.0	0.0755

TABLE 4.7 continued

(b) $CsDCl_2$

T(K)	T_1(mS)	T(K)	T_1(mS)
116.0	620	203.0	27.2
118.0	381	204.0	31.8
123.0	461	205.5	27.2
123.0	460	207.0	14.0
124.0	490	208.5	18.5
124.0	420	209.5	23.6
124.5	420	211.0	14.3
126.0	364	212.0	18.2
126.0	371	214.0	15.5
128.0	370	216.5	10.0
132.5	365	220.0	17.5
139.0	355	220.0	15.0
150.0	310	221.0	13.6
150.5	228	221.0	13.2
152.0	264	223.0	11.8
153.5	308	224.0	10.6
155.0	236	226.0	11.8
156.5	255	227.0	9.1
158.0	229	233.5	8.2
159.0	109	239.5	8.2
159.5	210	245.0	4.7
160.0	172	248.0	6.6
160.0	204	253.0	4.75
162.5	181	257.0	4.40
165.5	172	257.0	5.60
167.0	180	255.0	3.70
167.5	172	269.0	2.55
169.0	147	270.0	2.30
171.0	138	283.0	0.80
171.0	132	284.0	0.85
172.0	143	284.0	0.95
180.0	82	294.0	0.150
180.5	143	294.0	0.105
180.5	118	294.0	0.129
181.0	91	294.0	0.089
184.0	82	295.0	0.100
185.0	96	303.0	0.037
185.0	92	303.0	0.022
188.0	78.5	303.0	0.036
193.0	79.0		
194.5	57.0		
195.0	29.0		
195.0	27.0		
201.0	17.4		
201.0	21.5		
201.0	34.5		
202.5	32.0		
203.0	28.0		

TABLE 4.7 continued

(c) Me_4NHCl_2

T(K)	T_1(mS)	T(K)	T_1(mS)
95.0	510	305.0	15.3
139.0	170	305.0	11.9
153.0	115	306.0	15.3
164.0	100	306.0	9.7
170.5	85.0	306.0	7.4
198.0	59.0	314.0	7.1
205.0	45.0	314.0	6.4
205.0	44.5	314.0	4.3
206.0	52.5	320.0	3.6
208.0	49.4	325.0	4.3
208.0	53.7	326.0	4.1
209.0	51.0	327.0	3.46
242.0	37.0	328.0	3.64
278.0	24.5	328.0	4.54
283.0	14.7	328.0	4.30
287.5	16.4	336.0	2.80
301.0	21.5	338.0	2.70
301.0	19.8	341.0	1.30
305.0	19.0	343.0	1.37
305.0	17.7		

TABLE 4.7 continued

(d) Me_4NDCl_2

T(K)	T_1(mS)	T(K)	T_1(mS)
211.0	50.2	293.0	22.5
211.0	59.8	294.0	19.4
213.5	53.5	294.0	18.8
213.5	37.5	309.0	14.5
214.0	46.8	315.0	15.5
215.5	39.7	317.0	15.4
217.0	36.6	317.0	13.6
223.0	37.5	323.0	9.1
240.0	26.2	332.0	3.2
243.0	27.0	332.0	2.4
248.0	27.7	340.0	1.64
257.0	27.0	341.0	1.28
277.0	21.7	341.0	1.54
277.0	21.3	341.5	1.54
277.0	19.9	342.5	1.27

TABLE 4.7 continued

(e) $CsCl^1/3(H_3O^+HCl_2^-)$

T(K)	T_1(mS)
226.0	32
226.0	34
226.0	35
243.0	13.5
248.0	11.7
249.5	8.2
251.0	5.5
260.0	3.65
267.0	1.7
267.0	1.8
273.0	1.75
274.5	1.45
276.0	1.40
276.0	1.27
282.0	1.17
286.0	1.20
285.0	1.00
289.0	0.95
290.5	0.90
294.0	1.00
297.5	1.28
295.5	1.45
298.0	1.72
306.5	2.65
308.5	3.15
315.0	3.75

TABLE 4.7 continued

(f) $CsCl^{1}/3(D_3O^{+}DCl_2^{-})$

T(K)	T_1(mS)
249.0	18.0
262.0	6.3
265.0	4.3
268.0	4.5
271.0	2.2
285.0	1.65
284.0	1.05
289.0	0.78
292.0	0.82
296.0	0.90
301.0	1.00
301.0	1.07
313.0	1.35
313.0	1.45
322.0	1.65
332.0	1.70
332.0	1.90

Various theories for quadrupolar relaxation in terms of lattice and molecular motions are reported in the literature. Bayer and Ayant have developed theories for T_1 based on a molecular torsional oscillator [1.8, 4.30]. Van Kranendonk has considered quadrupolar relaxation by lattice vibrations in ionic crystals and applied the resulting theory to simple cubic lattices [1.12]. Das, Roy and Roy extended the Van Kranendonk treatment to body-centred cubic structures [4.31]. Yosida and Moriya took into account the variations in covalent bonding resulting from lattice vibrations [4.32]. Quadrupole relaxation by conduction electrons in a metal has been treated by Mitchell [4.33]. Woessner and Gutowsky have further developed the molecular torsional oscillator theory and also deal with molecular hindered rotations [1.10]. This has been also discussed by Tokuhiro [1.11] and Lotfulin and Semin [4.34]. As yet ^{35}Cl T_1 values have only been obtained for a small number of compounds. Spin-lattice relaxation times of ^{35}Cl in potassium chlorate have been interpreted by Chang in terms of the lattice vibration theory, the indirect (Raman) spin-phonon process being mainly responsible for the exchange of energy [1.17], likewise for ^{63}Cu resonance in cuprous oxide [1.10]. The ^{35}Cl T_1 value in p-dichlorobenzene was found to depend upon molecular torsional oscillations about an axis perpendicular to the plane of the ring [1.10]. Agreement with experiment was enhanced when the temperature dependence of the torsional oscillations was taken into account [1.13].

A selective excitation technique has been used to measure the individual transition probabilities W_1 and W_2 in sodium and potassium chlorate and p-dichlorobenzene. The results were consistent with the Bayer theory for the latter, but did not agree with the Chang theory for chlorate - again the Bayer theory was consistent with the measurements [4.35].

Quadrupolar relaxation of ^{35}Cl in 2,2dichloropropane agrees with a model based on field gradient fluctuations from reorienting methyl groups [1.10]. Hindered rotation is also a mechanism for relaxation in 1,2dichloroethane [1.10,1.11].

^{35}Cl Spin-lattice relaxation in (1) tetramethylammonium hydrogen dichloride and (2) caesium hydrogen dichloride.

Examination of Figures 4-5 and 4-6 relating to the T_1 data for these two salts reveals a certain similarity in the temperature dependences, and therefore the two will be discussed together.

(1) Tetramethylammonium hydrogen and deuterium dichlorides

In the plot of ln T_1 against reciprocal temperature two distinctly linear regions are apparent each of which is expected to be indicative of a thermally activated relaxation mechanism. In such cases the correlation time τ_c which gives the time-scale of the motion usually has the temperature dependence

$$\tau_c = \tau_o \exp (E/RT) \qquad (9)$$

at temperatures when T_1 is proportional to τ_c T_1 also has the exponential form.

A least squares straight line fit to the data in the two regions gives the following activation energies

	Temp. range (K)	$E_{act.}$ (kcals/mole)
Me_4NHCl_2	140-300	1.08 ± 0.03
	300-345	12.45 ± 0.62
Me_4NDCl_2	208-320	1.39 ± 0.12
	320-350	12.17 ± 1.56

FIG.4-5

Temperature Dependence of T_1

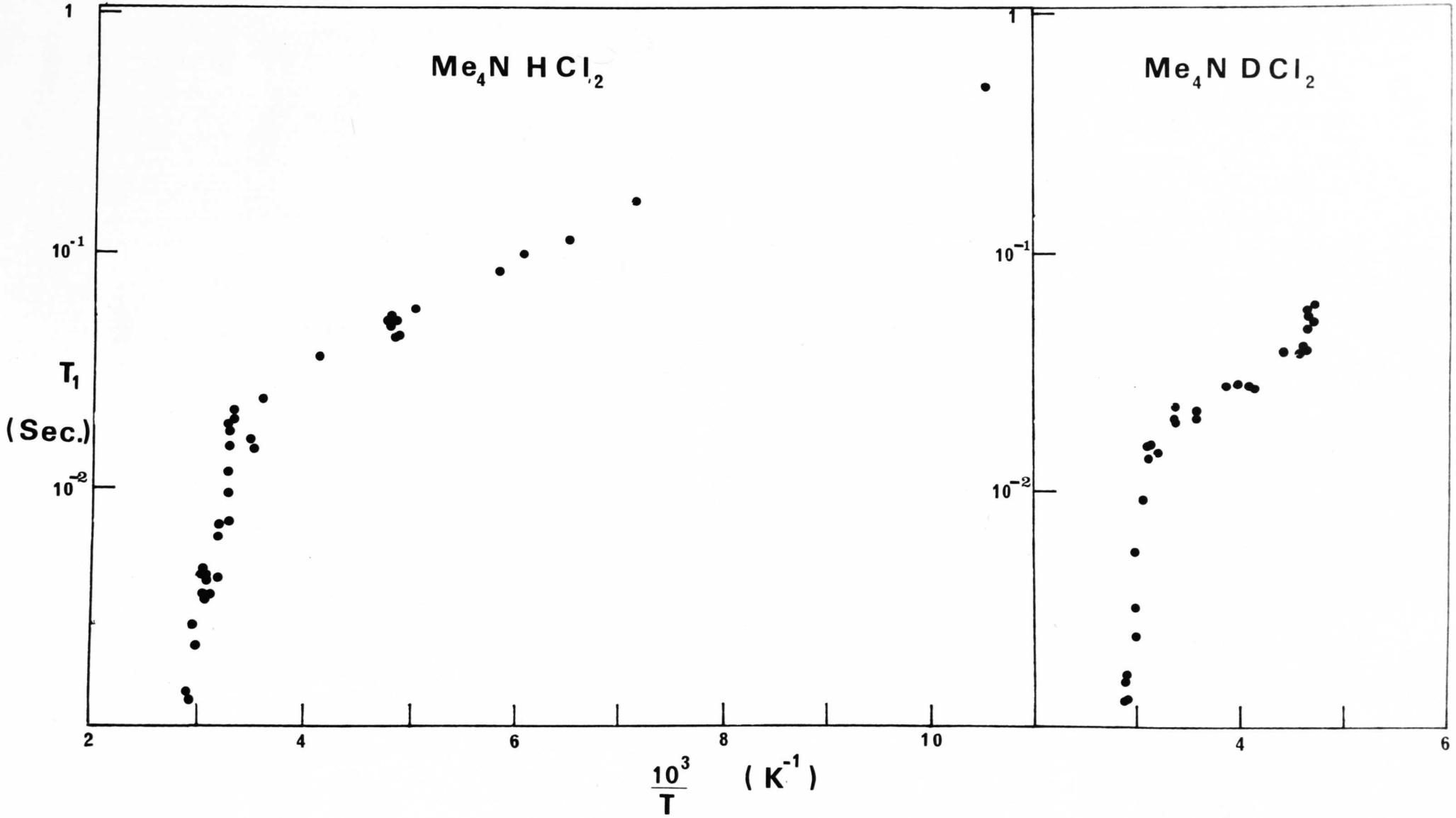

FIG. 4-6

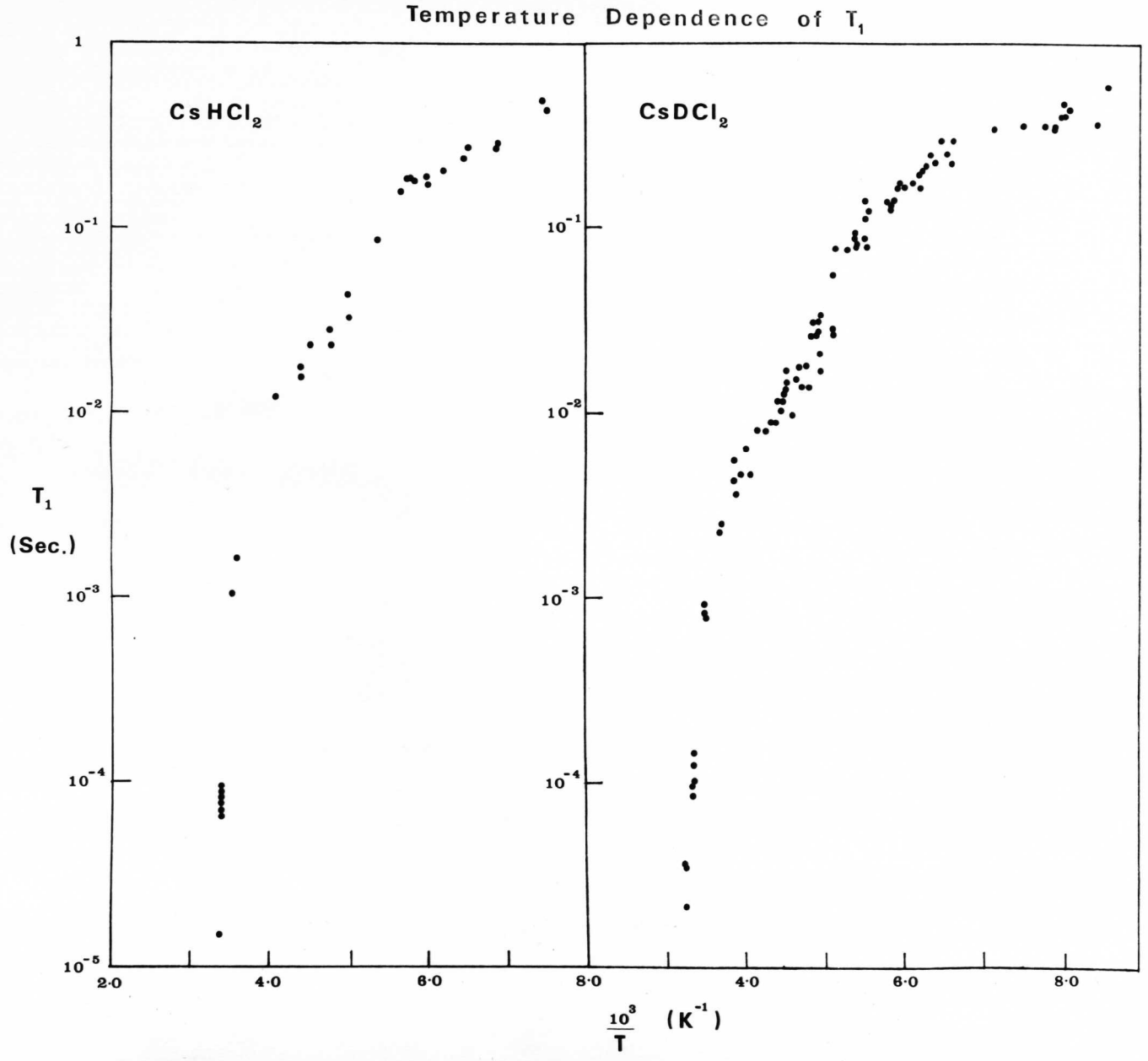
Temperature Dependence of T_1
$CsHCl_2$
$CsDCl_2$
1
10^{-1}
10^{-2}
10^{-3}
10^{-4}
10^{-5}
T_1
(Sec.)
2·0
4·0
6·0
8·0
$\frac{10^3}{T}$ (K^{-1})

(2) Caesium hydrogen and deuterium dichlorides

The temperature dependences of T_1 are indicated in Figure 4-6. Compared with the tetramethylammonium salt the T_1 values cover a great range, spanning five orders of magnitude. It is not surprising therefore that the caesium hydrogen dichloride signal as detected by an s.r.o, disappears before that from tetramethylammonium dichloride, as the temperature is lowered, (see Figure 4-1). The linear regions in the logarithm plot are less well defined than in the previous salt, and the variation in T_1 above 250 K is asymptotic. Least squares fitting produced the following activation energies:

	Temp. range (K)	Activation Energy (kcals/mole)
$CsHCl_2$	127-175	1.08 ± .08
	175-238	3.33 ± .17
$CsDCl_2$	116-150	0.59 ± .09
	150-185	1.97 ± .07
	185-258	4.13 ± .08

We shall now examine the possible relaxation mechanisms for these four salts.

(i) Molecular torsional oscillations

In this theory, due to Bayer and outlined in Chapter 1, the random fluctuating field gradients produced by the torsional oscillations have a finite spectral density at the n.q.r. frequency and bring about relaxation. Woessner and Gutowsky [1.10] have extended Bayer's expressions for the transition probabilities for $\Delta m = 1,2$. They are of the form

$$W_1 = \frac{A_1}{\tau_a} \text{ and } W_2 = A_2 \tau_a$$

where $A_1 = \frac{3}{2} \hbar\omega_Q^2 \sum_i (\omega_i^3 I_i)^{-1} \coth (x_i/2)$

$$A_2 = \frac{3}{16} \hbar\omega_Q^2 \sum_i (\omega_i I_i)^{-2} \left[(1 + e^{-x})(\sinh^2(x_i/2))\right]^{-1}$$

$$x_i = \frac{\hbar\omega_i}{kT}$$

and $$\frac{1}{T} = 2(W_1 + W_2) \qquad (10)$$

τ_a is the lifetime in one excited vibrational level.

The quadratic equation

$$A_2\tau_a^2 - \frac{\tau_a}{2T_1} + A_1 = 0 \qquad (11)$$

can be used to provide solutions for τ_a from experimental values of T_1, and values of A_1 and A_2 calculated from observed angular vibration frequencies.

Substitution of the 35 cm^{-1} lattice frequency observed in the neutron inelastic scattering spectra of both $CsHCl_2$ and $CsDCl_2$ gave imaginary values for the solutions to equation (11) indicating that in these compounds the observed T_1 values are too large for this lattice frequency to be dominant in providing the relaxation mechanism.

The bending frequency of 652 cm^{-1} in caesium hydrogen dichloride gave real solutions for τ_a but the slope of the predicted curve on a logarithm plot of T_1 against reciprocal temperature did not coincide with the experimental data and in fact corresponded to an activation energy of 1.9 kcals/mole.

In both salts, Figures 4-5 and 4-6 show that within the accuracy of the data the shift in T_1 upon deuteriation is small. Now it was noted in section 4.2(c) that deuteriation has a large effect on ν_2, the bending mode, reducing from 652 cm^{-1} in $CsHCl_2$ to 480 cm^{-1} in $CsDCl_2$. Therefore it is

unlikely that this vibration should be responsible for the relaxation in this compound. For a similar reason this applies also to the tetramethylammonium salts.

(ii) Relaxation through lattice vibrations

In the absence of motions with relatively narrow frequency distributions the field gradient fluctuations arising from the time dependences of ionic positions, overlap covalency and induced dipoles resulting from lattice vibrations may constitute the relaxation mechanism. The major part of the spectrum of lattice vibrations occur at frequencies above that of the quadrupole interaction so that direct energy exchange between the spin system and the lattice vibrations does not occur to a great extent. However Raman-type processes, in which the difference between initial and final phonon frequencies is equal to the n.q.r. frequency are more effective than the direct process because phonons of all frequencies can take part.

The probability of this type of Raman process is proportional to $[(n_\omega + 1)\, n_\omega]$, where n_ω is the number of incoming phonons. Since ω_Q is small compared with the phonon frequency, $n_\omega \sim n_{\omega 1}$ so that the probability is proportional to $\frac{e^x}{(e^x-1)^2}$ since $n_\omega = (e^x-1)^{-1}$. $x = \hbar\omega/kT$ as before. In the high temperature approximation ie for small values of x it is possible to use the expansion

$$e^x \sim 1 + x \quad \text{so that} \quad \frac{e^x}{(e^x-1)^2} \sim \frac{1}{x^2} \quad \text{or} \quad \frac{k^2T^2}{\hbar^2\omega^2}$$

In this case T_1 is inversely proportional to T^2.

In Fig. 4-7 $^1/T_1$ is plotted against T^2 and there are two regions in which a squared dependence on temperature is seen to hold. These regions

Fig. 4-7 Graphs of $1/T_1$ against T^2.

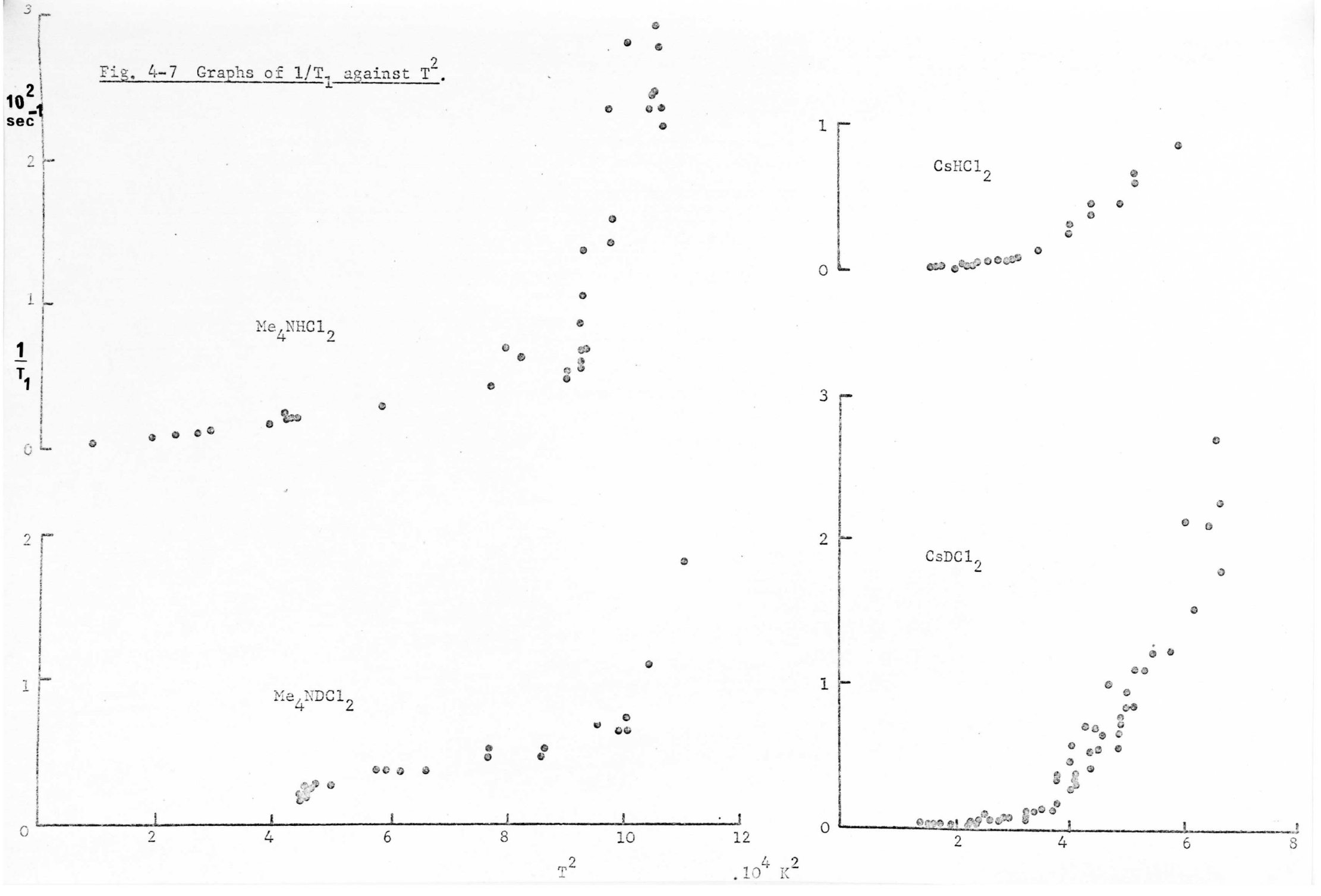

correspond to those in Figs 4-5 and 4-6 corresponding to energies of activation of 1-4 kcals/mole.

Thus the values for T_1 measured at temperatures below 250 K could in theory be explained by either a molecular torsional oscillator model or by relaxation via lattice vibrations. The fact that the torsional frequencies predicted by the relaxation data is inconsistent with measured molecular vibrational frequencies and also that a considerable deuteriation shift in T_1 values is not apparent from the measurements leads us to believe that lattice vibrations are probably responsible for this relaxation. An a priori calculation of the constants in the relation

$$\frac{1}{T_1} \propto T^2 (a - b/T^2) \qquad (12)$$

from the lattice phonon spectrum is extremely difficult and beyond our present concern.

(iii) Diffusion

Above 250 K, Fig. 4-6 shows that T_1 decreases dramatically with increase in temperature until it reaches the limiting value equal to T_2^*. In this situation the lifetime of the free induction decay is so short that for s.r.o. detection the signal has decayed before the next pulse is initiated, and so the signal is not detected. This happens with caesium hydrogen dichloride and deuterium dichloride. In this region of temperature and above, hydrogen chloride is lost from the sample at atmospheric pressure.

It is possible that this loss of hydrogen chloride is pre-empted by a diffusive motion of HCl molecules throughout the sample and this type of motion could be responsible for the large change in T_1 as the temperature is increased.

Figure 4-2 shows the unit cell of the Me_4NHCl_2 molecule as determined by Swanson and Williams [4.14]. It is seen that the symmetry connecting hydrogen dichloride ions is equal to the combination of a 180^o rotation plus a glide plane ie. a screw axis. Since a diffusive motion of the type described includes a rotational component to the motion we may apply the theory of relaxation through field gradient fluctuations generated by hindered rotations in the molecule. Such a theory has been used by Woessner and Gutowsky to treat the relaxation data in 2,2,dichloropropane which agrees with a model based upon field gradient fluctuations arising from reorienting methyl groups [1.10].

Hindered rotation is also a mechanism of relaxation in 1,2dichloroethane [1.10,1.11]. A quantitative theory for rotation has been developed by Lotfulin and Semin [4.34]. In this are derived expressions for the transition probabilities corresponding to $\Delta m = 1,2$ from which T_1 is given by the usual relation for spin $^3/2$ nuclei

$$\frac{1}{T_1} = 2(W_1 + W_2) \tag{13}$$

The general expression for the transition probability from state M to M-n is

$$W_{M,M-n} = \frac{1}{18\hbar^2} \left|(Q_{-n})_{M,M-n}\right|^2 \sum_m \left| P_{mn}(\cos\beta)e^{-im\gamma} \varphi'_m \right|^2 \frac{\sigma_n}{\sigma_n^2 + \omega_Q^2} \tag{14}$$

where $\sigma_n = \frac{1-\cos nX}{\tau_c}$

and $Q_2 = Q^*_{-2} = \frac{3}{2} P I_+^2$

$Q_1 = -Q_{-1} = \frac{3}{2} P[I_z I_+]$

$Q_o = \frac{\sqrt{6}}{2} P [3I_z^2 - I(I+1)]$

$I_\pm = I_x \pm iI_y$

$P = \frac{eQ}{I(2I-1)}$

$\varphi_{\pm 2} = \frac{1}{2} (\varphi_{xx} - \varphi_{yy}) \pm i\varphi_{xy}$

$\varphi_{\pm 1} = \mp \varphi_{xz} - i\varphi_{yz}$

$\varphi_o = \frac{\sqrt{6}}{2} \varphi_{zz}$

X = angle of rotation.

ω_Q = n.q.r. frequency (radian/sec).

For the $\Delta m = 1$ transition probability, n = 1 and $X = 180^\circ$ so $\sigma_n = \frac{2}{T_1}$ then the expression

$\frac{\sigma_n}{\sigma_n^2 + \omega_Q^2}$ reduces to $\frac{1}{2}$ $\frac{\tau_c}{1+(\frac{1}{2} \tau_c \omega_Q)^2}$

when the rate of rotation is slow compared with the n.q.r. frequency, ie $\omega_Q \tau_c > 1$, where τ_c is the lifetime in any one orientation, then this expression reduces further to $\frac{4}{\tau_c \omega_Q^2}$.

The full expression for W_1 is

$$W_1 = \frac{1}{18\hbar^2}\left(\cdot\ \frac{27}{16}\ e^2Q^2\right)\cdot\left(\frac{q^2}{4}\ \text{x}\ 0.398\right)\ \frac{4}{\tau_c\omega_Q}^2 \qquad (15)$$

using $2\omega_Q = \frac{eQq}{\hbar}$

$$W_1 = \frac{3.75}{\tau_c} \qquad (16)$$

For the $\Delta m = 2$ transition, $n = 2$ so that $\cos n X = 1$ therefore $1-\cos nX$ = zero. Therefore W_2 must also be zero, from equation (14).

Since $\frac{1}{T_1} = 2(W_1 + W_2)$ the expression for T_1 is

$$T_1 = \frac{\tau_c}{7.5} \qquad (17)$$

τ_c has the usual form of $\tau_c = \tau_o \exp(E/RT)$ so that a plot of $\ln T_1$ against $^1/T$ should have slope E/R and intercept ($\ln \tau_o$ - $\ln$ 7.5).

Fitting this expression to the T_1 data above 290 K for Me_4NHCl_2 gives a reasonable τ_o value of 1.53×10^{-10} secs. and an activation energy of 12.4 kcals/mole. This value of τ_o is consistentwith the assumption that $\omega\tau \gg 1$ for all temperatures within the range of measurement. The value of E must be the sum of the energies associated with a rotation and translational motion of an H-Cl molecule. This value would therefore be expected to be greater than that associated with the breaking of the hydrogen bond. The latter energy is likely to be in the region 4-7 kcal/mole, since these are the values of the heat of vaporisation of HCl and HF respectively. We should expect the hydrogen dichloride ion to have a bond energy within these limits, with a higher bond energy for the symmetrical structure.

When this theory is applied to all the data for the asymmetric dichlorides the following τ_o values and activation energies are predicted.

	τ_o(sec)	E_a(kcal/mole)		Temp range
Me_4NHCl_2	$1.53_{10}{}^{-10}$	12.4	>	290 K
	$2.6_{10}{}^{-2}$	1.1	<	290
Me_4NDCl_2	$2.35_{10}{}^{-10}$	12.2	>	290
	$1.3_{10}{}^{-2}$	1.38	<	290
$CsHCl_2$	$7.39_{10}{}^{-5}$	3.33		175-238
$CsDCl_2$	$8.42_{10}{}^{-6}$	4.13		182-278

Of these results only the T_1 data from Me_4NHCl_2 and Me_4NDCl_2 $\geq$ 290 K give sensible values of τ_o to provide an efficient relaxation mechanism. Also the energy involved with this diffusive motion is likely to be in excess of 4 kcals/mole. The rapid decrease in T_1 above 250 K in the caesium salt is most likely to be governed by this process. It is interesting to compare these results with those of a similar investigation on HCl and DCl.

In a study of quadrupolar coupling and relaxation of ^{35}Cl in the low temperature phases of HCl and DCl, Marram and Ragle discount the mechanism of classical reorientation of the molecular dipoles (H-Cl...H-Cl → H...Cl-H...Cl-) because this would result in a large temperature coefficient for ν_Q which was not observed [4.36]. There is a significant shift of T_1 to longer times on deuteriation which indicates that the proton mass or an inertial term is important in the molecular motion responsible for the relaxation. The motion is thermally activated with an energy of 2.7 kcal/mole in both

Text cut off in original

HCl and DCl. As the temperature is increased T_1 falls until it becomes equal to T_2^* (as in the present case). A minimum is predicted in T_1 at 2.5×10^{-5} sec. Mechanisms for relaxation based upon torsional oscillations and large amplitude reorientations are discounted because they predict correlation times that are too long by about 6 orders of magnitude. Marram and Ragle conclude that relaxation by some fluctuation in the intermolecular contribution to the field gradient is the most consistent with the experimental values of T_1. They postulate that the motion producing these fluctuations is a large amplitude dipolar reorientation, but that only a relatively quiescent fraction of the total sample is observed by n.q.r., especially at higher temperatures.

It may be that in the present case of the hydrogen dichloride anion the diffusive motion of HCl has an intermolecular effect on the field gradient of neighbouring hydrogen dichloride ions and that the quadrupole resonance is not observed in the ions in which diffusion is taking place. No T_1 isotope shift is observed because the motion does not only involve the proton, but the HCl molecule.

To summarise, then, it appears that in caesium and tetramethyl ammonium hydrogen dichlorides the T_1 measurements suggest that at lower temperatures, relaxation occurs by field gradient fluctuations due to vibrations of the lattice, and at higher temperatures (> 250 K (Cs^+) and > 300 K(Me_4N^+) near the dissociation temperature of the compound, the severe change in T_1 may be explained by diffusion of HCl molecules throughout the lattice.

(3) ^{35}Cl Spin Lattice Relaxation in caesium chloride, $^1/3$ hydronium dichloride and the deuteriated analogue.

The temperature dependences of the observed spin-lattice relaxation times in these salts are indicated in Figure 4-8. In both cases they clearly

FIG. 4-8

Temperature Dependence of T_1

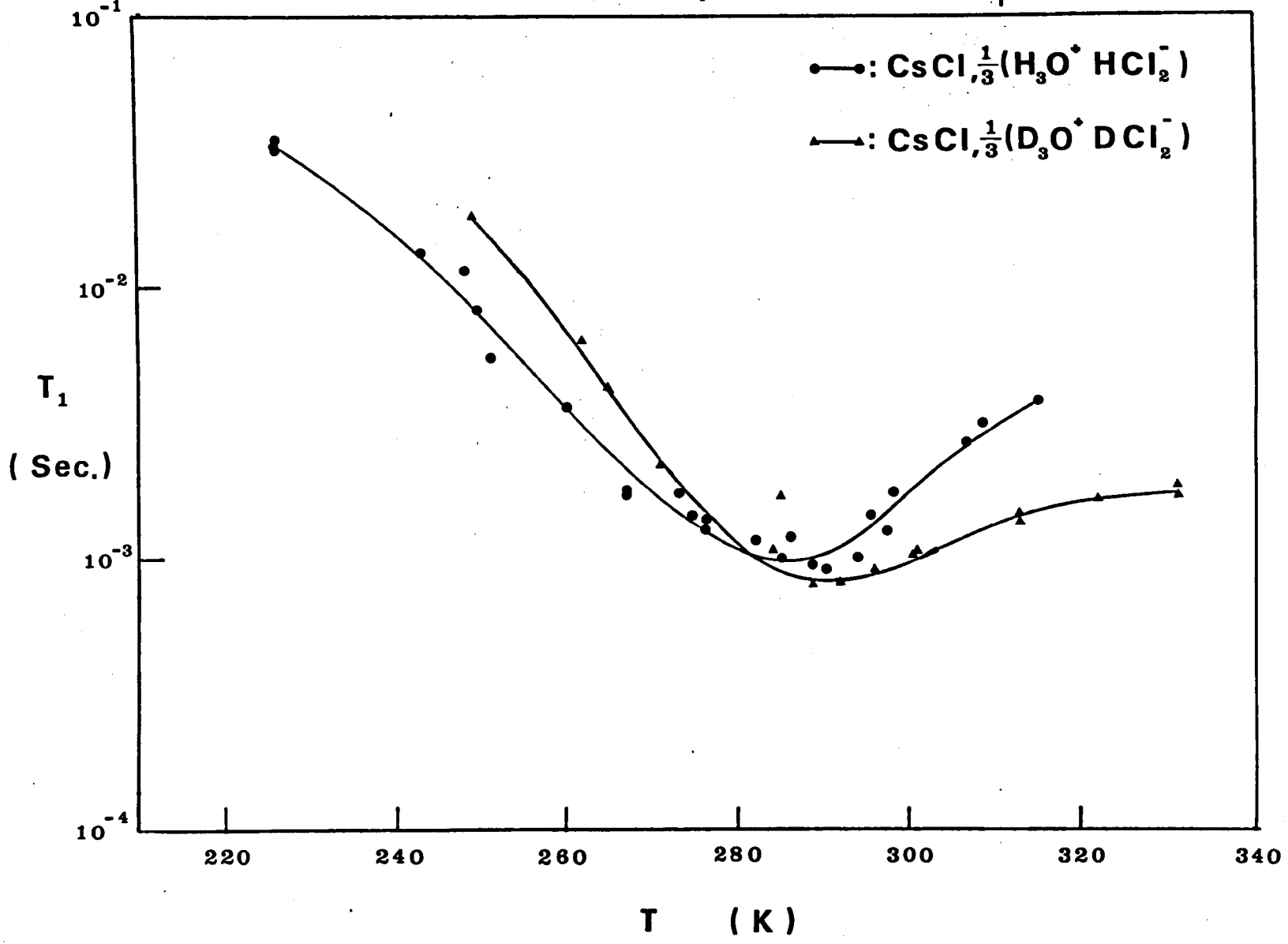

distinguish these salts from those discussed in the preceding section. An important feature is the appearance of an isotope shift in T_1 in these salts which are predicted to have symmetrically bonded hydrogen dichloride ions. On deuteriation the minimum in T_1 is shifted to a slightly higher temperature, and the activation energies governing the motions are changed. This deuteriation shift does not necessarily imply that the relaxation mechanism involves the central proton (or deuteron) in the hydrogen dichloride ion. Since the hydronium ion is also deuteriated, any fluctuations in field gradient generated by motion of this ion will also be subject to an isotope shift from which a shift in T_1 would follow. Of the various motions which are likely to account for relaxation effects, the torsional mode will have minimal effect since the moment of inertia of the hydrogen dichloride ion will be hardly changed on deuteriation and the torsional frequency is not expected to vary either. The bending mode frequency (ν_2) will change upon deuteriation - as will the inertial term. The Bayer theory for the HCl_2^- salt predicts a value for τ_a of 3.0×10^{-9}. For this motion to be a realistic model the excited state lifetime should be of the order of the inverse of the vibration frequency (4.2×10^{-12}sec).

Lotfulin and Semin have shown that a mechanism resulting from the fluctuating field gradients generated by the rotation of charged groups is most efficient in producing relaxation and in typical cases have calculated that a rotational mechanism, where this is geometrically feasible, produce a relaxation rate of up to three orders of magnitude greater than that from molecular angular motions [4.34].

The shift in the T_1 minimum to higher temperature on deuteriation is qualitatively consistent with a reorientational motion of the hydronium ions.

The activation energy for this motion, ie the barrier to rotation is obtained from a least squares fit to a logarithm plot of T_1 values on the low temperature side of the minimum, against reciprocal temperature. For the protonated salt, this activation energy is 8.06 $\pm$ 0.28 kcals/mole. and for the deuteriated salt, 10.50 $\pm$ 0.78 kcals/mole. Each hydronium ion is involved in three O-H...Cl hydrogen bonds so an estimate of the potential function barrier height is 2.69 $\pm$ 0.09 kcals/mole for the O-H...Cl bond, and 3.50 $\pm$ 0.26 kcals/mole for the O-D...Cl bond. We can compare these results with those from a proton spin lattice relaxation study of hydronium perchlorate [4.37].

In this compound the hydronium ion is also involved in three hydrogen bonds of average length (O-H...O) 2.66 Å and with internal angles of 115°. The barrier to rotation from the relaxation data is 4.8 kcals/mole. A phase transition due to the onset of hydronium ion reorientation occurs at 243 K., and this corresponds approximately to a minimum in T_1 at about 230 K. Hysterisis effects associated with the phase transition displace this minimum according to the direction of measurement. In the present compounds the minima occur at 285 K(H_3O^+) and 290 K(D_3O^+) respectively so it is not surprising that the measured activation energies for the rotational process are higher than that in hydronium perchlorate. Moreover the contraction from the sum of the Van der Waal's radii is greater (0.28Å) for the hydrogen dichloride salt than for the perchlorate salt (0.14Å).

Vibration spectra of the hydronium ion place ν_4, the degenerate bending mode, at 1600 cm^{-1} in hydronium perchlorate [4.38] and at 1700 cm^{-1} in the hydronium dichloride salt [4.19]. ν_2 is not well defined in the latter so a comparison is not possible. The only other band to be assigned in the low temperature phase of hydronium perchlorate is a band at 1021 cm^{-1} (223 K) which is believed to be due to a vibrational lattice motion of the hydronium ion.

This was not observed for the hydronium dichloride, possibly due to coincidence with the very broad ν_2 (500-1200cm^{-1}).

The variation of T_1 with temperature is rather similar to that recorded for ^{1}H spin-lattice relaxation in ammonium bromide and ammonium iodide in which reorientation of the ammonium group provides the relaxation mechanism [4.25]. It seems characteristic that the activation energy (slope) of the process is reduced after the onset of rotation, although theory predicts that the slopes on either side of the minimum should be equal since $\ln T_1 \propto \tau_c$ for $\omega_Q \tau_c \gg 1$, and $\ln T_1 \propto 1/\tau_c$ for $\omega_Q \tau_c \ll 1$.

Woessner and Gutowsky have derived an approximate theory for relaxation resulting from fluctuations in the external field gradient and have used this for treatment of their chlorine resonance results from 2,2dichloropropane in which methyl group rotation provides the relaxation mechanism. They assume an exponential form for the correlation function and derive

$$\frac{1}{T_1} = \frac{1}{12}\left(\frac{e^2Q^2}{\hbar^2}\right)\left[4\, V_{\mp 1}(0)\; V^*_{\mp 1}(0) + V_{\mp 2}(0)\; V^*_{\mp 2}(0)\right]$$

$$\left[\tau_c / (1 + \omega_Q^2\, \tau_c^2)\right] \qquad (18)$$

where $V_{\mp 1}(0)$ and $V_{\mp 2}$ are the temperature independent part of the transition inducing terms of the field gradient tensor. At the minimum point in T_1, $\omega_Q^2\, \tau_c^2 = 1$. so that

$$\frac{\tau_c}{(1 + \omega_Q^2\, \tau_c^2)} = \frac{1}{2\omega_Q} \qquad (19)$$

For an order of magnitude comparison of equation (18) with experiment, the expression in the first square brackets may be set equal to the square of a field gradient, eq' , which will be that generated by the rotational motion.

$$4 \quad V_{\pm 1}(0)\, V^{*}_{\pm 1}(0) \quad + \quad V_{\pm 2}(0)\, V^{*}_{\pm 2}(0) \quad = \quad (eq')^2 \qquad (20)$$

Since $\frac{e^2 Qq}{\hbar} = 2\,\omega_Q$, equation (18), when applied at the minimum point (T_1 = 1mS), becomes

$$\frac{1}{T_1} = 10^3 = \frac{1}{12} \quad \frac{\omega_Q}{(eq)^2} \quad (eq')^2 . \quad \frac{1}{2}$$

which gives an estimated value for eq' of 1.3% of the total field gradient, eq. This value appears reasonable in comparison with the value determined in 2,2dichloropropane of 6.5% from methyl group reorientation.

It is apparent from the crystal structure [4.9] that each chlorine atom in the hydrogen dichloride anion will have three nearest neighbour hydrogen atoms, each from different hydronium ions. Because of the disorder in the oxygen position in the hydronium ion chains (above or below a plane which bisects the hydrogen dichloride ion) there will be on average a net effect from only one hydrogen atom. From the molecular geometry this proton is 5.00Å from a dichloride chlorine, and angled at 78° from the axis of the hydrogen dichloride ion. The field gradient due to a charge e on the hydrogen atom is $e \left(\frac{3\cos^2 78 - 1}{125\text{Å}^3}\right) = -7.0 \times 10^{21}\ \text{cm}^{-3}$.

This would contribute to the n.q.r. frequency only +9.65 kHz. The contribution as calculated from the T_1 theory (1.3%) is 280 kHz. However the effect of an external charge on the chlorine field gradient will not only

be a direct one as calculated above. Two additional effects are important:

(1) a Lorentz field term, which results from the effect of the proton charge fluctuations on the charges on other ions in the lattice, for example Cs^+ or Cl^-. This is likely to be small, probably less than 2.

(2) The Sternheimer polarisation term (see Chapter 1).

Both (1) and (2) are not calculable in a straightforward manner, but Sternheimer factors are known to be large in ionic crystals (up to 100). Their overall effect could easily result in the 30-fold enhancement of field gradient, which is the difference between the calculated value and that derived from the measured T_1 value at the minimum position. An experimental estimate of the Sternheimer polarisation factor can therefore be obtained if an approximation is made for the Lorentz factor. Assuming the latter to be 2, this gives an estimated lower limit of -13.5 for the Sternheimer factor in this salt.

(c) Inverse Linewidth Parameter, T_2^*

The measured values of T_2^* in these dichlorides are given in Table 4.8. The large standard error is probably a consequence of the extremely short values (comparable with the pulse widths) and a non-negligible dead time. In addition the values were calculated from the best exponential fit, whereas the decay rate following the 90^o pulse, is not necessarily exponential.

Comparison of T_2^* values from linewidth measurements using s.r.o. detection compare reasonably with the values from the pulsed experiments. A comparison of the values at room temperature is shown overleaf.

	Approximate linewidth $\Delta\nu$, kHz.	$\frac{1}{\Delta\nu}$,μS.	Average T_2^* value from pulsed method. μS
$CsHCl_2$	40	25	15
$CsDCl_2$	42	24	31
Me_4NHCl_2	35	29	20
Me_4NDCl_2	40	25	27

The linewidth was measured from the separation of the first large "wings" to the signal, assuming the line shape to be approximately second derivative.

TABLE 4.8

	Temp (K)	T_2^*, μS.	
$CsHCl_2$	166	5.9	
	194	5.2	
	203	9.8	
	209	5.8	
	297	13.2	
	297	8.3	
	297	16.7	
	297	19.1	
	297	18.2	(σ = 3.6)
$CsDCl_2$	221	10.5	
	224	21.5	
	247	12.5	
	257	7.1	
	268	16.2	
	269	14.2	
	269	17.2	
	283	28.0	
	283	20.0	
	297	21.4	
	297	33.8	
	297	38.6	
	306	18.0	(σ = 7.7)
Me_4NHCl_2	77	10.7	
	228	18.9	
	228	17.5	
	279	18.9	
	279	16.2	
	301	24.2	
	301	21.5	(σ = 2.4)
Me_4NDCl_2	211	13.7	
	277	32.2	
	277	29.4	
	297	23.4	
	297	31.1	(σ = 6.8)

CHAPTER 5

A STUDY OF HYDROGEN BONDING IN HYDROGEN DI-CHLOROCARBOXYLATE ANIONS BY CHLORINE N.Q.R.

5.1 Introduction.

The acid salts of monobasic carboxylic acids form a large class of strongly hydrogen-bonded compounds, containing anions of the general formula $[RCOOH\cdots OOCR]^-$. As with hydrogen dihalide ions, the structure of the hydrogen bond can be of the symmetrical or asymmetrical form. In the present study the object has been to examine the n.q.r. spectra of such anions in which the group R contains a convenient quadrupolar nucleus, and from the spectra to assign the symmetry of the hydrogen bond. In the present case the most convenient nucleus instrumentally is ^{35}Cl so that hydrogen di-chlorocarboxylate anions are an obvious choice. The chlorine n.q.r. frequencies will be dependant upon the field gradient generated from the charge density on the nearest carboxylate group, which in turn is dependent upon the proton position in the hydrogen bond. Where this bond is clearly asymmetric, the proton is unequally divided between the two halves of the anion so that the n.q.r. spectrum, which responds only to the average proton position shows signals from both an acid and a carboxylate component.

It is to be expected also that the separation between the two groups of lines should be related to the degree of asymmetry of the hydrogen bond. Biedenkapp and Weiss have studied hydrogen di-trichloroacetate salts and in this way have predicted a symmetrical structure for the hydrogen bond in this anion [5.1]. The magnitude of the effect of the hydrogen bond on the n.q.r. frequency is of course small compared with that in the hydrogen dichloride ion where the field gradient is a direct consequence of the proton

position. In the acid salts, ν_Q is varied only through an indirect effect, acting via changes in charge density on neighbouring atoms of the carboxylate group. Even so, splittings of more than 1MHz are observed in some hydrogen dichlorocarboxylate anions.

X-ray structural studies of a number of acid salts of monobasic carboxylic acids by Speakman et.al. have been used to classify them into two groups. In both cases the hydrogen bonds are strong and are usually less than 2.5Å in length. In the Type A anion there is an element of symmetry at the mid-point between the two carboxylate groups. Speakman suggested that in this class where the carboxylate groups are crystallographically identical, the hydrogen bond is symmetrical [5.2]. Type B salts have crystallographically distinct carboxylate groups and this is apparent not only from the symmetry but also from their actual dimensions.

In the type A salts there appears to be more evidence in favour of a truly centred proton, rather than rapid proton tunneling between two equivalent asymmetric positions. Neutron diffraction data on a type A salt (potassium hydrogen di-aspirinate) shows a large thermal vibration of the proton along the H bond, and this has been interpreted as indicative of an anharmonic flat-bottomed single well potential function [5.3].

Proton magnetic resonance of potassium hydrogen bisphenylacetate and potassium hydrogen maleate gave weak, easily saturated signals in contrast to the strong and narrow line observed in KH_2PO_4 where proton tunneling is expected to provide a relaxation mechanism [5.4]. In the deuteriated species, the value of the deuterium quadrupole coupling constants also serves to differentiate them [5.5].

Most of the acid salts in the following series were prepared by Dr T.A. O'Shea using a method in which half an equivalent weight of the metal carbonate was used to neutralise a hot aqueous solution of the acid. After crystallisation,

excess water was removed under vacuum. Deuterium-substituted analogues were crystallised twice from deuterium oxide. The composition of the products were verified by elemental analyses [5.6]. Additional salts were prepared by the author, mainly for the series in Section 5.5, using a similar method.

In each of the following sections the n.q.r. spectra of each type of hydrogen dicarboxylate salt are discussed, with relevance to the particular hydrogen bond structure.

5.2 The Hydrogen Di-monochloroacetate Anion.

The ^{35}Cl n.q.r frequencies observed at 77 K in potassium, rubidium, caesium and ammonium hydrogen di-monochloroacetates are listed in Table 5.1, together with those of related compounds. A stick diagram is included for ease of comparison.

In the spectra of potassium and rubidium hydrogen di-monochloroacetates, two well separated lines are observed, both of which are intermediate in frequency between that of the free acid and that from the neutral salt. This widely separated doublet suggests an asymmetrically hydrogen bonded anion, HA_2^- consisting of distinct carboxylate and acidic portions, each of which gives rise to a single n.q.r. line. The infra-red spectra of these compounds similarly show features characteristic of both acid and salt [5.6]. The spectra are rationalised in terms of an asymmetric potential function with double non-equivalent minima, and proton tunneling is thought to be of low probability [5.6]. Since molecular vibrations are at a frequency much greater than that of the nuclear quadrupole precession frequency, the field gradient at the chlorine nucleus will be affected only by the average position of the proton, so that it is not possible to distinguish between a single minimum or double minima potential functions, if the latter is accompanied

by rapid proton tunneling. Two discrete n.q.r. signals are clearly consistent with the proton position (averaged over thermal vibrations) not centred in the hydrogen bond. Since the field gradient at the chlorine nucleus arises predominantly from the electrons in the C-Cl bond, the effect of the proton will contribute only a small part to the total field gradient and would be expected to act via the charge density on the neighbouring oxygen atoms. The second derivative of the potential arising from such charge will be

$$\frac{\partial^2 V}{\partial z^2} = \rho \int \left(\frac{3\cos^2\theta - 1}{r^3} \right) d\tau$$

where θ is the angle between the C-Cl bond and the element of charge, $d\tau$. The cubed dependence on the distance, r means that the nearest charge centres (oxygenatoms) to the chlorine nucleus will have the predominent effect. The angle θ will depend upon the conformation of the CH_2Cl group to the carboxyl plane. An approximate calculation indicates that whatever the conformation of this group the minimum value of θ is 56.5°, occuring when the C-Cl bond is perpendicular to the carboxyl plane. For values of θ greater than 55°, $\partial^2 V / \partial z^2$ is negative, so that an increase in oxygen charge density would be expected to decrease the chlorine n.q.r. frequency. In addition, the increase in oxygen charge density would reduce the chlorine frequency by a mechanism acting via polarisation of the C-Cl bonding electrons - an indirect effect. The frequency of the carboxylate salt would therefore be expected to be less than that for the free acid and this is observed experimentally. An increase in asymmetry parameter with increasing oxygen charge would also have a similar directional effect. Since the oxygen charge densities in the acid salt are expected to be intermediate between those of the simple salt and the free acid, the n.q.r. frequency is similarly intermediate.

TABLE 5.1

^{35}Cl QUADRUPOLE RESONANCE FREQUENCIES AT 77 K OF HYDROGEN DI-MONOCHLOROACETATES AND RELATED COMPOUNDS

	MHz	
$CH_2ClCOOH$	36.13, 36.43	
$CH_2ClCOOD$	36.15, 36.44	
$CH_2ClCOOK$	34.11	
$(CH_2ClCOO)_2HK$	34.79, 35.87	
$(CH_2ClCOO)_2DK$	34.62, 36.04	
$(CH_2ClCOO)_2HRb$ (1)	34.93, 35.72	intensity ratio 1:2 (a)
$(CH_2ClCOO)_2DRb$	34.61, 35.99	
$(CH_2ClCOO)_2HRb$ (2)	34.68	
$CH_2ClCOOCs$	35.10	
$(CH_2ClCOO)_2HCs$	34.97	
$(CH_2ClCOO)_2DCs$	34.95, 34.99	
$(CH_2ClCOO)_2HNH_4$	34.91, 35.13	(b)

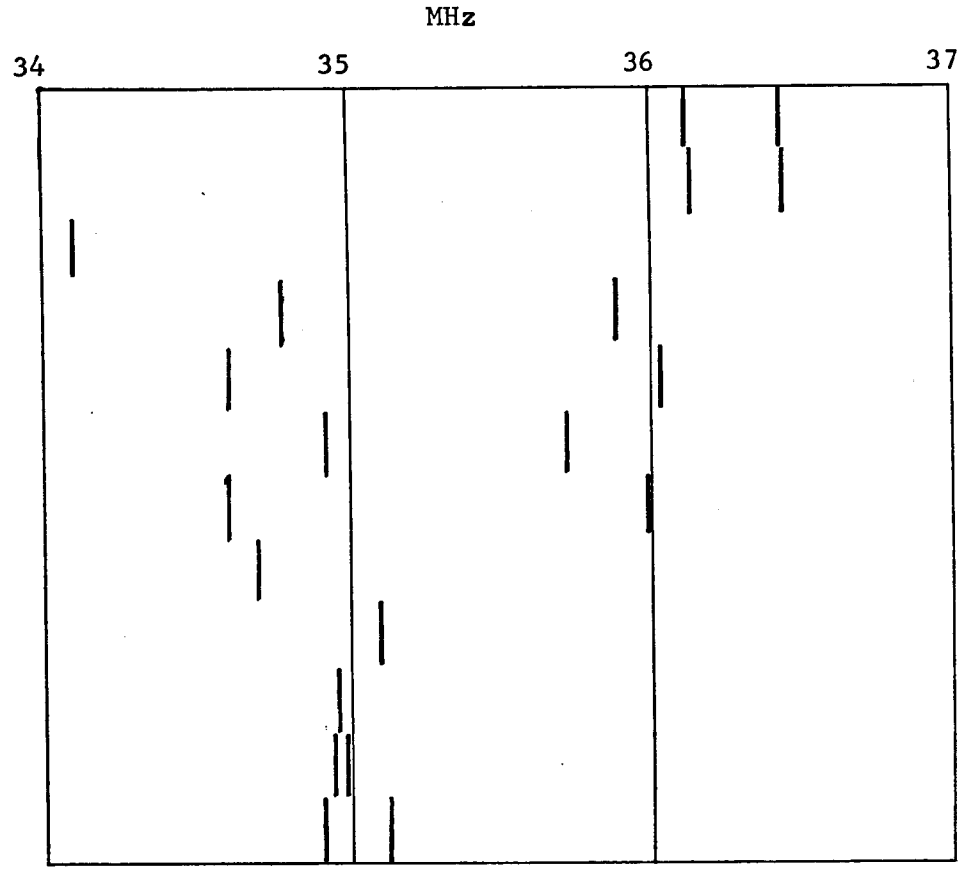

(a) most likely to have $H_2X_3^-$ structure. See text

(b) Sample provided by Dr J.C. Speakman

The spectra of these acid salts show an interesting isotope effect. Deuteriation causes a considerable increase in the line separation which can be rationalised in terms of the potential function assumed from the i.r. spectra [5.6]. The function has unequal double minima, formed from the superposition of two asymmetrical potential functions. The distribution of the proton between the two wells will change on deuteriation, the deuteron spending more time in the lower well. This results in an apparent contraction of the O-D bond relative to the O-H bond, when averaged over the vibrational states of the ion, making the hydrogen bond more asymmetric. The difference in oxygen charge densities on either side of the H bond correspondingly increases, and the chlorine n.q.r. frequencies are expected to follow this, as is indeed observed.

It follows therefore that the potassium hydrogen di-monochloroacetate falls into the type B category of Speakman for HA_2^- ions, in which the proton is not symmetrically located.

The rubidium salt appears to exist in several forms, since different samples gave different n.q.r. spectra. Sample (1) has a spectrum of two lines of unequal intensity at 34.93 and 35.72 MHz, the higher frequency (acid) line being the stronger. Sample (2) gave only a single line at 34.68 MHz (77 K). The neutral salt failed to give any signals so that it was not possible to check whether this line from sample (2) is in fact due to the presence of the neutral salt in the sample.

A frequency higher than this would be expected for a symmetrically-bonded acid salt. Potassium monochloroacetate has a chlorine resonance at 34.11 MHz and the caesium salt at 35.10 MHz, so that the frequency would seem appropriate to the rubidium neutral salt. A third sample appears to be a mixture of the two since all three signals appear. There is X-ray evidence that a rubidium acid salt of monochloroaceticacid can have the structure $H_2A_3^-$ instead of HA_2^-[5.7].

Such a structure would be consistent with the n.q.r. spectrum of sample(1) if the protons are associated mostly with the acid carboxylate groups.

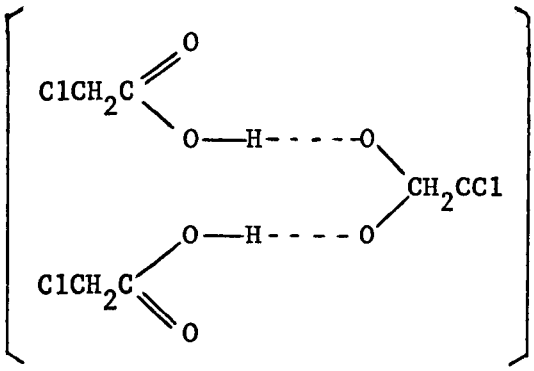

Such a structure might be expected to produce at least a small solid state splitting of the chlorine signals from the acid groups. The observed lineshapes of both lines are very complicated and it is not possible to definitely justify singlet structures. An elemental analysis of sample (1) is in closer agreement with $H_2A_3^-$ anion structure than with HA_2^-. Sample (2) however analysed closer to the stoichiometry of HA_2^-. The results of the analysis are given below:

	% Cl	% C	% H
Sample (1)	29.10	19.69	2.53
Sample (2)	25.63	17.35	1.86
Theoretical HA_2^-	25.93	17.56	1.84
Theoretical $H_2A_3^-$	28.90	19.59	2.19

The significant isotope shift noticed in sample (1) on deuteriation certainly indicates the asymmetry of the hydrogen bond. The splitting increases from 0.79 to 1.37 MHz. On the basis of n.q.r. evidence therefore it appears that sample (1) has the structure shown above*, but that of sample (2) cannot as yet be established.

* A very recent two-dimensional X-ray structure determination of a RbH_2A_3 salt indicates both $H_2A_3^-$ and symmetrical HA_2^- in the crystal [5.14]. The former ion is predicted to contain both an asymmetric and a centrosymmetric hydrogen bond. For this structure however, no appreciable n.q.r. deuteriation shift would be expected in the more intense line.

The chlorine n.q.r. spectrum of ammonium hydrogen di-monochloroacetate at 77 K shows also two lines, but the splitting is much smaller; 200 kHz, compared with 1.08 MHz of the potassium salt. The ammonium salt has in fact been found to be ferroelectric below 128 K [5.8].

A single crystal n.q.r. study by Yamamoto et al shows that the splitting rapidly decreases as the Curie point is approached, above which only one line is observed [5.9]. Differential thermal analysis showed the transition temperature to be sensitive to deuteriation, providing evidence that ordering of the protons in the hydrogen bonds is responsible for the ferroelectricity. It is suggested that the magnitude of the n.q.r. splitting may be directly proportional to the spontaneous polarisation [5.9]. A reduction in splitting with increased temperature is also observed for the rubidium acid salt. As in other type B salts, the splitting in the ammonium salt increases on deuteriation. In general the n.q.r. results for this salt are consistent with a double minimum vibrational potential function with a low barrier height of about 90 cm^{-1} (kT at 128 K) above the ground vibrational state. In such a system the O-O distance is expected to be short. An X-ray structure determination reported in [5.9] by personal communication from M. Ichikawa * gives this as 2.43Å, which is as short as many class A (symmetrically bonded) salts [5.2]. Alternatively a somewhat higher barrier to proton motion is also feasible provided that tunnelling occurs at a rate faster than ν_Q above the Curie point.

The same situation occurs with caesium hydrogen di-monochloroacetate. Only one signal is observed at 77 K so that both chlorine atoms in the anion must be crystallographically equivalent. The proton may be therefore either truly symmetrical, or rapid tunnelling may occur between two equivalent asymmetrical proton positions. On deuteriation little or no shift in ν_Q is apparent since the average position of the proton (deuteron) remains unaltered.

* Now reported in [5.15].

The lineshape also becomes more complex, indicative of a fine doublet structure. This splitting would be consistent with a low central barrier potential function ($\sim 55\ cm^{-1}$ - kT at 77 K).

If the conformation of the carbon-chlorine bond to the carboxyl plane is approximately constant throughout this series of monochloroacetate salts, then the magnitude of $\Delta\nu$, the splitting of the chlorine lines at 77 K predicts the following order of increasing hydrogen bond strength.

$$K < Rb < NH_4 < Cs.$$

This order is consistent with the results of the i.r. study by O'Shea [5.6].

5.3 The Hydrogen Di-dichloroacetate Anion.

The n.q.r. frequencies recorded at 77 K for KHA_2, KDA_2, $RbHA_2$, $RbDA_2$ (where A = $CHCl_2COO^-$), together with those of the neutral salt and acid KA and HA, are given in Table 5.2. In general the frequencies for the double salts fall between those of the acid and neutral salt, but the situation may be complicated by conformational effects. Conformational splitting of ν_Q arises from the differences in proximity of chlorine atoms in the same $CHCl_2$ group to the main centres of electron density, the oxygen atoms of the nearest carboxylate group. For example in the carboxylate ion, where oxygenatoms are equivalent this splitting is expected to be zero for conformation (1), and a maximum value for conformation (2).

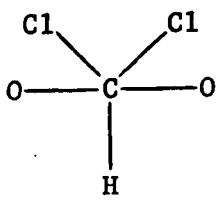

(1)

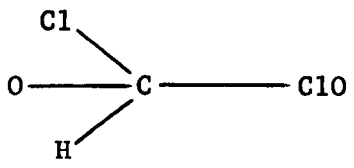

(2)

TABLE 5.2

^{35}Cl QUADRUPOLE RESONANCE FREQUENCIES AT 77 K OF HYDROGEN DI-DICHLOROACETATES

	MHz.
$CHCl_2COOH$	38.81, 37.98
$CHCl_2COOK$	36.40, 36.65
$(CHCl_2COO)_2HK$	36.98, 36.99
	37.50, 38.96
$(CHCl_2COO)_2DK$	36.87, 37.00
	37.68, 39.08
$(CHCl_2COO)_2HRb$	36.25, 37.71
	38.03, 38.72
$(CHCl_2COO)_2DRb$	36.16, 37.83
	38.22, 38.63

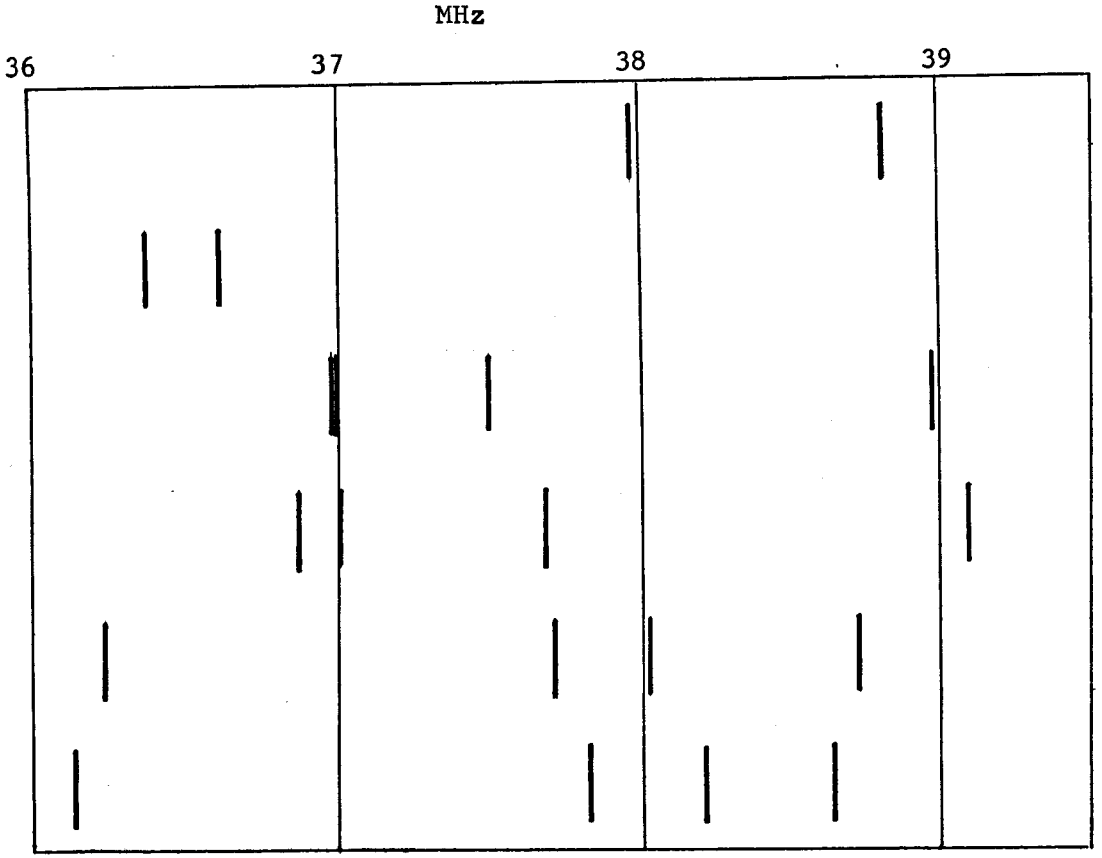

Solid state splittings may in addition be present so that without information of the symmetry within the unit cell it is not always possible to interpret the n.q.r data in terms of definite conformations. However, where the splitting is large (greater than 0.5 MHz) solid state effects can usually be discounted.

In potassium dichloroacetate, conformation (1) is excluded on evidence of the i.r. splitting of the two CCl_2 modes [5.6]. The observed n.q.r. splitting of 250 kHz, if not due to solid state splittings, would also favour an asymmetrical conformation, between that of (1) and (2). In KHA_2, a close doublet at lower frequency from the carboxylate half of the anion, would however suggest a conformation more like (1). In the infra-red the two CCl_2 modes are also close [5.6]. The other half of the anion may have an opposite conformation since the upper splitting is $\sim$ 1.5 MHz. Part of this splitting will arise from inequivalence of the oxygen charges. Rubidium hydrogen di-dichloroacetate shows a totally different n.q.r. spectrum. The carboxylate part of the anion (lower frequency lines) has a large splitting which favours conformation (2), and also agrees with i.r. results.

The effect of deuteriation on the n.q.r. spectra of these acid salts is not easily explained. In the previous section it was shown that whatever the conformation of the CH_2Cl group with respect to the rest of the anion, the frequency shift due to increasing electron density on the oxygen atoms is always in the same direction (ie. negative). This should be true also for the dichloroacetates. Therefore similar frequency shifts on deuteriation to those found in the hydrogen di-monochloroacetates are expected - an increased separation of the two groups of lines. This is observed in KDA_2 but not in $RbDA_2$. To maintain an increased separation between the two groups of lines it is necessary to assign the highest and lowest frequencies to chlorine atoms attached to the same carbon atom, and for the centre two lines

to correspond to chlorines in the acidic half of the anion. The former splitting is 2.4 MHz - a large value to attribute to only a conformational effect. In the alternative assignment in which the upper two lines (38.22 and 38.63 MHz) correspond to the acidic half of the anion and the lower two (36.16 and 37.83 MHz) to the carboxylate part, it is not evident why the splitting of the former should decrease and the latter increase on deuteriation - unless of course a conformational change takes place. If this is ruled out, then conformation (2) is most likely for the carboxylate part of the anion, in view of the very large splitting involved.

The present data indicates that no rotations of the $CHCl_2$ groups are taking place at frequencies comparable with or greater than ν_Q, in which case only one line per group might be observed, at a very much reduced frequency [5.10] The number of lines observed together with the considerable deuteriation shifts are consistent with the lack of a symmetry centre midway between oxygen atoms and therefore we can classify both potassium and rubidium hydrogen di-dichloroacetates as Type B salts in the Speakman classification.

5.4 The Hydrogen Di-trichloroacetate Anion.

The n.q.r. spectrum of rubidium hydrogen di-trichloroacetate (Table 5.3) differs from the spectra of the other rubidium hydrogen di-chloroacetates in two ways:

(1) The number of lines observed is only half that of the total number of chlorine atoms in the anion. In the monochloro- and dichloro-acid salts, two and four lines were observed respectively.

(2) There is negligible shift of ν_Q on deuteriation.

It follows from (1) that the trichloro groups in both halves of the anion must be crystallographically equivalent and therefore the hydrogen bond should

have a centre of symmetry. The same is true of the potassium salt [5.1]. O'Shea reports that the vibration spectra are also consistent with an anion of C_i symmetry, as is that of hydrogen di-trifluoroacetate [5.6].

The lack of a shift in ν_Q on deuteriation is to be expected from either a truly symmetrical hydrogen bond, or a bond in which rapid proton tunnelling occurs between two equivalent, asymmetrical proton positions. In either case the centre of maximum probability of the proton position will not change on deuteriation, provided that the tunnelling rate is greater than that of the n.q.r. frequency. In addition little change in the O····O distance is to be expected.

The three line spectrum arises from a fixed conformation of the CCl_3 group with respect to the carboxylate plane. Since the effect of charge on the oxygen atoms is to reduce ν_Q, a low frequency doublet and a higher frequency singlet is consistent with the following conformation, provided that the oxygen charges are comparable in magnitude.

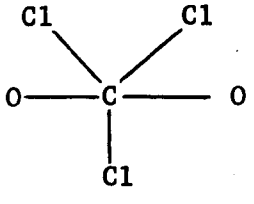

Since three distinct signals are observed at 77 K no rotation of the CCl_3 occurs at this temperature. Indeed three lines are observed up to 219 K in the potassium acid salt, as the results of Biedenkapp and Weiss show [5.1]. At this point the onset of hindered rotation could very well be responsible for the loss of signal.

On deuteriation of potassium hydrogen di-trichloroacetate there appears to be a fine splitting of the resonance lines. Although a slight proton impurity in the deuterated sample was suspected the line centres fail to

coincide with those measured in the KHA_2 sample. The effect is analogous to that found in caesium deuterium di-monochloroacetate, where again a fine splitting is observed. In terms of the proton tunneling model the effect is possibly attributable to a fall in the tunnelling rate below that of the n.q.r. frequency (3×10^7 Hz), or alternatively, to a reduction in the vibrational levels below the central barrier in the potential function.

5.5 Hydrogen Di-chlorobenzoate Anions

Since the chlorine atom in this type of ion is more remotely situated from the hydrogen bond than in previous anions the difference in ν_Q between the salt and the corresponding acid is smaller. The n.q.r. spectrum still provides symmetry information for each half of the anion. Table 5.4 gives the n.q.r. frequencies for series of ortho, meta, and para-substituted hydrogen dichlorobenzoates. Frequencies of the corresponding acids and neutral salts are also given for comparison. As previously, the frequency for the acid salt lies between that of the acid and the neutral salt.

The single line evident in the spectra of potassium, rubidium and ammonium hydrogen di-parachlorobenzoates is indicative of a symmetrical hydrogen bond - a Type A structure. The signal from the rubidium salt which was observed at room temperature also showed a narrowing of the line at the higher temperature ($\Delta\nu$ = 60 kHz at 77 K, 130 kHz at 298 K). The lineshapes at 77 K are certainly complicated and this may be an indication that the ground vibrational state is comparable with the height of the central potential barrier, ie. the line is starting to split. However, broadening of the line due to relaxation effects alone cannot be ruled out. The X-ray structure by Mills and Speakman shows the hydrogen bond in the potassium to be strong and short (O-O distance 2.457Å) and the centre of symmetry at the bond centre classifies the anion as Type A [5.11]. The ammonium and rubidium salts are also said to be isomorphous with the potassium salt.

TABLE 5.3

^{35}Cl QUADRUPOLE RESONANCE FREQUENCIES AT 77 K OF HYDROGEN DI-TRICHLOROACETATES

	MHz
CCl_3COOH	39.97, 40.16, 4Q24
$CCl_3COOLiH_2O$	38.37, 38.47, 39.12, 39.22,39.85*
$(CCl_3COO)_2HK$	39.11, 39.15, 39.75
$(CCl_3COO)_2DK$	39.06, 39.12,39.17,39.68,39.76
$(CCl_3COO)_2HRb$	39.11, 39.22, 40.18
$(CCl_3COO)_2DRb$	39.12, 39.22, 40.18
CCl_3COOK	-
CCl_3COORb	-

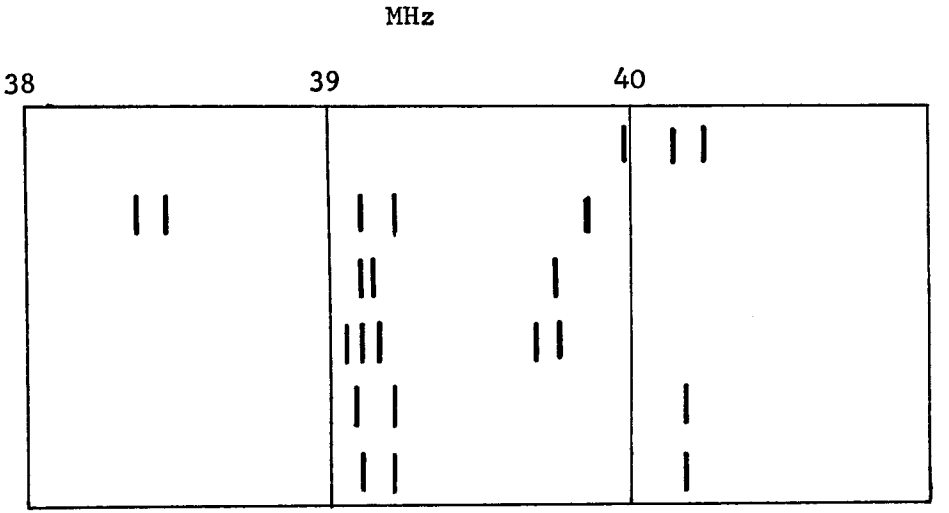

* The high frequency line is possibly a doublet. The six lines therefore agree with two molecules in the asymmetric unit as found in the crystal structure [5.13]. In [5.1] eight lines were found using a frequency-modulated spectrometer.

The singlet evident in the n.q.r. spectrum of potassium hydrogen di - metachlorobenzoate suggests that it too has the Type A symmetrical structure.

The anomalous frequency from p-chlorobenzoic acid, which is lower than that in the neutral salt may be attributable to a mesomeric effect in which the C-Cl bond can possess a degree of π character.

The n.q.r. spectra of potassium hydrogen di-ortho-chlorobenzoate appear to differentiate it from the para-and meta- substituted salts. The two widely-separated lines possibly indicate that the anion exists in acidic and carboxylate forms simultaneously, consistent with a Type B hydrogen bond structure in which the proton is not symmetrically located. The rubidium salt shows a doublet at 77 K but at frequencies very close to that of the free acid. The weaker of these (36.36 MHz) is probably due to a free acid impurity in the sample. The frequency of the remaining line is too high to be attributable to a Type A structured anion and it is more likely to be due to the acidic half of a Type B anion. The line from the carboxylate half of the anion has not been detected however. Similarly no signal was observed from rubidium ortho-chlorobenzoate.

The appearance of line multiplicity in ammonium ortho-chlorobenzoate at 77 K which does not exist at room temperature suggests a phase change associated with the onset of rotation of the ammonium ion. It is unfortunate that the ammonium acid salt failed to give an n.q.r. spectrum.

5.6 The Hydrogen chloromaleate and Hydrogen dichloromaleate Anions.

The hydrogen chloromaleates are examples of intra-molecularly hydrogen-bonded salts. The hydrogen bond in potassium hydrogen chloromaleate has been identified by neutron diffraction to contain a symmetrically located hydrogen atom - even though the oxygen atoms are chemically and crystallographically distinct [5.12]. In this respect they differ basically from the previous symmetrically-bonded acid salts.

The widely separated doublet in the spectrum of potassium hydrogen dichloromaleate indicates that the crystal environments of the two chlorine atoms are not identical and that the structure probably contains non-equivalent oxygen atoms as in the monochloromaleate. However, the hydrogen bond remains symmetrical, as is evident from the lack of a deuteriation shift in the n.q.r. spectra. Also the doublet frequency is almost exactly midway between that of the neutral salt and the acid (see Table 5.5). The single line (at 37.72 MHz) for potassium hydrogen chloromaleate is to be expected from the crystal structure in which only one chlorine crystal site is evident [5.12]. N.q.r frequencies given in this chapter which relate to compounds included in the vibration spectra study by O'Shea have been previously reported in [5.6].

TABLE 5.4

^{35}Cl QUADRUPOLE RESONANCE FREQUENCIES OF CHLOROBENZOATES, MHz.

	Room temp	77K	
p-ClC_6H_4COOH	34.24	34.68	
" K		35.48	
" NH_4	34.87	-	(34.92 at 285 K)
" Rb	34.88	35.29	
(")$_2$HK		35.39	
(")$_2$$HNH_4$		35.18	
(")$_2$HRb	34.79	35.30	
σ-ClC_6H_4COOH	35.65	36.31	
" D		36.31_5	
" K	34.13	-	
" NH_4	34.48	35.05, 35.18, 35.27	
" Rb	-	-	
(")$_2$HK		35.35, 36.22	
(")$_2$HRb	35.54	36.04, 36.36vw	
(")$_2$$HNH_4$	-	-	
m-ClC_6H_4COOH		35.23	
" K		34.74	
(")$_2$HK	34.53	34.88	

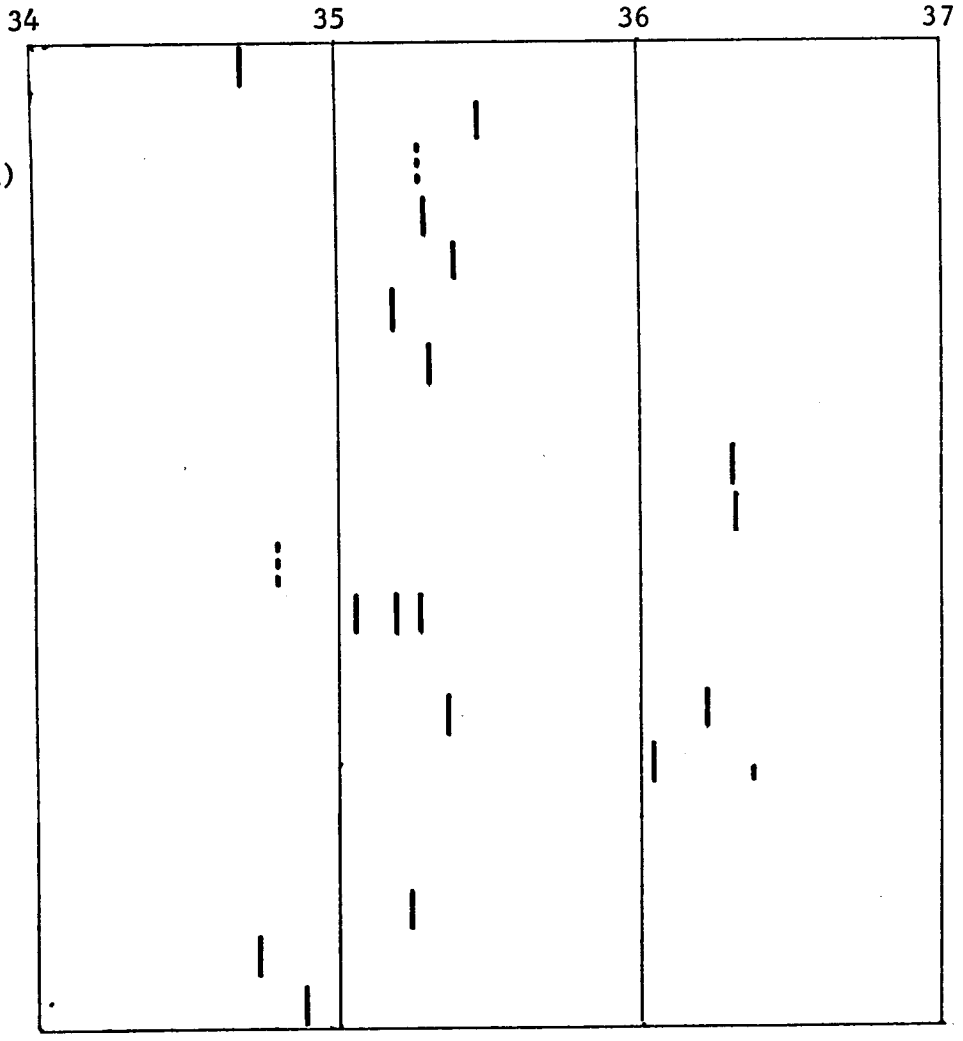

(Dotted lines in the chart indicate values extrapolated to 77 K)

TABLE 5.5

^{35}Cl QUADRUPOLE RESONANCE FREQUENCIES AT 77 K OF CHLORO- AND DICHLOROMALEATES, MHz.

Dichloromaleic acid	37.69, 38.14
Potassium dichloromaleate	35.48, 35.98
Potassium hydrogen dichloromaleate	36.59, 37.17
Potassium deuterium dichloromaleate	36.58, 37.17
Potassium hydrogen chloromaleate	37.72
Dichloromaleic anhydride	37.98, 38.05
Chloromaleic anhydride	37.16

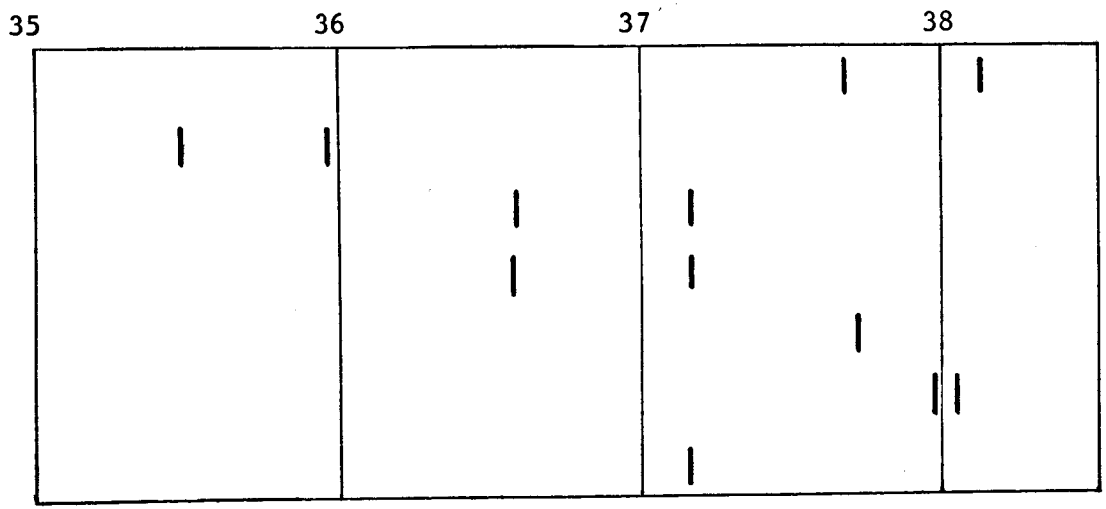

CHAPTER 6

CHLORINE QUADRUPOLE RESONANCE IN MIXED LIGAND OCTAHEDRAL COMPLEXES.

6.1 General.

N.q.r. studies of halogen ligands attached to transition metals have been mostly confined to ions of the type MX_6^{2-} [6.1] and MX_4^{2-}[6.2]. In the present study, the complexes are of the form trans-L_2MCl_4 where M is a number of third row transition metals, and the complex L_3IrCl_3, affording the opportunity of studying the cis- and trans- influence of a variety of ligands and the effect of the changing electronic configuration of the transition metal on the ^{35}Cl n.q.r. frequency. The complexes were prepared and kindly provided by Dr B. Bell and Prof. J. Chatt and were particularly suitable because the structures of identical or similar complexes have been determined recently [6.3]. Details of their preparation are given in [6.4].

The n.q.r. spectra were recorded as usual on the Decca prototype spectrometer. The L_2MCl_4 complexes showed a reduction in signal intensity as the temperature was lowered and searches were therefore normally carried out at room temperature. The response from the Ir(III) complex was more normal, in that stronger resonances were obtained at 77 K. Unfortunately not all the complexes examined gave detectable n.q.r. signals for example, all attempts to find a signal from $[(PEt_3)_2IrCl_4]$ were unsuccessful. Possibly the paramagnetism of iridium(IV) (d^5) may have been responsible for this, but on the other hand the Re(IV) complex (d^3) gave signals. Searches on the following complexes were also unsuccessful: mer-$(PEt_3)_3OsCl_3$ (d^5) mer-$(PEt_2Ph)_3IrCl_3$(d^6), fac-$(PEt_3)_3IrCl_3$(d^6),

mer-$(PEt_2Ph)_3ReCl_3(d^4)$, trans-$(PEt_3)_2WCl_4(d^2)$, trans-$(EtCN)_2MoCl_4(d^2)$.

Table 6.1 lists the chlorine-35 n.q.r. frequencies observed in the complexes trans-L_2MCl_4 (M = Re, Os, Pt; L = PEt_3, PEt_2Ph, $AsEt_3$) and in mer-$(PEt_3)_3IrCl_3$, at three different temperatures. The values in the first column are those at the lowest observable temperature or at 77 K, and in columns 2 and 3 are the values at ambient and above ambient temperatures. The latter were obtained by means of a hot oil bath surrounding the sealed probe unit. The temperature in this case was monitored by a Cu/Constantan thermocouple with a pre-calibrated Philips automatic measuring bridge (PR2210U). Temperatures are accurate to $\pm$ 1 K. The temperature dependences of the transition frequencies were obtained using both the warm-up technique (see Chapter 3) and also constant temperature slush-baths. N.q.r. frequency versus temperature plots are shown in Fig. 6-1 to 6-6 for each of the complexes studied.

There is evidence of a low temperature phase transition in trans-$(PEt_3)_2OsCl_4$ (see Fig. 6-2). At temperatures above 100 K two lines were detected, indicating two crystallographically distinct chlorine sites in the unit cell. Since the room temperature structure has two molecules per unit cell, all four chlorine atoms in the molecule are equivalent. However at 77 K the spectrum shows further splitting, due presumably to non-equivalence of two of the equatorial chlorine atoms. No phase transitions are evident from the spectra of the other complexes in the temperature ranges studied.

FIG. 6-1. Temperature dependence of the ^{35}Cl n.q.r. frequencies in trans-$(PEt_3)_2ReCl_4$.

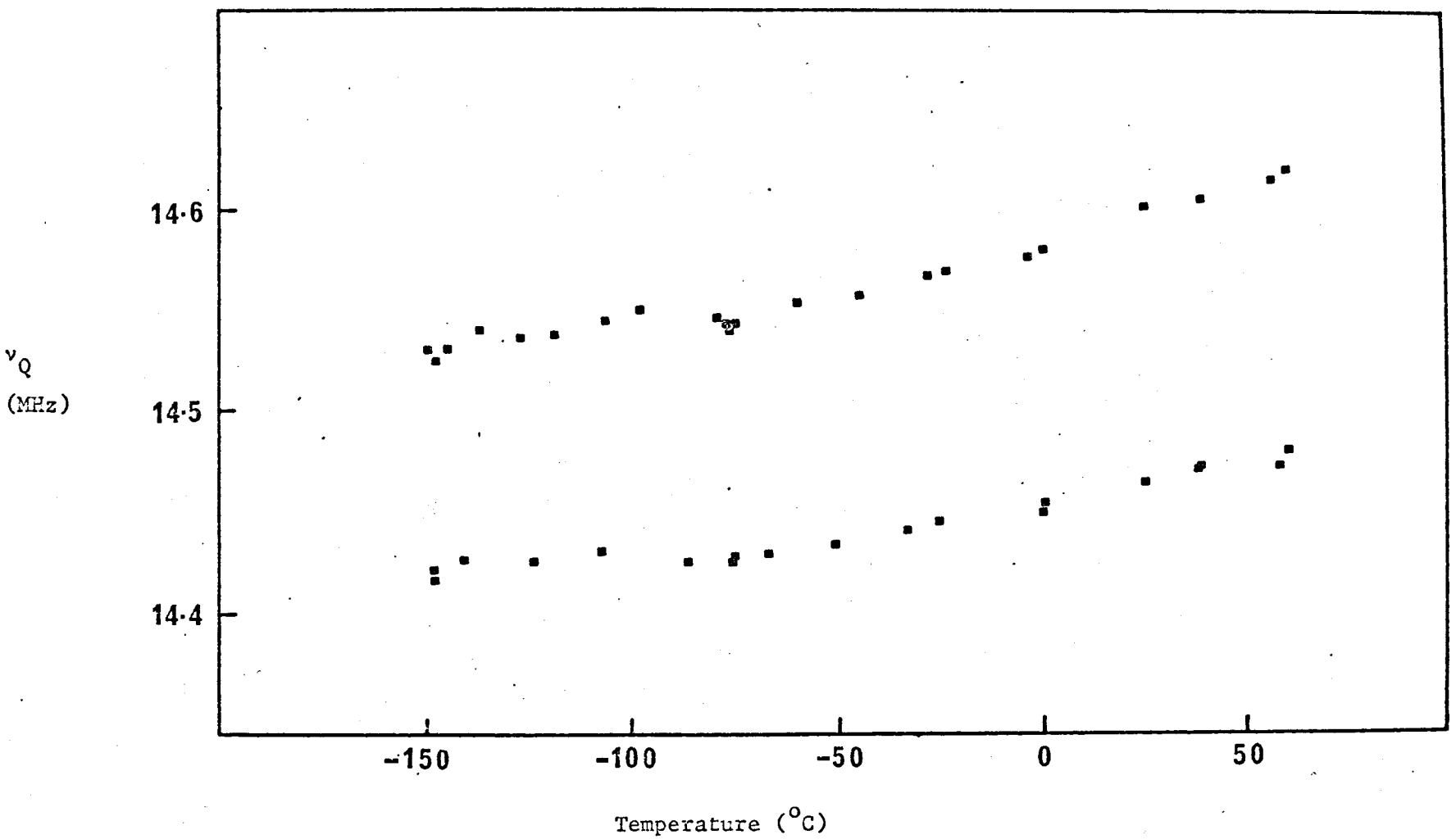

FIG 6-2. Temperature Dependence of the ^{35}Cl n.q.r. frequencies in trans-$(PEt_3)_2 OsCl_4$.

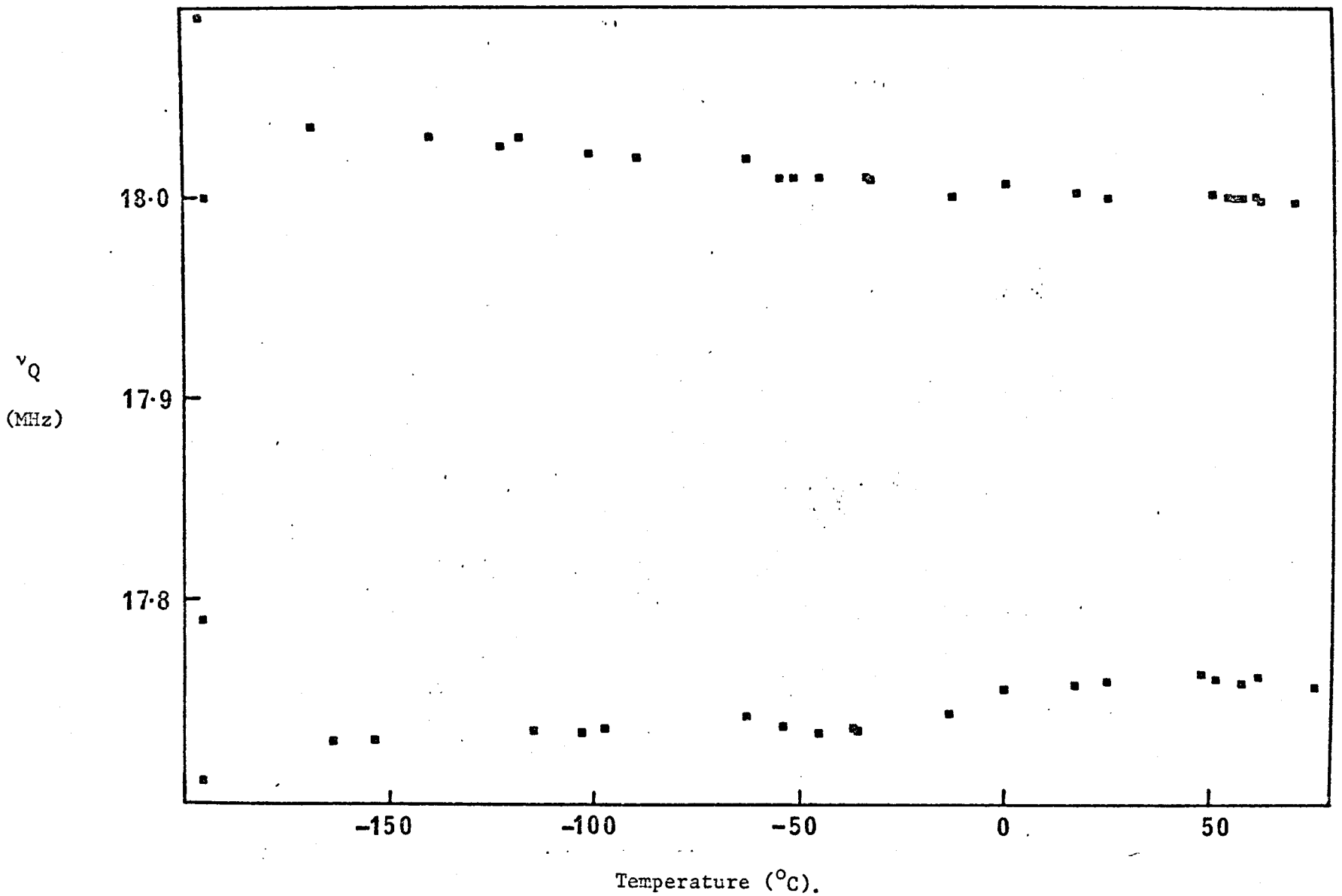

FIG. 6-3 Temperature dependence of the ^{35}Cl n.q.r. frequencies in trans-$(PEt_2Ph)_2OsCl_4$.

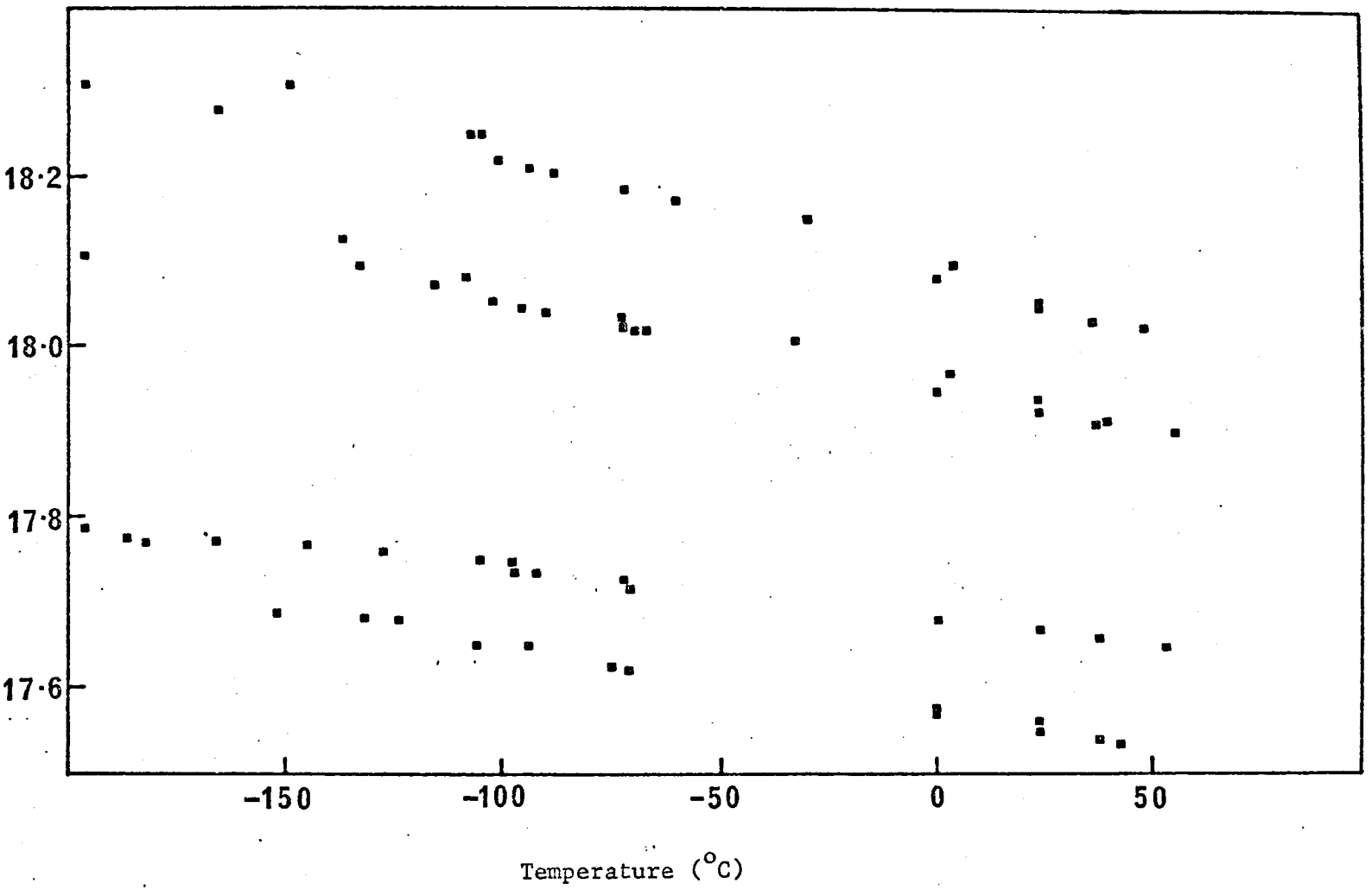

FIG 6-4. Temperature Dependence of the ^{35}Cl n.q.r. frequencies in trans-$(AsEt_3)_2OsCl_4$.

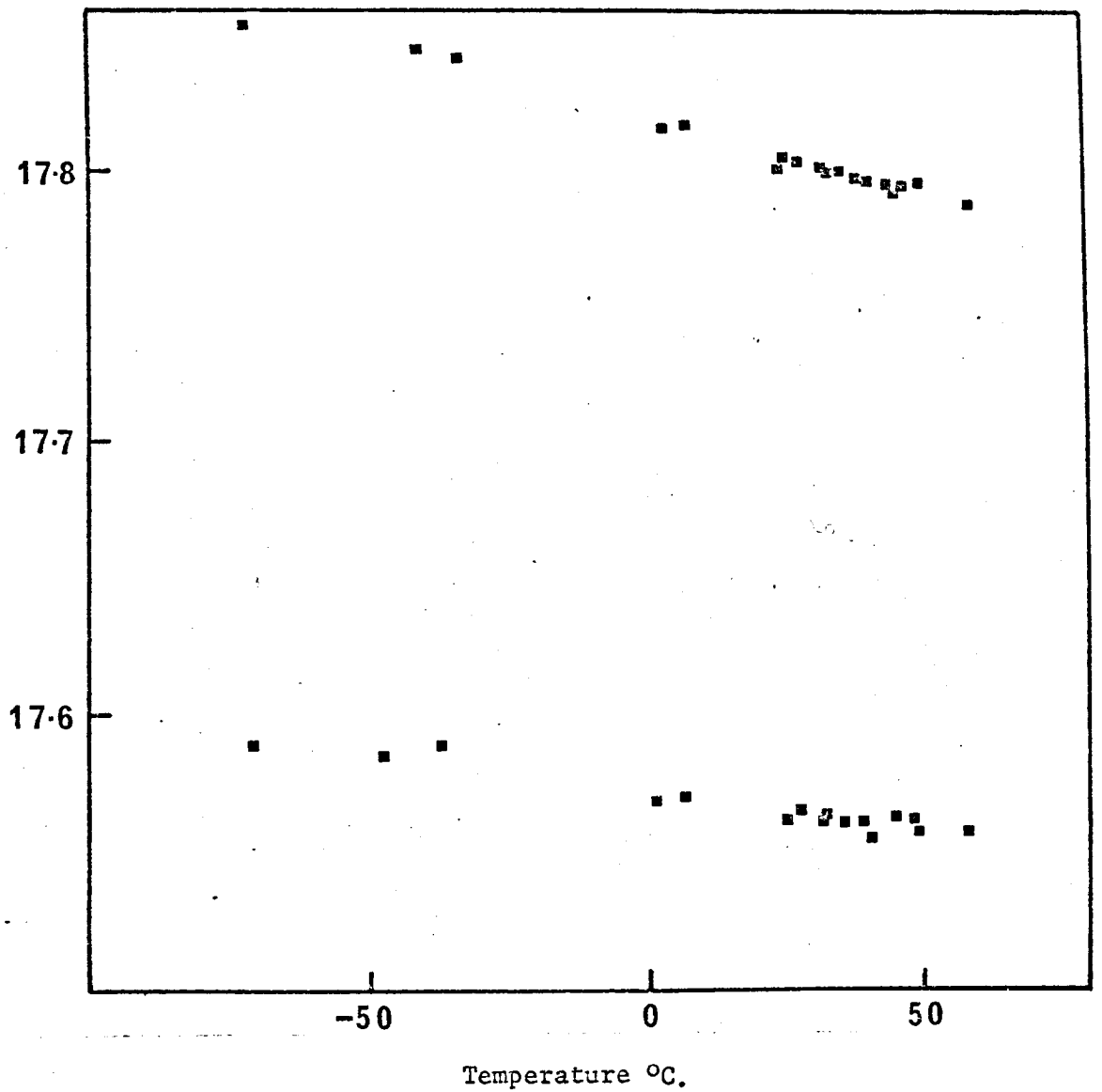

FIG 6-5. Temperature Dependence of the ^{35}Cl n.q.r. frequencies in trans-$(PEt_3)_2PtCl_4$.

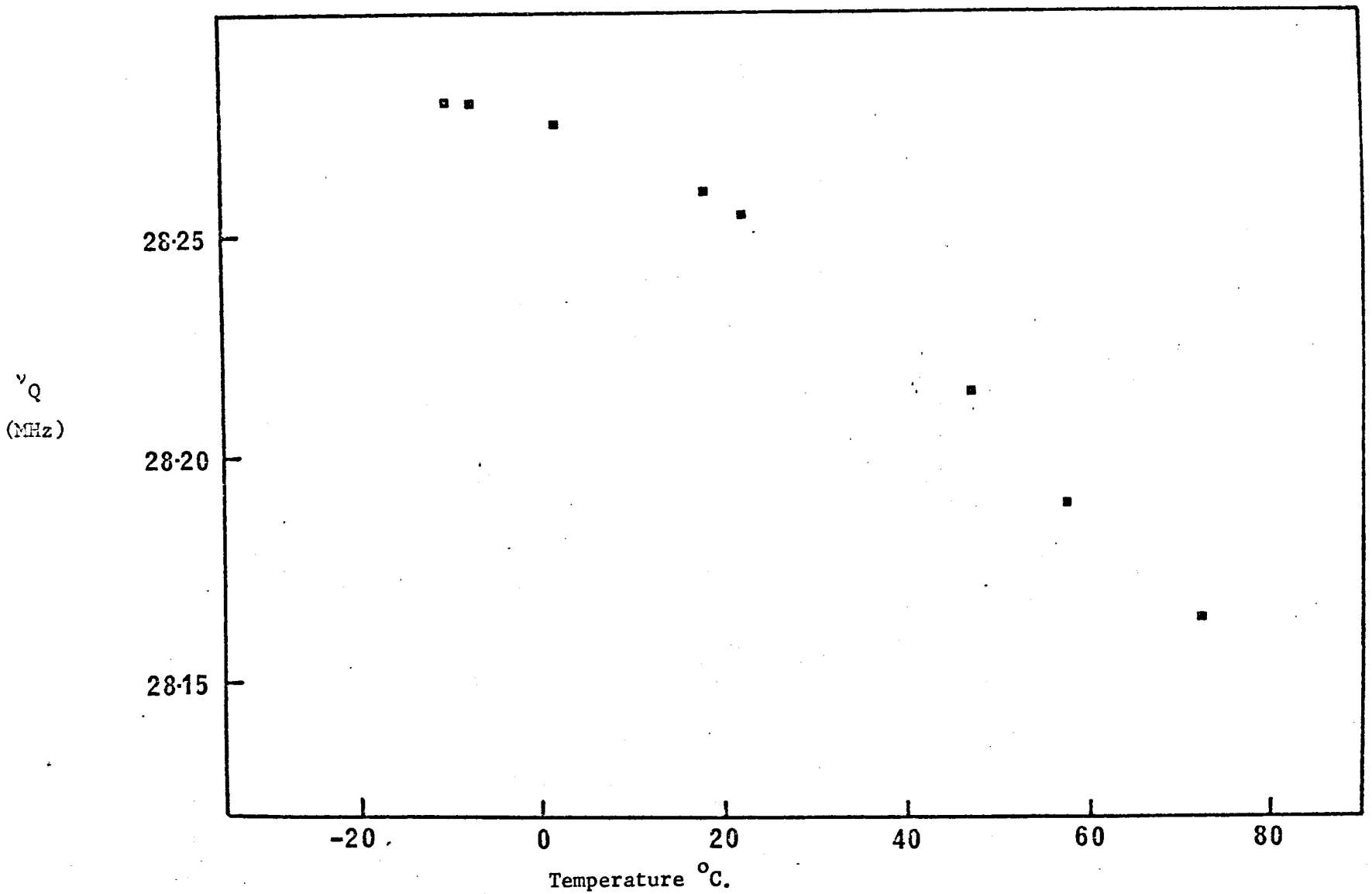

FIG 6-6. Temperature Dependence of the ^{35}Cl n.q.r. frequencies in mer-$(PEt_3)_3IrCl_3$.

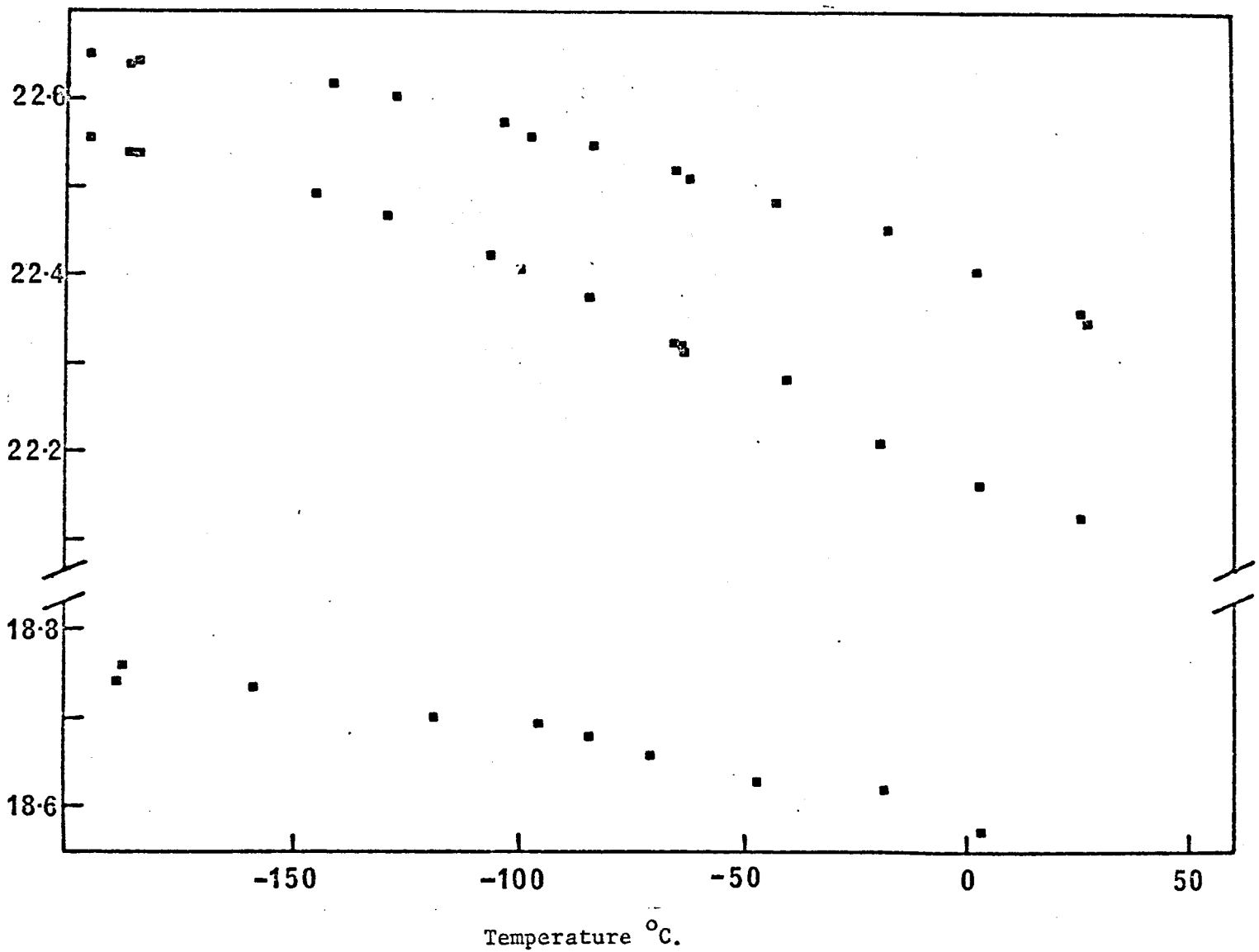

TABLE 6.1

^{35}Cl NQR FREQUENCIES OBSERVED IN TRANS-$[L_2MCl_4]$ COMPLEXES AT TEMPERATURES BELOW ABOVE AND AT AMBIENT.

	Low Temp. K	ν_Q MHz	Ambient Temp. K	ν_Q MHz	High Temp. K	ν_Q MHz
$(PEt_3)_2ReCl_4$	125	14.42	293	14.46_5	333	14.48
	127	14.53	"	14.60	"	14.62
$(PEt_3)_2OsCl_4$	77	17.71				
	"	17.79	296	17.76	349	17.76
	"	18.00	"	18.00	344	18.00
	"	18.09				
$(PEt_2Ph)_2OsCl_4$	77	-	297	17.56	316	17.54
	"	17.78	"	17.67	326	17.66
	"	18.10	"	17.92_5	328	17.90
	"	18.31	"	18.05	321	18.02
$(AsEt_3)_2OsCl_4$	201	17.59	297	17.57	331	17.56
	"	17.85_5	"	17.80_5	"	17.79
$(PEt_3)_2PtCl_4$	263	28.28	295	28.25_5	345	28.16_5
L_3MCl_3						
mer-$(PEt_3)_3IrCl_3$	77	18.74	297	18.55		
	"	22.55	"	22.13		
	"	22.65	"	22.35		

6.2 The Resonance Frequencies.

Table 6.2 shows a comparison of the present n.q.r. data with those for the corresponding K_2MCl_6 series reported in [6.1].

TABLE 6.2

COMPARISON OF NUCLEAR QUADRUPOLE RESONANCE FREQUENCIES IN K_2MCl_6 AND TRANS-L_2MCl_4 COMPLEXES

(MHz at room temperature)

M	K_2MCl_6	trans-L_2MCl_4	$\Delta\nu$
W	10.22	-	-
Re	13.89	14.47, 14.60	+0.64
Os	16.84	17.76, 18.00	+1.04
Ir	20.73	-	-
Pt	25.82	28.26	+2.43

The effect of the cation on the n.q.r. frequency is fairly small and a series of $PtCl_6^{2-}$ salts all have values within $\pm$ 3% [6.1]. In both MCl_6^{2-} and the trans-L_2MCl_4 series there is an expected increase in covalency in the metal-chlorine bond (increase in ν_Q) from tungsten to platinum. Furthermore the bond covalency is greater in the mixed ligand complex for the same metal atom; that is, replacement of chlorine by a phosphine ligand increases the covalency of the cis-bond.

In the meridional Ir(III) complex there are two chlorine atoms trans to each other and a chlorine atom trans to a phosphine (Figure 6-7). The doublet at 22.2 MHz is assigned to the former and the lower line at 18.5 MHz to the latter [6.5]. As before, the chlorines cis to phosphine are at a higher frequency than those in $IrCl_6^{2-}$, and also the frequency of the chlorine trans to the phosphine is lowered by a corresponding amount, i.e. the ionic character of that Ir-Cl bond has increased. The n.q.r. frequency of a chlorine atom cis to a ligand L is therefore a measure of the cis-influence of that ligand, and similarly a trans-placed chlorine atom can measure trans-influence. In Tables 6.1 and 6.2 the osmium series of complexes provide the following order of increasing cis-influence.

$$Cl < AsEt_3 < PEt_2Ph < PEt_3 \qquad \text{(See Fig. 6-8)}$$

Covalency of the Os-Cl bond cis to the Os-L bond is increasing from left to right. The order correlates with reactivity studies on the rate of replacement of chlorine in trans-L_2PtCl_2 by weak nucleophiles where the reaction rates increase in the order [6.6]:

$$L = PEt_3 < AsEt_3 < \text{pyridine}$$

The same trend is observed in the n.q.r. of trans-L_2PdCl_2 complexes (illustrated in Fig. 6-9) and is taken to be the order of their electron donating power [6.7].

This trend still continues when the central metal atom is changed (Fig. 6-10). If the σ donorability of the ligand is estimated by a parameter, Δr, the difference between the observed M-L bond length and the sum of the covalent radii, then as the σ donor properties of a ligand

FIG. 6-7

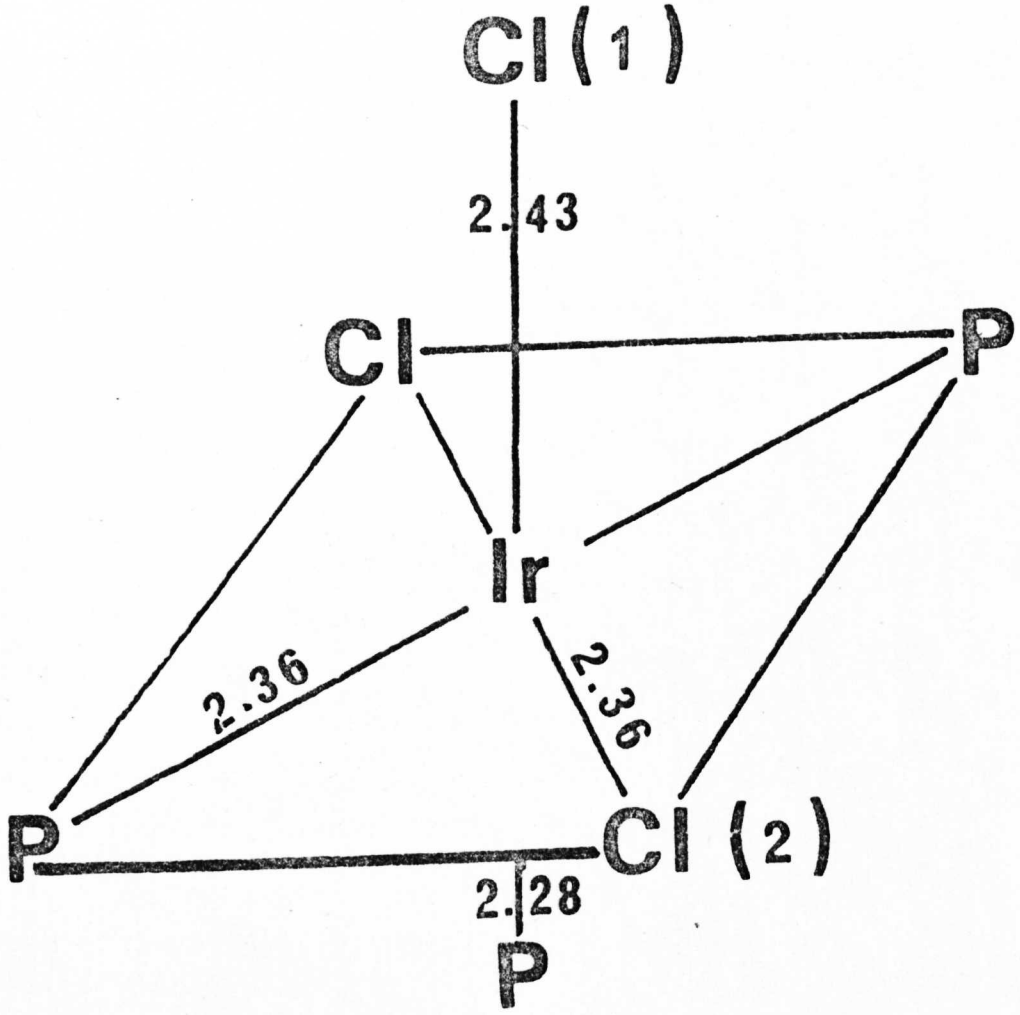

$\nu(1)$: 18.55 MHz.

$\nu(2)$: 22.11, 22.35 MHz.

Text cut off in original

FIG.6-8

Effect of Ligand on ν_Q in trans $OsCl_4L_2$

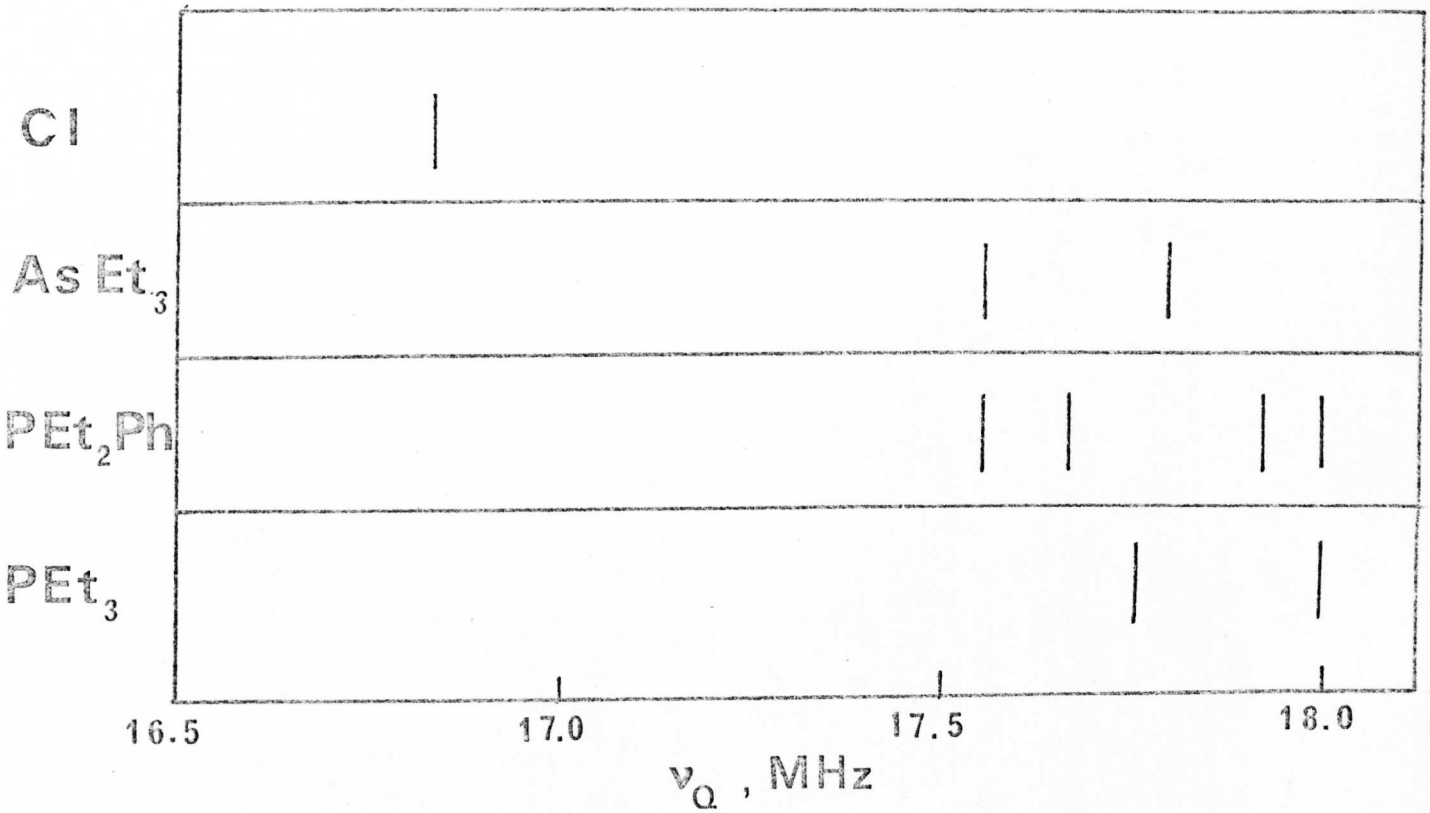

FIG.6-9

ν_Q in trans $PdCl_2L_2$

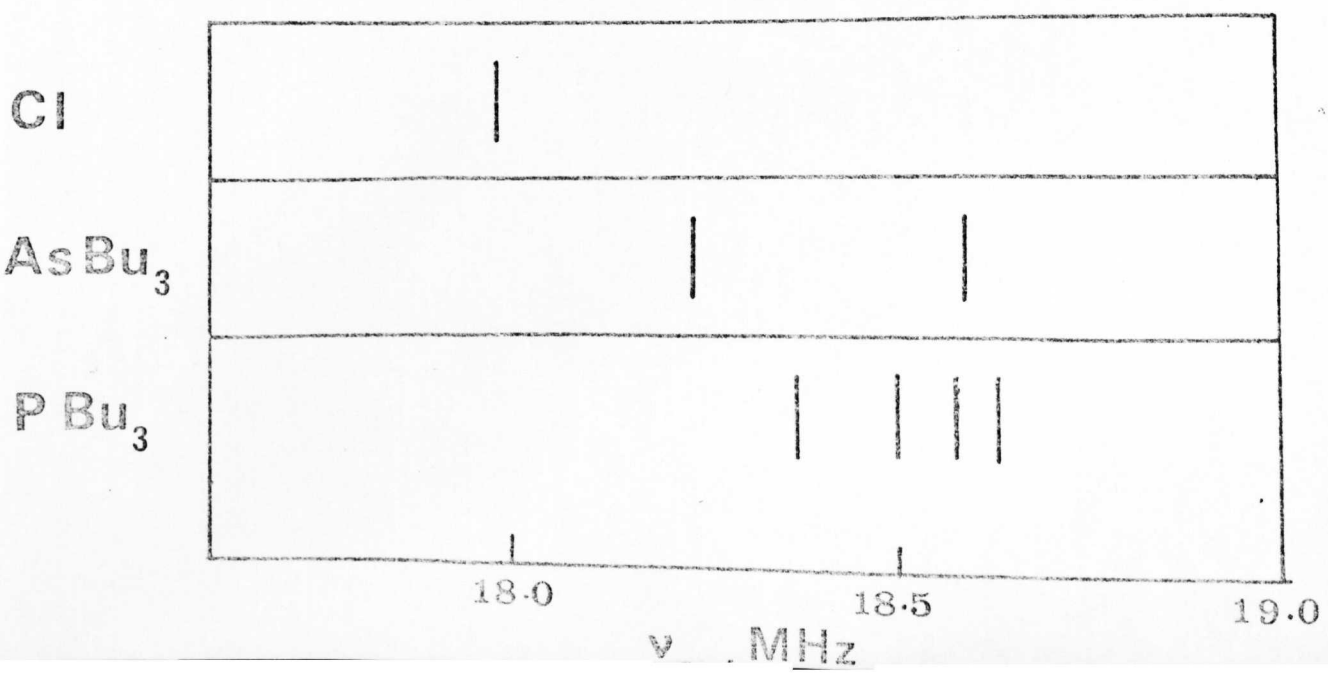

Text cut off in original

FIG. 6-10

Ligand Covalency / cis Cl ν_Q Shift

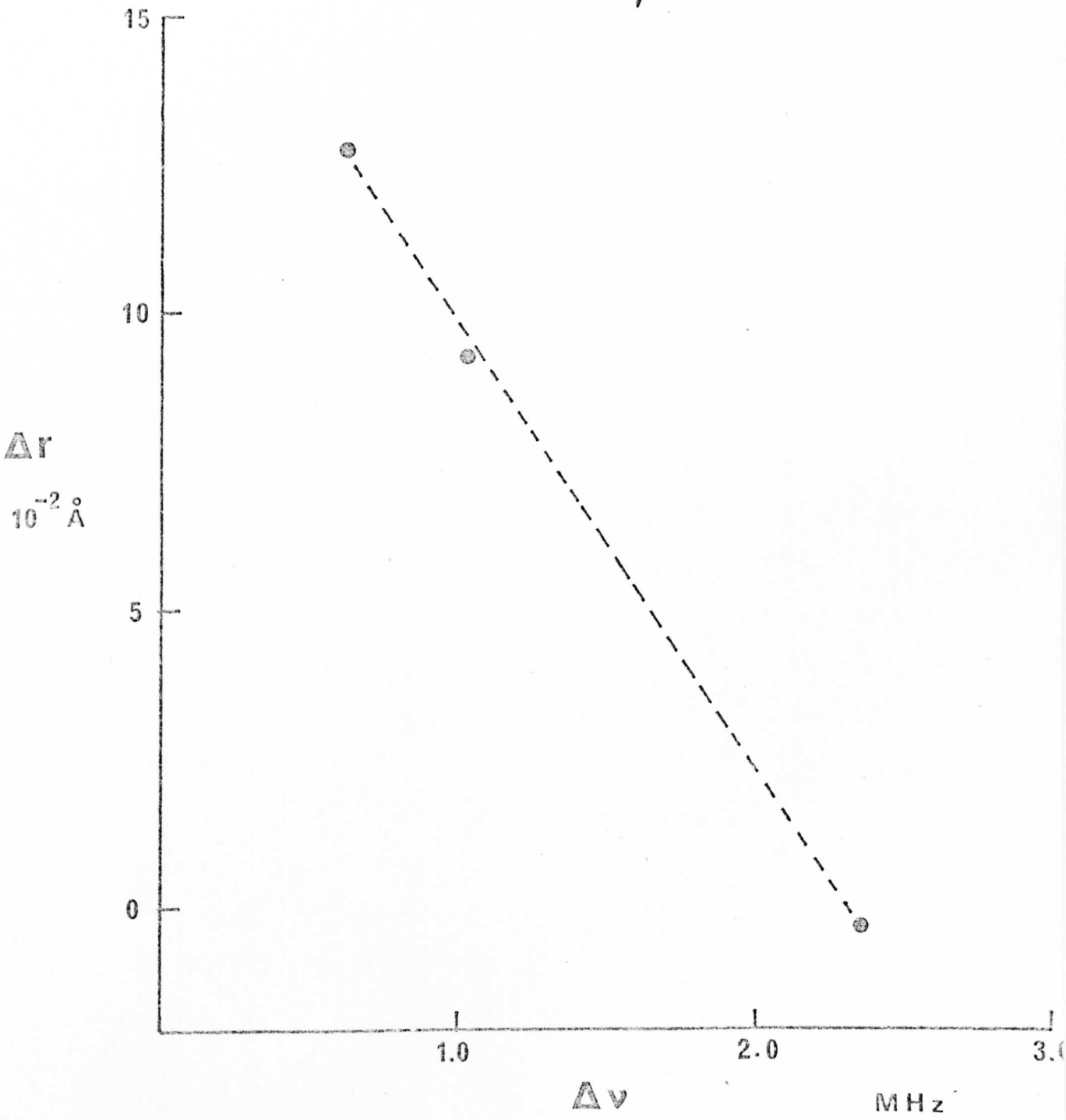

to a metal atom increases (ie. Δr decreases), the value of $\Delta\nu$, which is our measure of cis-influence (the difference between the n.q.r. frequency in L_2MCl_4 and that in K_2MCl_6) is seen to increase. If this increase occurs in a regular manner as the available data suggests, from Re, through Os to Pt, then the relationship might be used to estimate M-L bond lengths in similar M(IV) complexes, eg. an observed $\Delta\nu$ value of 1.04 MHz for trans$(AsEt_3)_2OsCl_4$ would correspond to an Os-As distance of 2.557 Å.

The opposite direction of the frequency shifts associated with the cis- and trans-chlorine atoms in mer-L_3IrCl_3 (compared with the frequency in K_2IrCl_6) is consistent with the Syrkin trans-effect theory [6.8] In this theory a ligand which weakens the trans bond simultaneously strengthens the cis bond. This follows from the order of metal atomic orbital energy levels ($5d < 6s < 6p$) which are used for the hybrid molecular orbitals. A ligand which forms a strong covalent bond to the metal will use a metal hybrid orbital of more 5d and 6s than 6p, and the trans bond consequently will have a greater 6p character and be weaker. The cis bonds can also use s-d hybrids and remain stronger than the trans bond. That the mechanism operates through a sigma effect has been indicated by measurements in Pt(II) and Pt(IV) complexes of ^{195}Pt-P nuclear spin coupling constants, which respond to changes in s character [6.8]. It is found that the cis coupling constants are significantly greater than those for the trans bonds, hence a larger s component is predicted in the cis Pt-P bonds. In addition, n.q.r. measurements on L_2PtCl_2 complexes indicate an inverse linear dependence of the Pt-Cl bond length with ν_Q[6.9]. Any Pt-Cl π bonding mechanism would be expected to have the opposite effect, according to the Townes-Dailey equation.

There remains the question of whether π bonding is important in the two series of octahedral complexes (L_2MCl_4 and MCl_6^{2-}). We shall consider both points of view in turn. Firstly we shall assume that the amount of π character does indeed change with the electronic configuration of the metal atom, and so affect the n.q.r. frequency. This is in line with previous treatments of the n.q.r. data from the hexahalometallates [6.1, 6.10, 6.11], in which the amount of π character is said to increase linearly with increasing number of vacancies in the metal atom d shell. The actual value set for π is extrapolated from the value estimated from the observed hyperfine interaction in the e.s.r. spectrum of $IrCl_6^{2-}$, which has one 5d vacancy and π was estimated at 5.4% [6.12]. If the extrapolation is linear (as in [6.1] [6.10]) according to the number of t_{2g} vacancies, ie. π = 10.8% for the osmium (d^4) complex and 16% for the rhenium (d^3) complex, then the chlorine atomic charges as given by the Townes-Dailey equation are as shown in column (1) of Table 6-3. Chlorine sp hybridisation has been neglected since this is small in transition metal chloro compounds [6.13]. An alternative estimate of π character has been proposed from the optical electronegativities [6.14]. π is given by the following equation

$$\pi = 0.054 \quad n \ (\Delta\chi_{Ir} \ / \ \Delta\chi_{M})$$

where $\Delta\chi_M = \chi_{opt\ M} - \chi_{opt\ Cl}$ and n is the number of t_{2g} orbital vacancies. The π values obtained for Os(IV), Re(IV) and W(IV) in the hexachlorometallate series are 8.1, 9.7 and 10.0% respectively [6.14]. These values have been used to calculate the atomic charges shown in column (2). Also shown in Table 6.3 are the Townes-Dailey chlorine atomic charges for negligible π bonding (column (3)), M-Cl bond lengths and also the e.s.c.a binding energies of the chlorine 2p electrons.

TABLE 6.3

COMPARISON OF CHLORINE ATOMIC CHARGES WITH BOND LENGTHS AND 2p BINDING ENERGIES

Trans-$(PEt_3)_2MCl_4$	Chlorine atomic charges, e			M-Cl distance, Å.	Chlorine 2p binding energy, eV.
	(1) using π from linear extrapolation	(2) π from optical electronegativities	(3) negligible π		(± 0.2)
Re	-0.49_5	-0.64	-0.73	2.331(3)*	198.4
Os	-0.51	-0.59	-0.67	2.319(3)*	197.9
Pt	-0.49	-0.49	-0.49	2.332(5)	198.2
mer-$(PEt_3)_3IrCl_3$	(Cl. trans to Cl.)		-0.59_5	2.361(6) a	-
	(Cl trans to P)		-0.66	2.429(6) a	-

* Data obtained on $(PMe_2Ph)_2MCl_4$. Figures in brackets are standard deviations on the last significant figure [6.3]

a " " " mer$(PMe_2Ph)_3IrCl_3$

The postulate that π bonding is considerable in the osmium and rhenium complexes does have the advantage that chlorine charges do then follow the trend seen in the bond lengths and electron binding energies ie. a slight minimum at osmium, and are fairly realistic in view of the similar electronegativities of the metal atoms. However, the differences observed in the last two columns are fairly small and it must be remembered that the bond lengths relate to complexes with different ligands in two of the cases. The experimental error on e.s.c.a data is of the order of 0.2eV. Table 6.3 illustrates the sensitivity of the chlorine charge to the amount of π character in the bond as derived from the Townes-Dailey theory. Support for the π bonding hypothesis has in the past come from studies of the temperature dependence of the n.q.r. frequencies. The temperature coefficients obtained for the present complexes will now be discussed.

6.3 The Temperature Dependence of ν_Q.

In Figure 6-1 to 6-6 are shown the temperature dependences of the chlorine n.q.r. frequencies in trans-L_2MCl_4 (L = PEt_3, M = Re, Os, Pt; L = PEt_2Ph, $AsEt_3$, M = Os and mer-$(PEt_3)_3IrCl_3$. The temperature coefficients for our purposes will be defined as the slopes of the curves at room temperature and are shown in Table 6.4. together with the values obtained for the hexachlorometallates [6.1]. This definition of the temperature coefficient is an approximate one only, but in what follows we will be interested mainly in the order of the values.

Both series show a departure from the Bayer-type temperature dependence (negative $d\nu_Q/dT$ and $d^2\nu_Q/dT^2$) as the number of metal d electrons decreases, and this phenomenon has been hitherto interpreted as indicative of a link between the temperature coefficient and the extent of π bonding in the M-Cl bond [6.1, 6.10, 6.11]. This

hypothesis is not without inconsistencies however. For instance, K_2ReCl_6 which has a positive temperature coefficient at room temperature, has a

TABLE 6.4

TEMPERATURE COEFFICIENTS, dv_Q/dT, (kHz/K)

M	L	trans-L_2MCl_4	MCl_6^{2-}
W	-	-	+ 0.44
Re	PEt_3	+ 0.42	+ 0.13
Os	PEt_3	- 0.07	- 0.22
Os	PEt_2Ph	- 0.94	"
Os	$AsEt_3$	- 0.39	"
Ir	-	-	- 0.54
Pt	PEt_3	- 1.38	- 1.00
		mer-L_3MCl_3	
Ir	PEt_3	- 0.99 (Cl trans to P) - 1.95 (Cl trans to Cl)	- 0.54

negative value below a phase transition point at 110 K. Above this temperature there is partial rotation of the octahedral anion relative to the lattice, and it is difficult to see why this motion should bring about a large change in the π bonding within the anion. Moreover, one of the resonances in $(NH_4)_3IrCl_6.H_2O$ has a positive temperature coefficient and yet no p → d π bonding is expected since all metal d orbitals are fully occupied. [6.15].

From the available experimental evidence on octahedral chloro-complexes there appears to be a general dependence of the temperature coefficient on the charge on the chlorine atom. Fig. 6-11 shows a graph of temperature coefficient against ν_Q, which itself is a measure of charge on the chlorine atom. It is notable that $PbCl_6^{2-}$ falls in line with the data for other MCl_6^{2-} ions, even though no π bonding is possible in this case. Frequencies below 13-15 MHz are most likely to be associated with a positive temperature dependence of ν_Q. In the limit - the chlorine ion - the "temperature coefficient" is also positive, in the sense that the analysis of the microwave spectrum of the ion-pair lithium chloride shows an increase in the ^{35}Cl quadrupole coupling constant of 0.4 MHz per vibrational level (that is, its negative value gets more negative [6.15]. In the light of such evidence the generalisation that a positive temperature coefficient is synonymous with a degree of π bonding, is not necessarily a valid one.

We shall now consider the second alternative, in which π bonding is <u>not</u> assumed to change appreciably with changing central metal atom. Chlorine frequencies of less than about 15 MHz, which are often associated with positive temperature coefficients, fall into a region which is midway between the ionic situation, where the electric field gradient is generated by other ions in the lattice, and the covalent (or Townes-Dailey) model, in which the field gradient is exerted by the bonding electrons within the molecule. To take into account the additional effects of neighbouring charges on the n.q.r. frequency, two different contributions must be considered. Firstly there is a <u>direct</u> effect which occurs as a result of an additional electrostatic field gradient acting on the chlorine nucleus from the neighbouring point charges. Secondly there is an <u>indirect</u> effect, which arises from polarisation of the

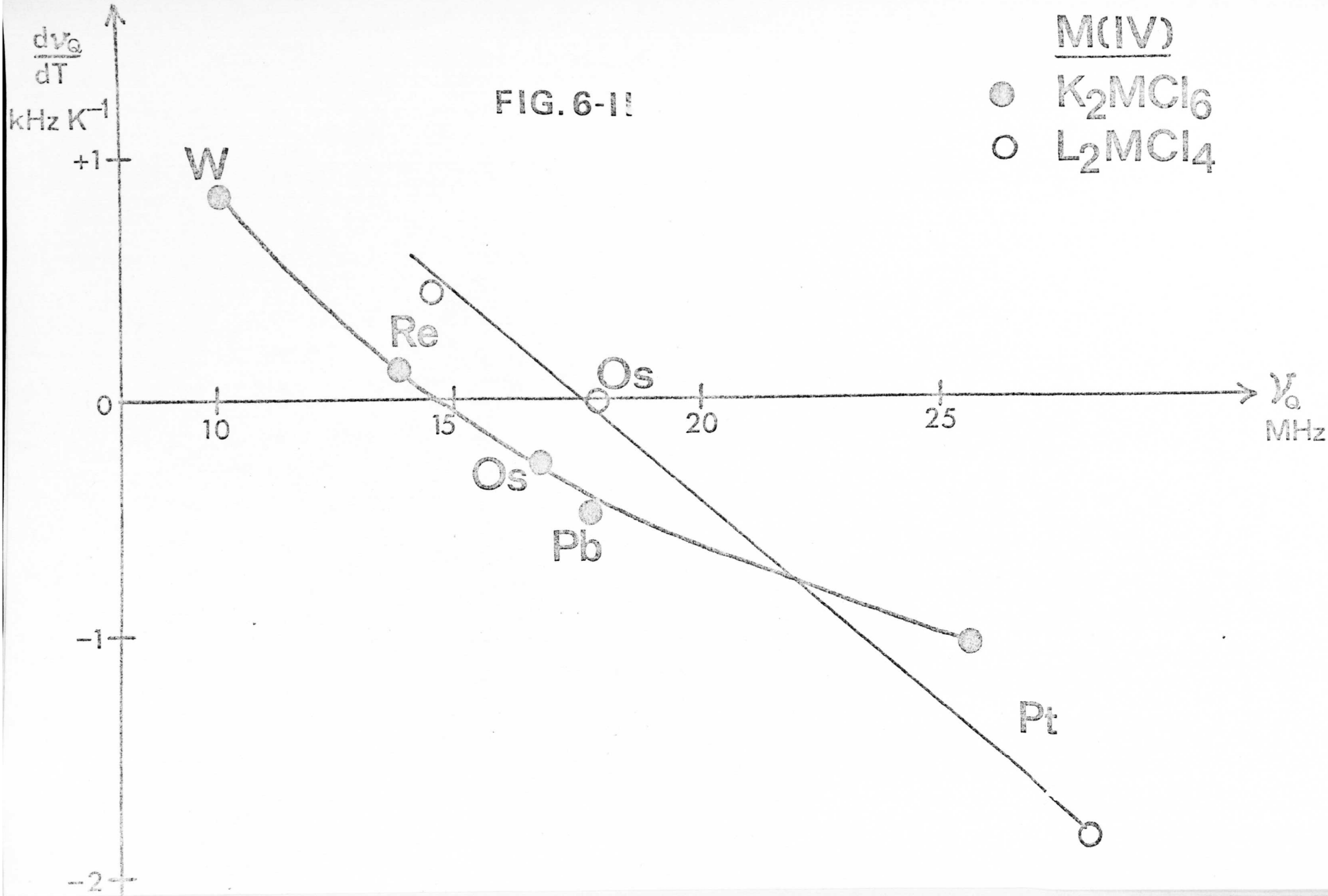
FIG. 6-1
M(IV)
K_2MCl_6
L_2MCl_4
$\frac{d\nu_Q}{dT}$
kHz K^{-1}
+1
0
−1
−2
W
Re
Os
Os
Pb
Pt
10
15
20
25
ν_Q
MHz

bonding electrons in the M-Cl bond by the neighbouring charge centres. Of the two the second effect appears to be the more important. Both are angularly dependent - the first varies as $\frac{3\cos^2\theta - 1}{r^3}$, the second as $\frac{\cos\theta}{r^2}$. The relative magnitudes of the two effects are estimated more easily for the MCl_6^{2-} series. It is evident from the crystal structure of K_2PtCl_6 that the cationic and interanionic contributions to these charge effects will be small because of their relatively large distance from a particular chlorine nucleus and in any case they should be largely independent of M. The calculation is therefore restricted to the octahedral anion itself. For a charge of -q(e) on chlorine atoms and $+q_m(e)$ on the metal atom the direct effect amounts to

$$(2q_m - 0.957q)\ 1.375/a^3 \text{ MHz}$$

where a is the M-Cl distance, in this case 2.33Å. q_m is related to q by the expression;

$$q_m = \text{formal charge on M} - (\text{Coordination number})\ (1-q)$$

In this case $q_m = 4-6\ (1-q)$.

If we consider a change of the chlorine charge of 0.2e, from -0.5e to -0.7e (due to changing M), then the magnitude of the direct effect changes from -0.16 MHz to -0.40 MHz, a shift of only 0.24 MHz. This will however be enhanced by a Sternheimer factor, the magnitude of which is difficult to estimate, but the effect could be appreciable.

We shall now consider the corresponding shift in the <u>indirect</u> effect. The magnitude of the electric field along an M-Cl bond in the octahedral anion MCl_6^{2-} amounts to

$$\frac{q_m}{a^2} - \frac{1}{\sqrt{2}} \cdot \frac{4q}{2a^2} \quad \frac{-q}{4a^2} = (q_m - 1.66q)\ 1.44\ 10^6/a^2 \text{ (kV/cm)}$$

The change in electric field intensity at a chlorine site associated with a change of charge q from -0.5e to -0.7e is from 0.45. 10^5 to 2.75. 10^5 kV/cm ie. 2.3 kV/cm. This may be related to a shift in the n.q.r. frequency via an experimentally determinable Stark coefficient and the appropriate Lorentz factor, which relates the externally applied electric field to the internal field. The correct values for both of these quantities are unknown, but the Stark coefficient for mercury-chlorine bonds has been measured (117 Hz. $(kV/cm)^{-1}$) [6.17]. Assuming a Lorentz factor of unity for the moment, the n.q.r. shift corresponding to the 0.2e change in chlorine charge by this effect would be very large, -27 MHz. The use of the correct Lorentz factor would however reduce this severely, but it is still evident that a relatively small change in chlorine charge could produce a large change in the n.q.r. frequency by this mechanism. It has also been shown that there is a correlation between the Stark coefficient and bond polarisability [6.18]; thus the effect might be largest for the weakest bonds.

If this type of mechanism could account for the relatively low frequencies in the earlier metal complexes without the invocation of π bonding, how then may the positive temperature coefficients be justified? In fact the intra-anionic electric field effect can also make a contribution to these, as discussed below.

The calculations of electric field and electric field gradient depend upon the values of the inverse square and inverse cube of the interatomic distances respectively, averaged over the vibrational states of the molecule. If ξ is the displacement from the equilibrium internuclear distance, r_e ie. $\xi = (r - r_e)/r_e$, then the relevant averaged bond distances for a diatomic molecule may be expressed as:

$$\langle r^{-2} \rangle^{-\frac{1}{2}} = r_e[1 + \langle \xi \rangle - \frac{3}{2} \langle \xi^2 \rangle]$$

$$\langle r^{-3} \rangle^{-\frac{1}{3}} = r_e[1 + \langle \xi \rangle - 2 \langle \xi^2 \rangle] \qquad [6.19]$$

and

$$\langle \xi \rangle_v = -3a_1 \left(\frac{B_e}{\omega_e}\right)(v + \tfrac{1}{2})$$

$$\langle \xi \rangle_v = 2 \left(\frac{B_e}{\omega_e}\right)(v + \tfrac{1}{2})$$

where B_e is the equilibrium rotational constant, ω_e is the fundamental vibration frequency, v is the vibrational quantum number and a_1 is the first anharmonicity constant. Now if the vibrational motion is approximately harmonic which is a reasonable assumption at low temperatures where only the lowest vibrational levels are populated, then a_1 is zero and therefore $\langle \xi \rangle$ is zero. However $\langle \xi^2 \rangle$ is non-zero and positive; hence as far as the electric field and electric field gradient operators are concerned, there is an <u>apparent</u> contraction in the internuclear distance as the temperature rises and v increases. Although these formulae are strictly applicable to only a diatomic molecule, we can use them to obtain an estimate of the magnitude of this apparent contraction using available r.m.s. amplitudes of vibration calculated at 0 K and 298 K from spectroscopic data [6.20]. By extrapolation from the values for $PbCl_4$, $HfCl_4$, PbF_4 and PtF_6 the mean amplitudes of vibration of M-Cl (M = Re,Pt) and Cl···Cl are estimated and given overleaf.

Estimated mean amplitudesof vibration in MCl_6^{2-} (Å)

Temp (K)	M-Cl	Cl····Cl
0	0.040	0.072
298	0.048	0.130

For M-Cl the values of the apparent contraction change very little from 0 to 298 K; $6.3.10^{-4}$ Å for $<r^{-3}>^{-1/3}$, and $4.7.\ 10^{-4}$ Å for $<r^{-2}>^{-\frac{1}{2}}$. There is a somewhat greater apparent decrease in the Cl···Cl distance however. $<r^{-3}>^{-1/3}$ is reduced by $7.1.\ 10^{-3}$Å and $<r^{-2}>^{-\frac{1}{2}}$ by $5.3.\ 10^{-3}$Å between 0 and 298 K. This will mainly affect the contributions to ν_Q from the four neighbouring chlorine atoms, the magnitude of which changes by +0.38 kHz ($ReCl_6^{2-}$) and +0.27 kHz ($PtCl_6^{2-}$)from 0 to 298 K by the direct mechanism. The corresponding values due to the indirect effect are somewhat larger: + 112 kHz and + 80 kHz, which correspond to temperature coefficients of +0.37 and +0.26 (kHz/K). These are to be compared, after due allowance for the additional negative Bayer term, with the observed values of +0.13 (K_2ReCl_6) and -1.0 kHz/K (K_2PtCl_6). The present model predicts that the rhenium complex has the more positive value but underestimates the difference in magnitude between the two cases.

A further mechanism by which the temperature coefficient may be influenced is through a change in the contribution from the chlorine non-bonding orbitals. As the chlorine charge builds up through the series from platinum to rhenium the lone pair orbitals on chlorine may be expected to expand, with consequent reduction in ν_Q. The increase of vibration amplitudes perpendicular to the M-Cl direction as the temperature increases could increase repulsion between adjacent p orbitals and some contraction of these could result, which would have the effect

of raising the n.q.r. frequency. On a qualitative basis this is consistent with the observed positive temperature coefficients for the tungsten and rhenium complexes where the chlorine charge is considerable.

In conclusion, the calculations indicate that non-bonding interactions, particularly the intra-molecular electric field effect, can have a non-negligible effect on the chlorine n.q.r. frequency in these complexes and that these effects are most important when the relevant bonds are weak and atomic charges are high.

CHAPTER 7

ELECTRIC FIELD EFFECTS IN CHLORINE QUADRUPOLE RESONANCE

7.1 Introduction.

It has been shown recently that the acetylacetonato complexes of several elements are suitable structures for the study of first-order electric field effects in molecules [7.1-3]. In this way, the field-dependence of the n.m.r. ^{1}H shift in CH and CH_3 groups [7.1], ^{13}C-^{1}H spin-spin coupling constant [7.2] and the ^{13}C shift [7.3] have been estimated. In the case of ^{35}Cl quadrupole coupling constants, the electric field model has the possibility of some kind of comparison with experiment from the magnitude of the Stark coefficient [7.4, 6.17]. The ^{35}Cl quadrupole resonance of some 3-chloroacetylacetonato-complexes has therefore been studied in order to investigate further the validity of the electric field model.

The complexes were prepared by Dr A. Barabas and Dr E. Isfan (Institute of Atomic Physics, Bucharest). Details of the preparation are given in [7.5].

The ^{1}H and ^{13}C n.m.r. spectra were recorded by Dr J.C. Hammel using a Perkin-Elmer R10 high resolution spectrometer. The ^{13}C spectra required the use of a signal averager (Northern Scientific NS-544-PE). The Decca spectrometer was used to record the n.q.r. frequencies at liquid nitrogen temperature.

7.2 Results and Discussion.

The ^{35}Cl quadrupole resonance frequencies in six complexes of 3-chloroacetylacetone are recorded in Table 7.1; in three cases the

corresponding ^{37}Cl frequencies were also found at values lower by the usual factor of 1.2688. In $SbCl_4$ (3-Cl-acac), four low frequency lines were also observed (Table 7.1) and are assigned to Sb-^{35}Cl resonances; the values compare with those observed in $SbCl_4$(acac) at 77 K (24.28 and 25.79 MHz). In the boronium $SbCl_6^-$ complex, a complex multiplet was observed between 24.1 and 24.6 MHz at 77K; these lines are assigned to the $SbCl_6^-$ ion. No resonance for the Cr(III) Al(III) and Si(IV) complexes could be found in the 30-40 MHz region.

The ^{13}C shifts of the ^{13}CO, ^{13}CCl and $^{13}CH_3$ groups in several 3-chloroacetylacetonato-complexes are recorded in table 7.2, together with the shift (in brackets) from the parent unchlorinated derivative.

The figure is a stick diagram of the ^{35}Cl quadrupole resonance frequencies which show a reasonably clear division into two groups, the non-polar complexes near 36MHz, and the polar or charged complexes near 38MHz. Within each group, crystal effects or changes in the coordinating atom have a smaller effect compared with the difference of 2MHz between groups. Just as in the case of the ^1H and ^{13}C shifts and $J(^{13}C\text{-}H)$, it appears that the polarity or charge on the complex is the predominant factor, and the observed differences in quadrupole resonance frequency may then be ascribed to linear electric field shifts. Three quantitative checks on this description can be made. It is assumed that differences due to a change in the asymmetry parameter or in the effects of thermal motion can be neglected.

(1) Firstly the electric fields in the polar BF_2(3-Cl-acac) and cationic $B(3\text{-Cl-acac})_2^+$ complexes are compared; the dipole moment of the former and the charge (+1) of the latter are located on the boron atom. The ratio of electric fields (in the C-Cl direction) at a distance R from

FIG. 7-I

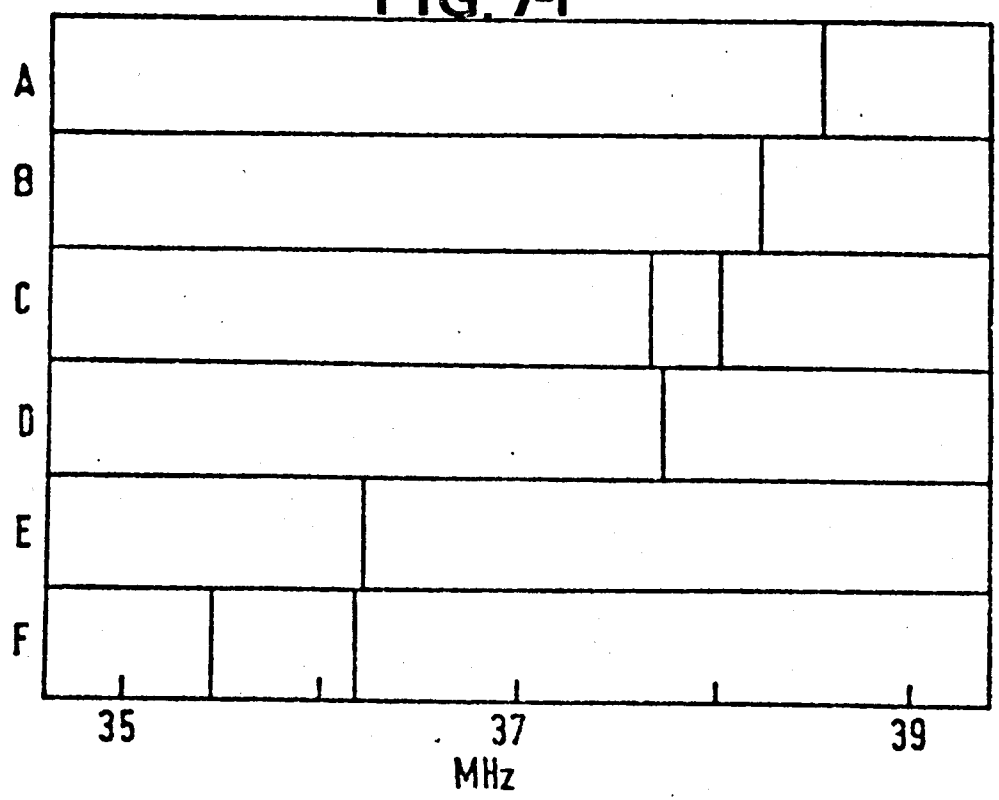

^{35}Cl N.q.r. frequencies (MHz, at 77°K) in some 3-chloroacetyl-acetonato-complexes

A	$[B(3\text{-Cl-acac})_2]^+SbCl_6^-$	D	$BF_2(3\text{-Cl-acac})$
B	$SbCl_4(3\text{-Cl-acac})$	E	$Co(3\text{-Cl-acac})_3$
C	$[B(3\text{-Cl-acac})_2]^+ClO_4^-$	F	$Be(3\text{-Cl-acac})_2$

the boron atom is $2\mu/eR$. By taking a ratio of the shifts the effect of many of the serious approximations of the model are reduced [7.2]. It is now assumed that the additional field at the chlorine site in the polar complex relative to a non-polar one can be estimated using the experimental dipole moment of BF_2 acac. in the above expression [7.6]. The ratio of cationic/polar electric fields along the C-Cl bond is 1.30 evaluated at the bond centre and 1.61 at the Cl nucleus. The ratios of the measured n.q.r. frequency shifts, $\Delta\nu_{cationic}/\Delta\nu_{polar}$ are 1.46 for the $SbCl_6^-$ salt and 1.10 for the ClO_4^- salt. The choice of bond centre gives better agreement.

(2) Alternatively the charge distributions assumed in (1) can be used to calculate values for the electric field, E_z, in each case (a) at the centre of the C-Cl bond and (b) at the Cl nucleus. Values for the shift in observed n.q.r. frequency per unit electric field may then be calculated, and these appear in Table 7.3.

In addition the electric field has been estimated from the observed chemical shifts of the unchlorinated species [7.2,7.7] and by using the equation relating the two quantities [7.8, 7.9]. The coefficients calculated in this way also appear in Table 7.3 and are in reasonable agreement with values obtained from the assumed charge distribution. E_z calculated at the bond centre gives the more consistent values. The sign and numerical values are consistent with Musher's calculations for the dichloro-substituted benzenes [7.9].

A check on some of the assumptions come from the ^{13}C chemical shifts in Table 7.2; the changes in the ^{13}CO and $^{13}CH_3$ shifts produced by chlorination in the 3-position are small and in the case of the latter much less than the displacement of + 4 p.p.m. on going from a non-polar complex like Al $acac_3$ to BF_2acac [7.3]. Only the ^{13}C shift of the 3-carbon

atom is appreciable, so that the distribution of the more distant charges is probably little afffected.

(3) The coefficients in Table 7.3 should be related in sign and magnitude to those of the Stark shift of ^{35}Cl n.q.r. frequencies [7.4]. For ^{35}Cl in carbon-chlorine bonds an experimental value of 59.0 Hz $kV^{-1}cm.$ has been obtained. For comparison with those in Table 7.3 which relate to the internal field, this value should be divided by the appropriate Lorentz factor. The latter has been estimated by Bloembergen as 1.6 in p-dichlorobenzene; using this factor a value for the internal field Stark coefficient of 37.3 is obtained which agrees in sign and fairly well in magnitude with those in Table 7.3.

The calculations support the conclusion that the differences in ^{35}Cl quadrupole resonance frequency between the polar or charged complexes on the one hand and the non-polar complexes on the other are due mainly to first-order electric field shifts.

The work reported in this chapter is published in [7.10].

TABLE 7.1

^{35}Cl AND ^{37}Cl QUADRUPOLE RESONANCE FREQUENCIES (IN MHz) IN SOME 3-CHLOROACETYLACETONATO-COMPLEXES

Compound	$\nu_Q(^{35}Cl, MHz)$ at 77 K	$\nu_Q(^{37}Cl, MHz)$ at 77 K
$Be(3\text{-}Cl\text{-}acac)_2$	35.47, 36.18_5	27.96, 28.52
$Co(3\text{-}Cl\text{-}acac)_3$	36.23	-
$BF_2(3\text{-}Cl\text{-}acac)$	37.72	-
$[B(3\text{-}Cl\text{-}acac)_2]^+ClO_4^-$	37.77, 38.02	-
$SbCl_4(3\text{-}Cl\text{-}acac)$	38.22	30.12_5
	24.18, 24.71	19.05, 19.50
	26.27, 26.53	20.72, 20.93
$[B(3\text{-}Cl\text{-}acac)_2]^+SbCl_6^-$	38.53	30.37

TABLE 7.2

^{13}C SHIFTS (p.p.m.) IN SOME 3-CHLOROACETYLACETONATO-COMPLEXES; VALUES IN PARENTHESES ARE SHIFTS FROM UNCHLORINATED DERIVATIVE

Compound	Solvent	$\delta(^{13}CO)$ (p.p.m)*	$\delta(^{13}CCl)$ (p.p.m.)*	$\delta(^{13}CH_3)$ (p.p.m)*	Scans
$H(3\text{-}Cl\text{-}acac)$	$CDCl_3$	4.0	86.2	171.3	150
		(+2.4)	(-6.8)	(+2.1)	
$Be(3\text{-}Cl\text{-}acac)_2$	$CDCl_3$	0.0	83.2	170.2	1250
		(-1.2)	(-9.6)	(+1.0)	
$Al(3\text{-}Cl\text{-}acac)_3$	$CDCl_3$	+1.6	-	167.6	1090
		(-0.6)		(+1.4)	
$Co(3\text{-}Cl\text{-}acac)_3$	$CDCl_3$	+2.6	-	-	1110
		(-1.4)			

* p.p.m. from $^{13}CS_2$ as external reference.

TABLE 7.3

RATIO OF SHIFT OF ^{35}Cl N.Q.R. FREQUENCY (IN Hz) TO INTRA-MOLECULAR ELECTRIC FIELD ALONG C-Cl BOND (IN kV cm^{-1})

	From charge distribution		From chemical shift	
	(a) E_z at bond centre	(b) E_z at ^{35}Cl nucleus	(a) E_z at bond centre	(b) E_z at ^{35}Cl nucleus
BF_2(3-Cl-acac)	22.0	41.3	19.6	36.7
$B(3\text{-Cl-acac})_2^+ClO_4^-$	16.3	25.0	14.6	22.4
$B(3\text{-Cl-acac})_2^+SbCl_6^-$	21.9	33.7	19.7	30.3

CHAPTER 8

CHLORINE QUADRUPOLE RESONANCE OF THE TETRACHLOROPHOSPHONIUM CATION

8.1 Introduction.

In the solid state, phosphorus pentachloride can exist in both molecular and ionic forms, of which the latter is the more stable. The n.q.r. spectrum of the stable form shows a difference of 2-3 MHz between the ^{35}Cl resonances of the cation (PCl_4^+) and those of the anion (PCl_6^-); a group of lines near 32 MHz has been assigned to the cation and a similar group near 29-30 MHz to the anion [8.1, 8.2, 3.6].

The work described in this chapter consists of an n.q.r. study of a series of phosphorus pentachloride addition compounds, PCl_5X, the results of which favour an ionic structure $[PCl_4^+][XCl^-]$ in each case. The compounds in the series were prepared by Dr K.B. Dillon [8.3].

^{35}Cl quadrupole resonance frequencies were observed using the Decca spectrometer (chapter 3). The intensities of the lines were found to be greatest at 77 K so that searches were normally carried out at this temperature.

8.2 The Resonance Frequencies.

The observed quadrupole resonance frequencies in a series of PCl_5 addition compounds together with those of the ionic form of PCl_5 are listed in Table 8.1.

The spectrum of PCl_5 showed ten lines at 77 K, a group of four near 32 MHz and six near 29-30 MHz; assignment of the former group to the PCl_4^+

TABLE 8.1

OBSERVED ^{35}Cl N.Q.R. FREQUENCIES OF THE TETRACHLOROPHOSPHONIUM ION *

IN $[PCl_4^+][X^-]$ AT 77 K.

	$[X^-]$	ν_Q, MHz.	
(a)	PCl_6^-	32.285	
		32.395	
		32.425	
		32.615	
		28.405	
		29.720	
		30.040	assigned to PCl_6^-
		30.075	
		30.470	
		30.580	
(b)	ICl_2^-	32.710	
(c)	$AlCl_4^-$	32.135	
		32.210	
(d)	$FeCl_4^-$	32.20	
		32.28	
(e)	$HfCl_5^-$	32.27	
(f)	$Ti_2Cl_9^-$	32.11	Intensity ratio: 1
		32.24	2
		32.39	2
		32.515	1
(g)	$SnCl_5^-$	32.125	
		32.360	(106 K)
		25.40	^{37}Cl of PCl_4^+
		22.04	^{35}Cl of $SnCl_5^-$
		22.08	" "
		20.32	" "

* unless otherwise stated resonance frequencies quoted are assigned to ^{35}Cl in PCl_4^+.

ion and the latter to the PCl_6^- ion is consistent with previous work and the relative P-Cl bond distances. Previously groups of three and four [8.1], two and four [8.2], and five and five [3.6] lines have been reported for this compound at 77 K. The room temperature crystal structure [8.4] does not distinguish between chlorine atoms in the tetrachlorophosphonium cation but a phase transition at 110 K [8.1] is expected to be responsible for the difference in the number of equivalent chlorine sites at 77 K and at room temperature.

Throughout the series of compounds listed in Table 8.1 a line or group of lines were observed near 32 MHz and these are assigned to ^{35}Cl resonance from the PCl_4^+ ion, consistent with the spectrum of PCl_5. Further evidence for the presence of PCl_4^+ is provided by the observed value of the ^{31}P n.m.r. chemical shift which in all cases lies in the region of -85 p.p.m. [8.3] in agreement with previous values for the ion. From $[PCl_4^+][ICl_2^-]$ and $[PCl_4^+][HfCl_5^-]$ only one resonance line was observed in each case, indicating at least mm symmetry for the cation. This is in agreement with the crystal structure of the former compound in which the cation symmetry is $\bar{4}$, [8.5]. Two lines were detected from $[PCl_4^+][AlCl_4^-]$, $[PCl_4^+][FeCl_4^-]$ and $[PCl_4^+][SnCl_5^-]$. The crystal structure of the second of these reported two fold symmetry for the PCl_4^+ ion and the n.q.r. spectra are consistent with this [8.6]. From the similarity of the spectra it is expected that the tetrachlorophosphonium ion in the $[AlCl_4^-]$ compound has similar symmetry. The two lines observed from $[PCl_4^+][SnCl_5^-]$ in the 32 MHz region have a larger splitting and also somewhat different temperature dependences (see Fig. 8-1). It is probable that they relate to different PCl_4^+ ions within the unit cell.

Three other lines were also observed at lower frequencies in this compound: a medium intensity doublet at 22.04 and 22.08 MHz and a broad,

weak line at 20.32 MHz. These are ascribed to ^{35}Cl resonance from the $SnCl_5^-$ ion. The frequencies are between those found in $SnCl_4$ (23.72, 24.14, 24.23, 24.29 MHz at 77 K) [8.7] and those reported for the $SnCl_6^{2-}$ ion (15.61, 15.65 MHz at 77 K) [8.8]. Unfortunately no lines were observed from a sample of $[Pr_4N^+][SnCl_5^-]$, which it was hoped would confirm the assignment.

The spectrum of $[PCl_4^+]$ $[Ti_2Cl_9^-]$ showed a quadruplet of lines, of relative intensities 1:2:2:1. The room temperature crystal structure indicates two different PCl_4^+ ions in the unit cell, each with a mirror plane, so that six different chlorine sites are expected [8.9]. It appears that at 77 K, the inequivalence between two sites, in two cases, is very small and that the use of Zeeman modulation (used for sensitivity reasons) prevented the resolution of fine splitting. However at higher temperatures some splitting of the third line was observed (see Fig. 8-2).

8.3 The Temperature Dependence of ν_Q.

In Figures 8-1 and 8-2 the temperature dependences of the resonance frequencies are shown, over the ranges in which lines were observed. In most cases resonances faded out before room temperature was reached and this is probably due to the onset of hindered rotation of the tetrachlorophosphonium ion.

Above 120 K the change of frequency with temperature is reasonably linear and the wide variation in slopes suggests that different torsional frequencies of the PCl_4^+ ion are associated with the n.q.r. frequency reduction in each case. By means of the Bayer expression for the temperature coefficient, $\partial\nu/\partial T$ (Chapter 1 equation (28)), the frequency of the torsional motion (or libration) of the cation may be estimated,

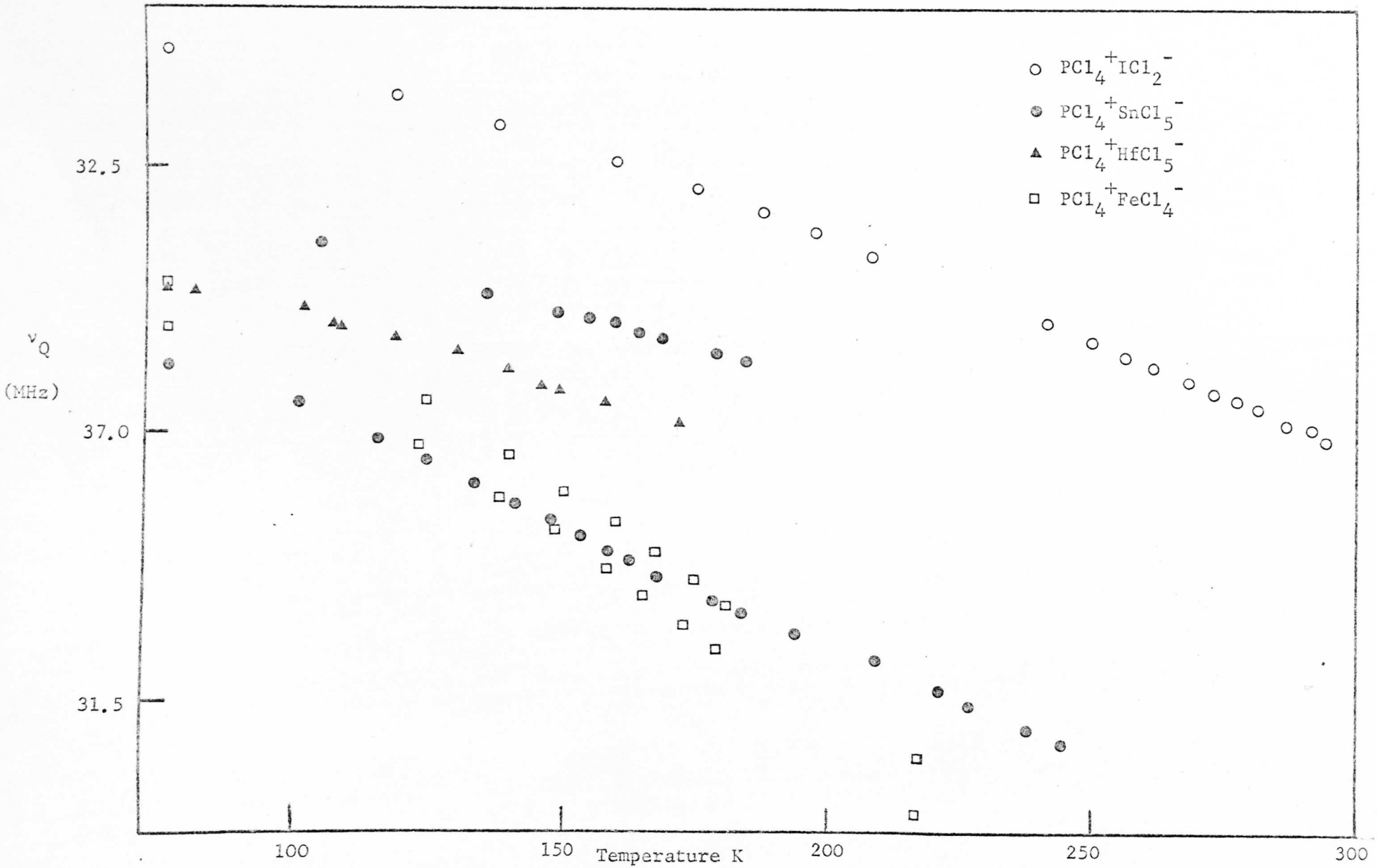

Fig. 8-1 Temperature Dependence of ν_Q in PCl_4^+

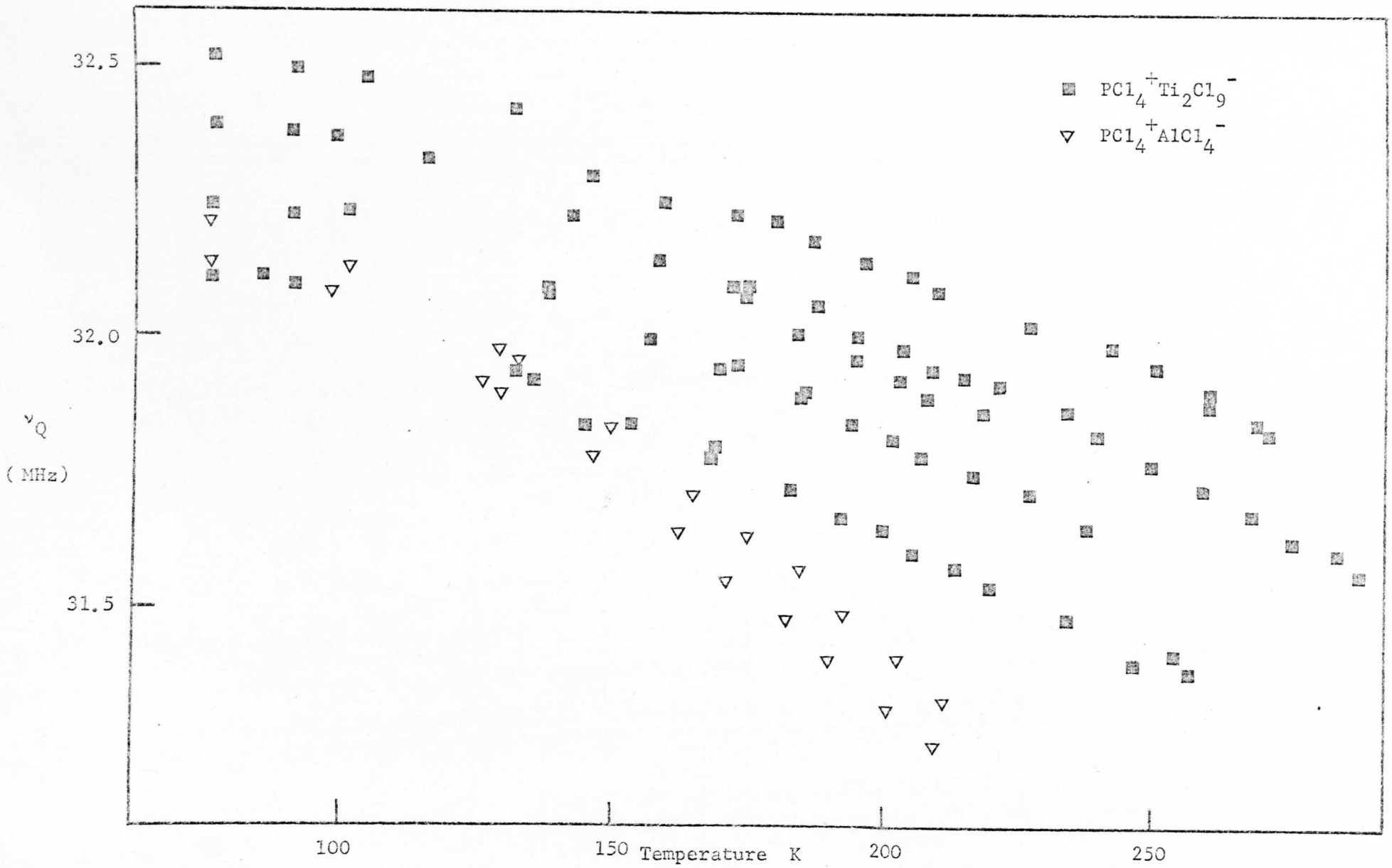

Fig. 8-2 Temperature Dependence of ν_Q in PCl_4^+

subject to various assumptions already mentioned. The intra-ionic vibrations contribute little to the value of the temperature coefficient; for example the two bending motions ν_2 (171 cm^{-1}) and ν_4 (251 cm^{-1}) contribute only 0.12 and 0.06 kHz K^{-1} respectively to the value of $\partial \nu / \partial T$ at 150 K. The values of librational frequencies obtained using the Bayer theory (single mode model) for a common temperature, 150 K, are given in Table 8.2. The moment of inertia of the PCl_4^+ ion about a C_2 axis was taken as 618.10^{-40} $g.cm^2$ [8.1]. The value of ν_o, the n.q.r. frequency at 0 K was estimated from a smooth extrapolation of the frequency/temperature plots.

The libration frequencies do not seem to depend upon the size of the counter ion but are probably more dependent upon the individual crystal packing. The frequencies are calculated assuming only one ionic librational mode is important in each case. A possible explanation for the large temperature coefficients observed for $[PCl_4^+][FeCl_4^-]$ and $[PCl_4^+][AlCl_4^-]$ is that perhaps more than one librational motion may be present where both ions are tetrahedral and of similar size. The lattice may then be a close approximation to that of a close-packed array of spheres (near cubic or hexagonal symmetry) permitting easy motion of the ions. For the $[AlCl_4^-]$ complex for example, a frequency of 34.3cm^{-1} is obtained for a triply degenerate motion about the C_2 axes of the PCl_4^+ ion.

A further experiment worthy of consideration would be to study the temperature dependence of the spin-lattice relaxation time of a resonance for a particular complex, from which it should be possible to estimate the barrier height to the hindered rotational motion of the PCl_4^+ ion. This value should correlate approximately with the thermal energy at the

TABLE 8.2

LIBRATION FREQUENCIES OF THE PCl_4^+ ION.

Anion	ν_o MHz.	$(\partial\nu/\partial T)_{150}$ kHz K^{-1}	ν_1 cm^{-1}
$HfCl_5^-$	32.3	-3.0	31.3
ICl_2^-	32.8	-3.1	31.3
$SnCl_5^-$ (1)	32.2	-4.6	26.0
" (2)	32.5	-2.8	32.8
$Ti_2Cl_9^-$	32.4	-4.3	26.2
$FeCl_4^-$	32.4	-7.4	20.2
$AlCl_4^-$	32.3	-7.8	19.8

disappearance point on the frequency/temperature graph, if this point is associated with the onset of rotation of the ion.

The resonance frequency for the rapidly rotating ion may be predicted using the expression of Dodgen and Ragle for rotation in trans 1,2dichloroethane [8.10]. The n.q.r. frequency is reduced, on rotation, by a factor $\left(\frac{3\cos^2\theta-1}{2}\right)$ where θ is the angle between the field gradient axis of symmetry and the rotation axis. For rotation about a two-fold axis $\theta \sim 55^{\circ}$, so that the expected frequency is very low indeed, near 210 kHz, and is well below the range of the present instrument.

REFERENCES

Chapter 1

1.1 M.H. Cohen and F. Reif, Solid State Physics 5, 321 (1957).

1.2 C.P. Slichter, "Principles of Magnetic Resonance" (Harper and Row, New York, 1963).

1.3 J.A.S. Smith, J. Chem. Education. 48, 39 (1970).

1.4 T.P. Das and E.L. Hahn, "Nuclear Quadrupole Resonance Spectroscopy" Solid State Physics Suppl. 1. (Academic Press, New York 1958).

1.5 M.H. Cohen, Phys. Rev. 96, 1278 (1954).

1.6 Y. Morino and M. Toyama, J. Chem. Phys. 35, 1289 (1961).

1.7 N. Bloembergen, E.M. Purcell, R.V. Pound, Phys. Rev. 73, 679, (1948).

1.8 H. Bayer, Z. Phys. 130, 227 (1951).

1.9 T. Kushida, G.B. Benedeck and N. Bloembergen, Phys. Rev. 104, 1364 (1956).

1.10 D.E. Woessner and H.S. Gutowsky, J. Chem. Phys, 39, 440 (1963).

1.11 T. Tokuhiro, J. Chem. Phys. 41, 438 (1964).

1.12 J. Van Kranendonk, Physica, 20, 781 (1954).

1.13 T. Tokuhiro, J. Chem. Phys. 41, 1147 (1964).

1.14 A. Abragam, "The Principles of Nuclear Magnetism", O.U.P. (1961). p. 472.

1.15 R.G. Barnes and R.D. Engardt, J. Chem. Phys. 29, 248 (1958).

1.16 H.W. Dodgen and J.L. Ragle, J. Chem. Phys. 25, 376 (1956).

1.17 C.E. Chang, USA Office of Scientific Research report (TN-55-401), from Physics Department, University of Washington. (1955) See also Das and Hahn.

1.18 S. Alexander and U. Ganiel, J. Chem. Phys. 43, 4060 (1965).

Chapter 2

2.1 C.H. Townes and B.P. Dailey, J.Chem.Phys. 17, 782 (1949).

2.2 E.A.C. Lucken "Nuclear Quadrupole Coupling Constants". Academic Press, London 1969.

2.3 H.C. Meal, J.Chem. Phys. 24, 1011 (1956).

2.4 R. Sternheimer, Phys. Rev. 80, 102 (1950);
" " 84, 244 (1951);
" " 86, 316 (1952);
" " 95, 736 (1954).

2.5 W. Gordy, Disc. Faraday Soc. 19, 14 (1955).

2.6 B.P. Dailey and C.H. Townes, J. Chem. Phys. 23, 118 (1955).

2.7 F.A. Cotton and C.B. Harris, Proc. Nat. Acad. Sci. 56, 12 (1966).

2.8 M.A. Whitehead and H.H. Jaffé, Trans. Faraday Soc. 57, 1854 (1961).

2.9 J. Hinze, M.A. Whitehead and H.H. Jaffé, Theoret. Chim. Acta, 1, 209 (1963).

2.10 J. Hinze and H.H. Jaffé, J. Am. Chem. Soc. 84, 540 (1962).

2.11 E. Scrocco and J. Tomasi, Theoret. Chim. Acta. 2, 386 (1964).

2.12 D. Schoemaker, Phys. Rev. 149, 693 (1966).

2.13 G.R. Bird and C.H. Townes, Phys. Rev, 94, 1203 (1954).

2.14 R. Bersohn, J. Chem. Phys. 22, 2078 (1954).

2.15 L. Pauling, "The Nature of the Chemical Bond". Cornell University Press. (1939)

2.16 A.F. Wells, J. Chem. Soc. 55, (1949).

2.17 F.A. Cotton and C.B. Harris, Inorg. Chem. 6, 369 (1967).

2.18 " " " " Inorg. Chem. 6, 376 (1967).

2.19 V. Rehn, J. Chem. Phys. 38, 749 (1963).

2.20 M. Suhara, T. Yonemitsu and T. Tonomura, Bull. Chem. Soc. Japan 38, 2205 (1965).

Chapter 3

3.1 N. Bloembergen, E.M. Purcell and R.V. Pound, Phys. Rev. 73, 679 (1948).

3.2 T.C. Wang, Phys. Rev. 99, 566 (1955).

3.3 J.A.S. Smith and D.A. Tong, J. Sci. Instruments, 1, (ser 2), 8 (1968).

3.4 H.G. Dehmelt and H. Krüger, Naturwissenschaften, 37, 11 (1950).

3.5 C. Dean and M. Pollack, Rev. Sci. Instruments, 29, 630 (1958).

3.6 D.A. Tong, Ph.D. Thesis (University of Leeds 1965).

3.7 M. Bloom, Phys. Rev. 94, 1396 (1954).

3.8 A. Abragam, "The Principles of Nuclear Magnetism", O.U.P. (1961) p. 44.

3.9 H.Y. Carr and E.M. Purcell, Phys. Rev. 94, 630 (1954).

Chapter 4

4.1 W. Dilthey, Ber. 36, 923 (1903).

4.2 - - Annalen. 344, 300 (1906).

4.3 F. Kaufler and E. Kunz, Ber. 42, 385, 2482 (1909).

4.4 F. Ephraim, Ber. 47, 1828 (1914).

4.5 H.F. Herbrandson, R.T. Dickerson and J. Weinstein, J. Am. Chem. Soc., 76, 4046 (1954).

4.6 T.C. Waddington, J. Chem. Soc., 1708 (1958).

4.7 R.E. Vallee and D.H. McDaniel, J. Am. Chem. Soc., 84, 3412 (1962).

4.8 R. West, J. Am. Chem. Soc. 79, 4568 (1957).

4.9 L.W. Schroeder and J.A. Ibers, J. Am. Chem. Soc., 88, 2601 (1966); " " Inorg. Chem. 7, 594 (1968).

4.10 C.J. Ludman and T.C. Waddington, personal communication.

4.11 R. Livingston, J. Phys. Chem., 57, 496 (1953).

4.12 H.C. Meal and H.C. Allen, Phys. Rev. 90, 348 (1953).

4.13 J.C. Evans and G. Y-S. Lo, J. Phys. Chem. 70, 2702 (1966); 71, 3697 (1967).

4.14 J.S. Swanson and J.M. Williams, Inorg. Nucl. Chem. Letters, 6, 271 (1970).

4.15 J.C. Evans and G.Y-S. Lo, J. Phys. Chem. 70, 11 (1966).

4.16 T.C. Waddington, J. Chem. Soc.,1708 (1958).

4.17 J.W. Nibler and G.C. Pimentel, J. Chem. Phys., 47, 710 (1967).

4.18 G.C. Stirling, C.J. Ludman and T.C. Waddington, J. Chem. Phys., 52, 2730 (1970).

4.19 L.W. Schroeder, J. Chem. Phys., 52, 1972 (1970).

4.20 F.P. Temme, T.C. Waddington and C.J. Ludman, to be published.

4.21 S.W. Peterson and H.A. Levy, J. Chem. Phys., 20, 704 (1952).

4.22 S-S. Chang and E.F. Westrum, J. Chem. Phys., 36, 2571 (1962).

4.23 E.A.C. Lucken, "Nuclear Quadrupole Coupling Constants" Academic Press 1969 p 290.

4.24 C.W. Fryer and J.A.S. Smith, J. Chem. Soc (A), 1029, (1970).

4.25 W.C. Hamilton and J.A. Ibers "Hydrogen Bonding in Solids", Benjamin, New York 1968 Ch.3.

4.26 R.E. Rundle, J. Phys., 25, 487 (1964).

4.27 C.T. O'Konski and T.J. Flautt, J. Chem. Phys., 27, 815 (1957).

4.28 I. Olovson and D.H. Templeton, Acta. Cryst. 12, 832 (1959).

4.29 S. Alexander and A. Tzalmona, Phys. Rev. 138 A, 845 (1965).

4.30 Y. Ayant, J. Phys. Radium, 17, 338 (1956).

4.31 T.P. Das, D.K. Roy and S.K. Gosh Roy, Phys. Rev. 104, 1568 (1956).

4.32 K. Yosida and T. Moriya, J. Phys. Soc. Japan, 11, 33 (1956).

4.33 A.H. Mitchell, J. Chem. Phys. 26, 1714 (1957).

4.34 P. Sh. Lotfulin and G.K. Semin, Phys. Stat. Sol. 35, 133 (1969); Soviet Physics - Crystallography 14, 700 (1970).

4.35 M. J. Weber, J. Phys. Chem. Solids, 17, 267 (1961).

4.36 E.P. Marram and J.L. Ragle, J. Chem. Phys. 41, 3546 (1964).

4.37 D.E. O'Reilly, E.M. Peterson and J.M. Williams, J. Chem. Phys., 54, 96 (1971).

4.38 R.C. Taylor and G.L. Vidale, J. Am. Chem. Soc. 78, 5999 (1956).

Chapter 5

5.1 D. Biedenkapp and A. Weiss, Ber. Bunsengesell. Phys. Chemie 70, 788 (1966).

5.2 J.C. Speakman, Chem. Comm. 32, (1967) and refs therein.

5.3 A. Sequeira, C.A. Berkebile and W.C. Hamilton, J. Mol. Structure, 283 (1967).

5.4 R. Blinc and D. Hadzi, Spect. Acta. 16, 853 (1960).

5.5 " " Nature, 212, 1307 (1966).

5.6 T.A. O'Shea, Ph.D. Thesis, University of Warwick, 1969.

5.7 J.C. Speakman - personal communication to J.A.S. Smith.

5.8 M. Ichikawa and T. Mitsui, Phys. Rev., 152, 495 (1966).

5.9 T. Yamamoto, N. Nakamura and H. Chihara, J. Phys. Soc. Japan, Suppl. 28, 112 (1970).

5.10 [1.4] p 64.

5.11 H.H. Mills and J.C. Speakman, J. Chem. Soc., 4354, (1963).

5.12 R.D. Ellison and H.A. Levy, Acta. Cryst., 19, 260 (1965).

5.13 D. Tuomi, Diss. Abs. 18, 840 (1958).

5.14 J.C. Speakman, Structure and Bonding, (1972) to be published.

5.15 M. Ichikawa, Acta Cryst. B28, 755 (1972).

Chapter 6

6.1 M. Kubo and D. Nakamura, Advan. Inorg. Radiochem., 8, 257 (1966) and references therein.

6.2 E.P. Marram, E.J. McNiff and J.L. Ragle, J. Phys. Chem. 67, 1719 (1963).

6.3 L. Aslanov, R. Mason, A.G. Wheeler and P.O. Whimp, Chem. Comm., 1, 30 (1970).

6.4 B. Bell, Ph.D. Thesis, University of Sussex 1971.

6.5 C.W. Fryer, personal communication.

6.6 U. Belluco, L. Cattalini, F. Basolo, R.G. Pearson and A. Turco, J. Amer. Chem. Soc., 87, 241 (1965).

6.7 C.W. Fryer and J.A.S. Smith, J. Organometallic Chem., 18, 35 (1969); J. Chem. Soc (A), 1029 (1970).

6.8 L.M. Venanzi, Chem. in Britain, 4, 162 (1968).

6.9 C.W. Fryer, Chem. Comm., 902 (1970).

6.10 T.E. Haas and E.P. Marram, J. Chem. Phys., 43, 3985 (1965).

6.11 T.L. Brown and L.G. Kent, J. Phys. Chem. 74, 3572 (1970).

6.12 J.H.E. Griffiths and J. Owen, Proc. R. Soc., A226, 96 (1954).

6.13 R. Bersohn and R.G. Shulman, J. Chem. Phys, 45, 2298 (1966).

6.14 T.L. Brown, W.G. McDugle and L.G. Kent, J. Am. Chem. Soc., 92, 3645 (1970).

6.15 P.J. Cresswell, J.E. Ferguson, B.R. Penfold and D.E. Scaife, J. Chem. Soc., Dalton no 3, 254 (1972).

6.16 [2.2] p 298.

6.17 " p 163.

6.18 J. Duchesne, M. Read and P. Cornil, J. Phys. and Chem. Solids, 24, 1333 (1963).

6.19 D.R. Herschbach and V.W. Laurie, J. Chem. Phys. 37, 1668 (1962).

6.20 S.J. Cyvin, "Molecular Vibrations and Mean Square Amplitudes" Elsevier (1968) p 221, 240.

Chapter 7

7.1 J.A.S. Smith and E.J. Wilkins, J. Chem. Soc (A), 1749 (1966).

7.2 J.C. Hammel, J.A.S. Smith and E.J. Wilkins, J. Chem. Soc. (A), 1461 (1969).

7.3 J.C. Hammel and J.A.S. Smith, J. Chem. Soc. (A), 2883 (1969).

7.4 N. Bloembergen, J. Chem. Phys. 35, 1131 (1961); J. Armstrong, N. Bloembergen and D. Gill, ibid., 1132.

7.5 E. Isfan and A. Barabas, Tetrahedron 26, 5057 (1970).

7.6 N.M.D. Brown and P. Bladen, Chem. Comm., 10, 304 (1966).

7.7 R.C. Fay and N. Serpone, J. Am. Chem. Soc. 90, 5701 (1968).

7.8 A.D. Buckingham, Canad. J. Chem., 38, 300 (1960).

7.9 J.I. Musher, J. Chem. Phys., 37, 34, 2372 (1962).

7.10 J.C. Hammel, R.J. Lynch, J.A.S. Smith, A. Barabas and E. Isfan, J. Chem. Soc. (A), 3000 (1969).

Chapter 8

8.1 H. Chihara, N. Nakamura and S. Seki, Bull. Chem. Soc. Japan, 40, 50 (1967).

8.2 J.V. DiLorenzo and R.F. Schneider, Inorg. Chem., 6, 766 (1967).

8.3 K.B. Dillon and T.C. Waddington, to be published.

8.4 D. Clark, H.M. Powell and A.F. Wells, J. Chem. Soc., 642 (1942).

8.5 W.F. Zelezny and N.C. Baenziger, J. Am. Chem. Soc., 74, 6151 (1952).

8.6 T.J. Kistenmacher and G.D. Stucky, Inorg. Chem. 7, 2150 (1968).

8.7 R. Livingston, J. Phys. Chem., 57, 496 (1953).

8.8 D. Nakamura, Bull. Chem. Soc. Japan, 36, 1662 (1963).

8.9 T.J. Kistenmacher and G.D. Stucky, Inorganic Chemistry, 10, 122 (1971)

8.10 [1.4] p 67.